STELLAR ROTATION IN M35: MASS-PERIOD RELATIONS, SPIN-DOWN RATES, AND GYROCHRONOLOGY[1]

Søren Meibom[2,3,4] and Robert D. Mathieu [4]

Department of Astronomy, University of Wisconsin - Madison, Madison, WI, 53706, USA

Keivan G. Stassun[4]

Physics and Astronomy Department, Vanderbilt University, Nashville, TN - 32735, USA

ABSTRACT

We present the results of a 5 month photometric time-series survey for stellar rotation over a $40' \times 40'$ field centered on the 150 Myr open cluster M35. We report rotation periods for 441 stars within this field and determine their cluster membership and binarity based on a decade-long radial-velocity survey, proper-motion measurements, and multi-band photometric observations. We find that 310 of the stars with measured rotation periods are late-type members of M35. The distribution of rotation periods for cluster members span more than two orders of magnitude from $\sim 0.1 - 15$ days, not constrained by the sampling frequency and the time-span of the survey. With an age between the zero-age main-sequence and the Hyades, and with ∼6 times more rotation periods than measured in the Pleiades, M35 permit detailed studies of early rotational evolution of late-type stars. Nearly 80% of the 310 rotators lie on two distinct sequences in the color-period plane, and define clear relations between stellar rotation period and color (mass). The M35 color-period diagram enables us to determine timescales for the transition between the two rotational states, of ∼60 Myr and ∼140 Myr for G and K dwarfs, respectively. These timescales are inversely related to the mass of the convective envelope, and offer constraints on the rates of internal and external angular momentum transport and of the evolution of stellar dynamos. A

---

[1]WIYN Open Cluster Study. XXXIII.

[2]*smeibom@cfa.harvard.edu*

[3]Now at Harvard-Smithsonian Center for Astrophysics, Cambridge, MA, 02138, USA

[4]Visiting Astronomer, Kitt Peak National Observatory, National Optical Astronomy Observatory, which is operated by the Association of Universities for Research in Astronomy, Inc. (AURA) under cooperative agreement with the National Science Foundation.

comparison to the Hyades, confirm the Skumanich (1972) spindown-dependence for G dwarfs on one rotational state, but suggest that K dwarfs spin down more slowly. The locations of the rotational sequences in the M35 color-period diagram support the use of rotational isochrones to determine ages for coeval stellar populations. We use such gyrochronology to determine "gyro-ages" for M35 from 134 Myr to 161 Myr. We use the M35 data to evaluate new color dependencies for the rotational isochrones.

Subject headings: open clusters and associations:general - stars:late-type - stars:rotation - stars:ages - stars:spots - binary stars:rotation

1. INTRODUCTION

Observations of coeval populations of late-type stars younger than the Hyades have revealed that they rotate with periods ranging over two orders of magnitude - from near breakup to periods similar to the Sun. Understanding why some stars deplete their angular momentum faster than others, which physical processes are at work, when, and to what extent, is a primary mandate for stellar evolution research.

The discovery from photometric and spectroscopic measurements in the Pleiades of sub 1-day rotation periods for K dwarfs (Alphenaar & van Leeuwen 1981; van Leeuwen & Alphenaar 1982; Meys et al. 1982; Soderblom et al. 1983) challenged prior understanding of the early angular momentum evolution for late-type stars, and sparked a renewed interest in the topic. Observations of mainly projected rotation velocities ($v\sin(i)$) of late-type stars in α Persei (50 Myr; Stauffer et al. (1985, 1989)), the Pleiades (100 Myr; Soderblom et al. (1983); Stauffer et al. (1984); Benz et al. (1984); Stauffer & Hartmann (1987); Soderblom et al. (1993a); Terndrup et al. (2000)), and the Hyades (625 Myr; Soderblom (1982); Benz et al. (1984); Radick et al. (1987)), and photometric studies of the Hyades (Lockwood et al. 1984; Radick et al. 1987), confirmed the coexistence of slowly and rapidly rotating stars in α Persei and the Pleiades, but found an absence of rapid rotators in the Hyades. Furthermore, the rapid rotators in the youngest clusters were found primarily among K and M dwarfs and not among G dwarfs.

The emerging evidence for an age- and mass-dependence of rapid rotation prompted new ideas about the rotational evolution of late-type stars. For example the suggestion of epochs of decoupling and recoupling of the stellar core and envelope (e.g. Stauffer et al. 1984; Soderblom et al. 1993b; Jianke & Collier Cameron 1993). The idea of decoupling - allowing the more shallow convective envelope of G dwarfs to spin down faster than the envelopes in

K and M dwarfs - had developed in parallel in models of stellar rotation (e.g. Endal & Sofia 1981; Pinsonneault et al. 1990; MacGregor & Brenner 1991; Barnes & Sofia 1996). However, the concept of decoupling, if permanent, is in conflict with helioseismic observations of the sun as a solid-body rotator (Gough 1982; Duvall et al. 1984; Goode et al. 1991; Eff-Darwich et al. 2002). Furthermore, recoupling - giving access to the angular momentum reservoir of the faster spinning core - was suggested by Soderblom et al. (1993b) as being necessary to explain the evolution beyond the age of the Pleiades of slowly rotating stars (Soderblom et al. 1993b).

Understanding the formation of the rapid rotators is a separate problem. The fastest spinning stars in the youngest clusters cannot be explained from Skumanich-style spin-down (Skumanich 1972) of the fastest spinning T Tauri stars. The rapid rotators can be explained only by introducing "magnetic saturation" of the angular momentum loss via stellar winds (Stauffer & Hartmann 1987; MacGregor & Brenner 1991; Barnes & Sofia 1996; Bouvier et al. 1997; Krishnamurthi et al. 1997; Sills et al. 2000), and by allowing the saturation threshold to depend on the stellar mass. The physical meaning of "saturation" is still unclear.

During the pre main-sequence (PMS) phase, large dispersions and substructure (bimodalities) in the rotation-period distributions has also been observed for coeval stellar populations. Here, a popular explanation for coeval rapid and slow rotators originates from the work of Koenigl (1991) and Edwards et al. (1993) on interactions between T Tauri stars and their circumstellar disks. "Magnetic disk-locking" was introduced to provide a means to brake the spin-up of the central star by transferring angular momentum from the star to the disk (e.g. Shu et al. 1994; Najita 1995, and references therein). Accordingly, rotation-period dispersions (bimodalities) should result if some stars lose their disks faster than others (e.g. weak vs. classic T Tauri stars). Whether magnetic disk-braking is a dominant process regulating stellar rotation during the early PMS remains under debate on both observational and theoretical grounds.

Recently, taking advantage of results from an increasing number of photometric monitoring programs of late-type stars in young main-sequence clusters, Barnes (2003) presented an interpretation of his own and other published rotation period data. Free of the ambiguities of $v\sin(i)$, Barnes identified, in each coeval stellar population, separate groups of fast and intermediate/slowly rotating stars with different dependencies on color (mass). He specifically proposed that coeval stars fall along two "rotational sequences" in the color vs. rotation period plane. From an analysis of these sequences and their dependencies on stellar age, Barnes (2003) proposed a framework for connecting internal and external magneto-hydrodynamic processes to explain the evolution in the observed period distributions, including bimodalities. This approach combines the ideas of (e.g. Stauffer et al. 1984;

Soderblom et al. 1993b) of an initial decoupling of the stellar core and envelope with reconnection of the two zones through a global dynamo-field at a later and mass-dependent time. It does not (yet) interface with PMS angular momentum evolution. Importantly, Barnes (2003) also proposed that the age-dependence of the location of the rotational sequences in the color-period plane, could be used to measure the age of a stellar population, much like the sequences in the color-magnitude diagram. Barnes (2007) further developed this idea of "gyrochronology". Determining the age of a late-type star from its rotation and color, had previously been suggested by Kawaler (1989).

Interpretation aside, it has become desirable and increasingly possible to eliminate the ambiguity of projected rotation velocities ($v \sin i$) by measuring photometric rotation periods from light modulation by spots on the surfaces of young late-type stars. While more labor and time intensive, photometric measurements of rotation periods in coeval populations, promise to reveal important details about dependencies of rotation on other stellar properties - most obviously mass and age, but likely also stellar activity, internal/external magnetic configurations, and binarity.

We present in this paper the results of an extensive time-series photometric survey for rotation periods and a decade-long spectroscopic surveys for membership and binarity for late-type stars in the field of the open cluster M35 (NGC 2168). The combination of time-series and multi-band photometry with time-series radial-velocity data enable us to explore the distribution of rotation periods vs. stellar color (mass) for *bona fide* single and binary members of M35.

M35 is a rich ($\gtrsim$ 2500 stars; Barrado y Navascués et al. (2001)) northern hemisphere cluster located ∼800-900 pc (Barrado y Navascués et al. 2001; Kalirai et al. 2003) toward the galactic anti-center ($\alpha_{2000} = 6^h\ 9^m$, $\delta_{2000} = 24^\circ\ 20'$; $l = 186.^\circ59$, $b = 2.^\circ19$). The age of M35 has been estimated to 150 Myr (von Hippel et al. 2002), 175 Myr (Barrado y Navascués et al. 2001), and 180 Myr (Kalirai et al. 2003). We adopt an age of 150 Myr, in agreement with the most recent age determination based on the isochrone method (Deliyannis 2008). At the distance of M35 the majority of cluster members are confined to within a $\sim 0.5^\circ$ diameter field, facilitating photometric and spectroscopic observations of a large number of stars through wide-field CCD imaging and multi-object spectroscopy. Older and much more populous than the Pleiades, and younger than the Hyades, M35 nicely bridges a gap in the age sequence of star clusters with comprehensive information about rotation and membership, permitting a more detailed study of the rotational evolution of late-type stars beyond the zero-age main-sequence (ZAMS).

We begin in Section 2 by describing our time-series photometric observations, our methods for data-reduction and for photometric period detection, and the information about

cluster membership available from our spectroscopic survey and the M35 color-magnitude diagram. In Section 3 we present the distribution of rotation periods in M35, discuss the short- and long-period tails in the context of our period detection limits, and assess the stability/lifetime of spots or groups of spots by comparison of our short- and long-term photometric data. Section 4 introduces the M35 color-period diagram and the observed dependencies of stellar rotation on mass. In Section 5 we discuss and interpret the M35 color-period diagram in the context of present ideas for stellar angular momentum evolution. In particular we use the diagram to estimate spin-down rates for G and K dwarfs, to test the time-dependence on rotational evolution from a comparison with measured rotation periods in the Hyades, determine M35's gyrochronology age, and to evaluate the best functional representation of the color-period dependence in the M35 data. Section 6 summarizes and presents our conclusions.

2. OBSERVATIONS, DATA REDUCTION, AND METHODS

2.1. Time-Series Photometric Observations

We photometrically surveyed stars in a region approximately $40' \times 40'$ centered on the open cluster M35 over a timespan of 143 days. The photometric data were obtained in the Johnson V-band with the WIYN [1] 0.9m telescope [2] on Kitt Peak equipped with a $2k \times 2k$ CCD camera. The field of view of this instrument is $20.5' \times 20.5'$ and observations where obtained over a 2×2 mosaic.

The complete dataset presented is composed of images from high-frequency (approximately once per hour for 5-6 hours per night) time-series photometric observations over 16 full nights from 2-17 December 2002, complemented with a queue-scheduled observing program over 143 nights from 22 October 2002 to 11 March 2003, obtaining one image per night interrupted only by bad weather and scheduled instrument changes. The result is a database of differential V-band light curves for more than 14,000 stars with $12 \lesssim V \lesssim 19.5$. The sampling frequency of the December 2002 observations allow us to detect photometric variability with periods ranging from less than a day to about 10 days. The long time-span of the queue-scheduled observations provide data suitable for detecting periodic variabil-

---

[1] The WIYN Observatories are joint facilities of the University of Wisconsin-Madison, Indiana University, Yale University, and the National Optical Astronomy Observatories.

[2] The 0.9m telescope is operated by WIYN Inc. on behalf of a Consortium of ten partner Universities and Organizations (see http://www.noao.edu/0.9m/general.html)

ity of up to $\sim$ 75 days, and for testing the long-term stability of short-period photometric variations. From this database we derive rotation periods for 441 stars.

Figure 1 shows the surveyed region (solid square) and the spatial distribution of the 441 rotators. The region is roughly coincident with that of Deliyannis (2008) in which they obtained UBVRI CCD photometry for $\sim$19,000 stars (dashed square). Also shown is the circular target region of our spectroscopic survey described in Section 2.4 and in Meibom & Mathieu (2005). The photometric survey was carried out within the region of the spectroscopic survey to optimize information about spectroscopic membership and binarity[3].

Figure 2 displays the time-series data from both programs for a photometrically non-variable star. Filled symbols represent the high-frequency observations and open symbols represent the queue-scheduled observations.

2.2. Basic Reductions, PSF Photometry, and Light Curves

Basic reductions of our CCD frames, identification of stellar sources, and computations of equatorial coordinates[4] were done using standard IRAF packages. Instrumental magnitudes were determined from Point Spread Function (PSF) photometry using the IRAF DAOPHOT package. The analytical PSF and a residual lookup table were derived for each frame based on $\sim$30 evenly distributed isolated stars. The number of measurements in the light curve of a given star vary because stars near the edges of individual frames may be missed due to telescope pointing errors, while bright stars near the CCD saturation limit and faint stars near the detection threshold may be excluded on some frames because of variations in seeing, sky brightness, and sky transparency. To ensure our ability to perform reliable time-series analysis on stars in our database, we have eliminated stars that appear on fewer than half of the total number of frames. The resulting database contains 14022 stars with a minimum of 75 measurements.

We applied the Honeycutt (1992) algorithm for differential CCD photometry to our raw light curves to remove non-stellar frame-to-frame photometric variations. We favor this technique for differential photometry because it does not require a particular set of comparison stars to be chosen *a priori*, nor does it require a star to appear in every frame.

---

[3]All of these mutually supportive studies are parts of the WIYN Open Cluster Study (WOCS; Mathieu (2000)).

[4]We used data from the STScI Digitized Sky Survey; The Digitized Sky Surveys were produced at the Space Telescope Science Institute under U.S. Government grant NAG W-2166.

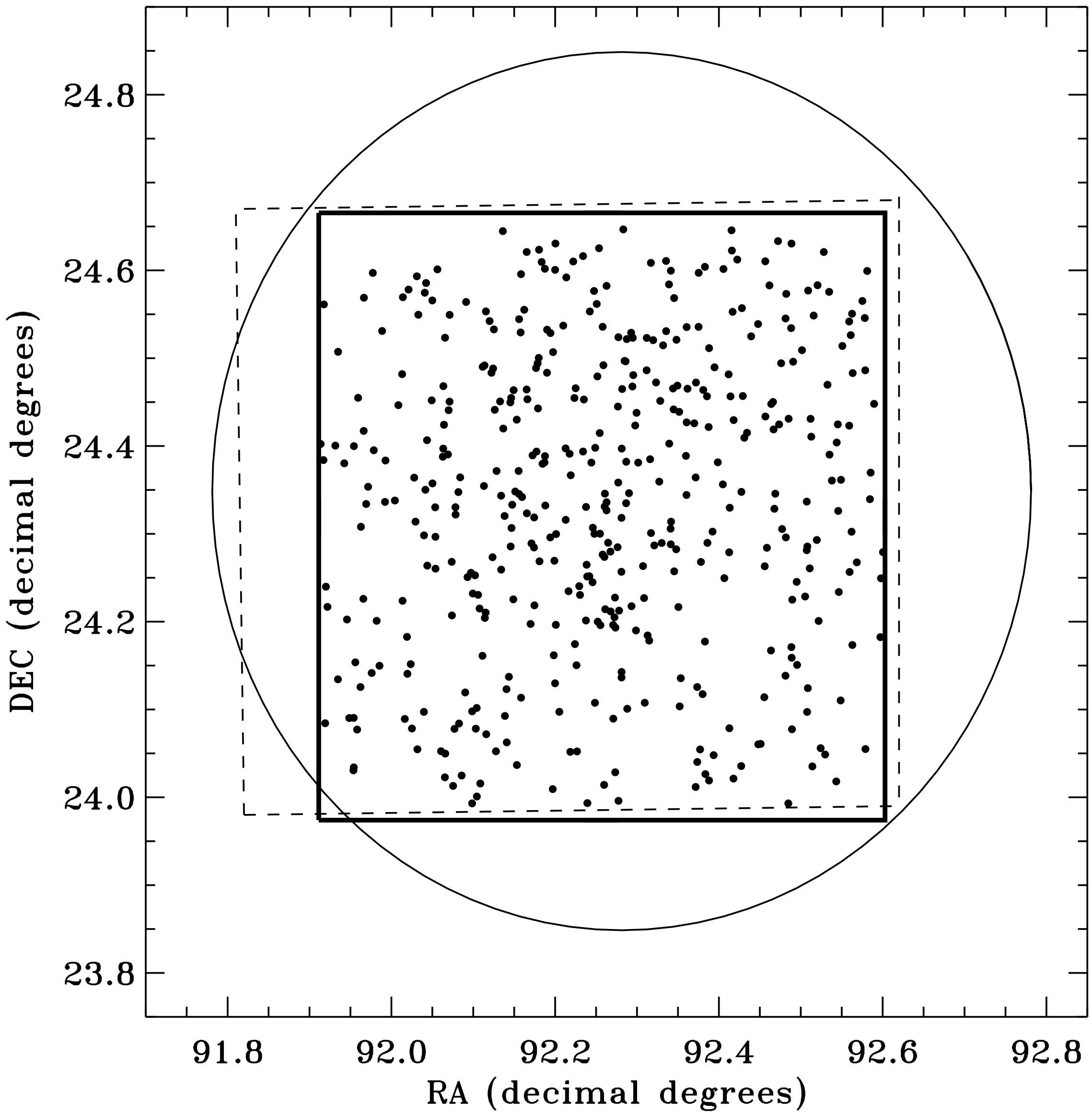

Fig. 1.— The locations and spatial extents of the photometric and spectroscopic surveys used in this study. The innermost solid square denotes the $40' \times 40'$ region of our time-series photometric survey. Within it we show the distribution of the 441 stars with measured rotation periods (black dots). The dashed rectangle displays the region of the multi-band photometric study by Deliyannis (2008) and the circle represents the 1-degree diameter field of our spectroscopic survey of M35 (Meibom & Mathieu 2005).

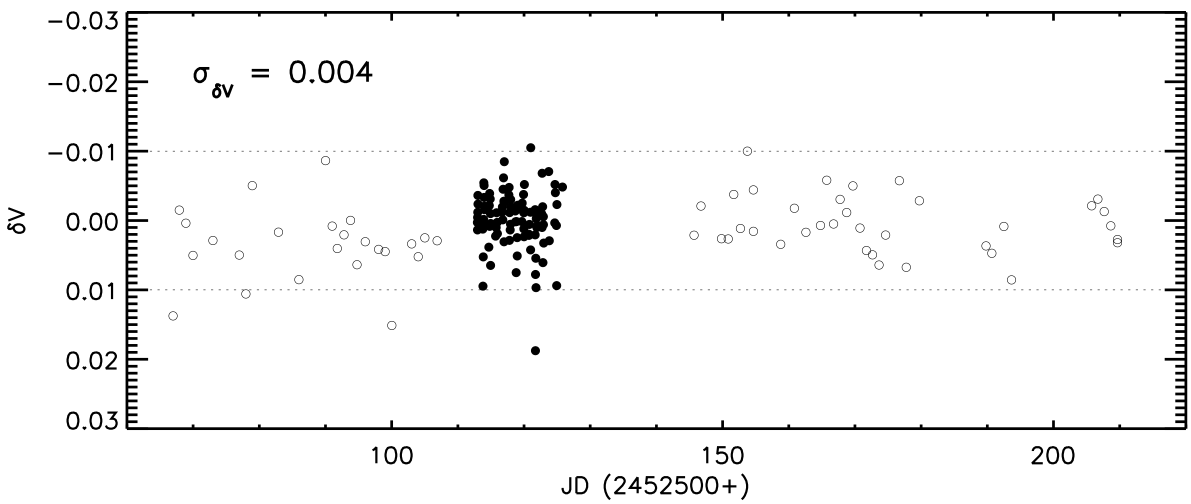

Fig. 2.— Sample time-series data from from our photometric database for a non-variable $V \simeq$14th magnitude star. Filled symbols represent measurements from the high-frequency December 2002 observing run and open symbols represent the low-frequency queue-scheduled observations. The data span a total of 143 days. The star was observed in all 157 images of the north-east quadrant of the 2 × 2 mosaic. The standard deviation ($\sigma_{\delta V}$) of the 157 measurements is $0\overset{\mathrm{m}}{.}004$, representative of our best photometric precision. The horizontal dotted lines denote $\delta V = \pm 0\overset{\mathrm{m}}{.}01$.

Figure 2 shows the light curve for a $V \sim$14th magnitude star. The standard deviation from 157 photometric measurements is $0\overset{\mathrm{m}}{.}004$, representative of our photometric precision at that brightness. Figure 3 shows the standard deviation of the photometric measurements as a function of the V magnitude for each star in the field of M35. The relative photometric precision is ∼0.5% for stars with $12 \lesssim V \lesssim 14.5$.

2.3. Photometric Period Detection

We employed the Scargle (1982) periodogram analysis to detect periodic variability in the light curves because of its ability to handle unevenly sampled data. We searched a grid of 5000 frequencies corresponding to periods between 0.1 day and 90 days. The lower search limit was set at a period ensuring critical sampling based on the Nyquist critical frequency for our high-frequency data ($f_c = 1/(2\delta t)$, where δt is the sampling interval of ∼1 hour. The upper limit was set at 90 days because a star with a 90-day period would complete about 1.5 cycle over the 143 nights of the survey.

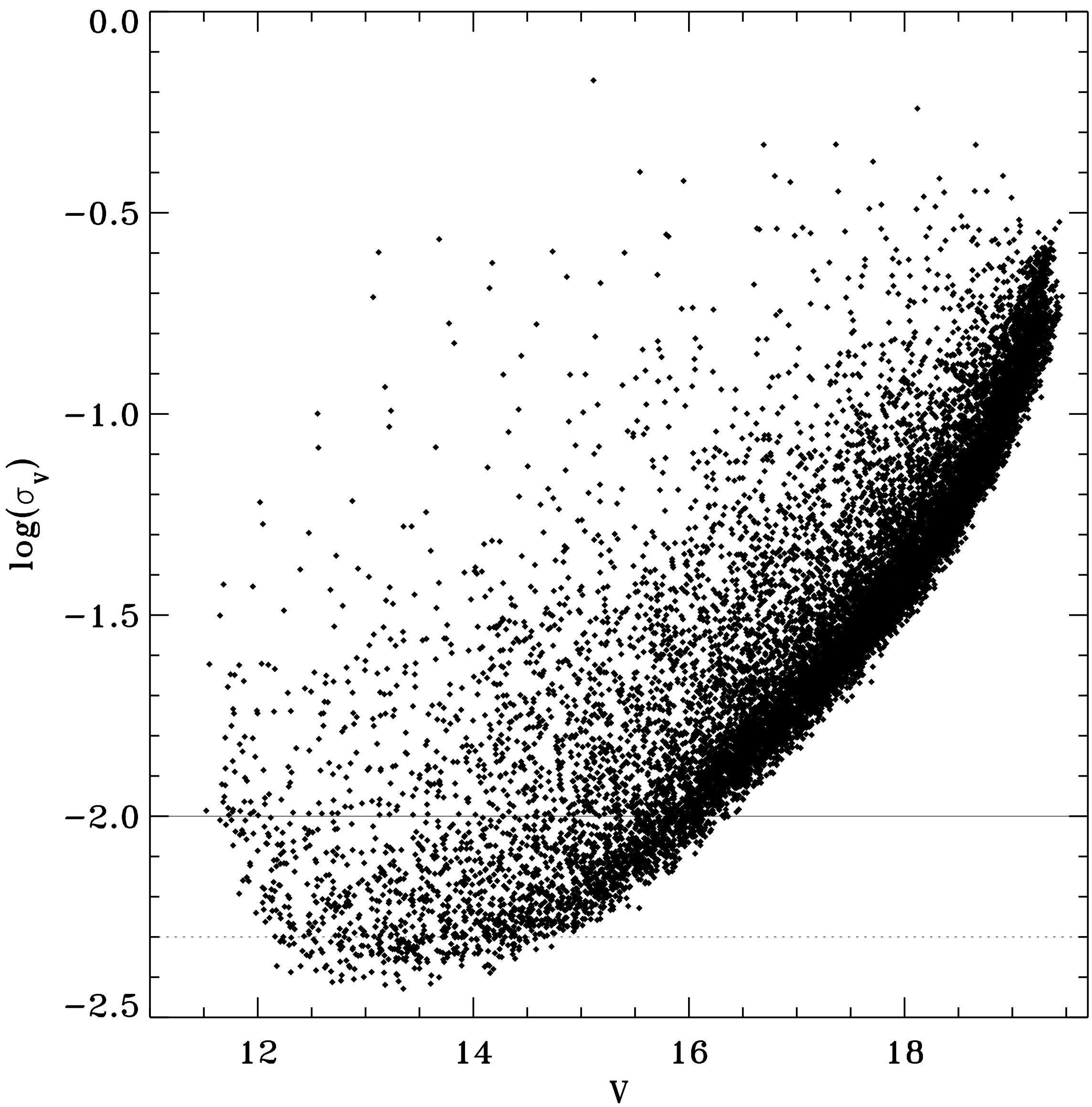

Fig. 3.— The logarithm of the standard deviation of all instrumental magnitudes as a function of V magnitude for 14022 stars in the field of M35. The number of measurements for each star range from 75 to 216. The solid and dashed horizontal lines represent σ_V of 0.01 (1%) and 0.005 (0.5%), respectively. A relative photometric precision of $\sim 0.5\%$ is obtained for stars with $12\overset{m}{.}0 \lesssim V \lesssim 14.5\overset{m}{.}0$.

A false alarm probability (FAP), the probability that a signal detected at a certain power

level can be produced by statistical fluctuation, was calculated as the measure of confidence in a detected period. An analytical expression for estimating a FAP is given by Scargle (1982) and Horne & Baliunas (1986). However, these methods are not entirely suitable when applied to time-series photometric studies of young stars because they only test against random fluctuations of a purely statistical nature (i.e., measurement errors) and do not account for correlated fluctuations intrinsic to the source such as variability on timescales long compared to the sampling frequency. For young stars our repeated measurements during a single night are not necessarily independent and uncorrelated. Consequently, the analytical expressions estimating a FAP will likely overestimate the significance of any measured periodic variability. Hence, we performed a two-dispersion Monte Carlo calculation to estimate the FAP of our detected periods, as per Herbst & Wittenmyer (1996) and Stassun et al. (1999). For each star, we generated a set of 100 synthetic light curves, each consisting of normally distributed noise with two dispersions: one representing the variability of the star during a night and one representing the night-to-night variability of the star. The former was estimated by taking the mean of each night's standard deviation, and the latter by taking the standard deviation of nightly means. With this approach, the test light curves can vary on timescales that are long compared to our sampling interval, allowing them to mimic the random slow variability of stellar origin that could produce spurious periodic behavior over our limited observing window. The maximum power of the 100 periodograms of the test light curves was adopted as the level of 1% FAP, and used as the initial threshold for detecting significant photometric variability. For all stars that met the FAP criterion we examined (by eye) the periodogram and raw and phased light curves. We report stellar rotation periods for 441 stars in our database (see Table 1 in Appendix B).

We do not have multiple seasons of observations or observations in multiple pass-bands at our disposal by which to confirm rotation periods of individual stars. However, the reliability of the derived periods is supported by an observed correlation between photometric period and rotational line broadening within a subset of 16 single cluster members. Figure 4 shows the projected rotation velocities measured by Barrado y Navascués et al. (2001) for 16 stars for which we have determined rotation periods. The shortest period stars ($P_r \lesssim 2.5$ days) show increasing $v \sin(i)$ with decreasing rotation period. For rotation periods of $\sim$ 4 days or longer the upper limits on the projected rotation velocities are consistent with slower rotation. For comparison, the solid, dashed, and dotted curves in Figure 4 indicate the relation between rotation period and the projected rotational velocity for a solar-like star with a 90°, 70°, and 50° inclination of the rotational axis, respectively. Thus, for all 16 stars, the projected rotation velocities are consistent with the measured rotation periods.

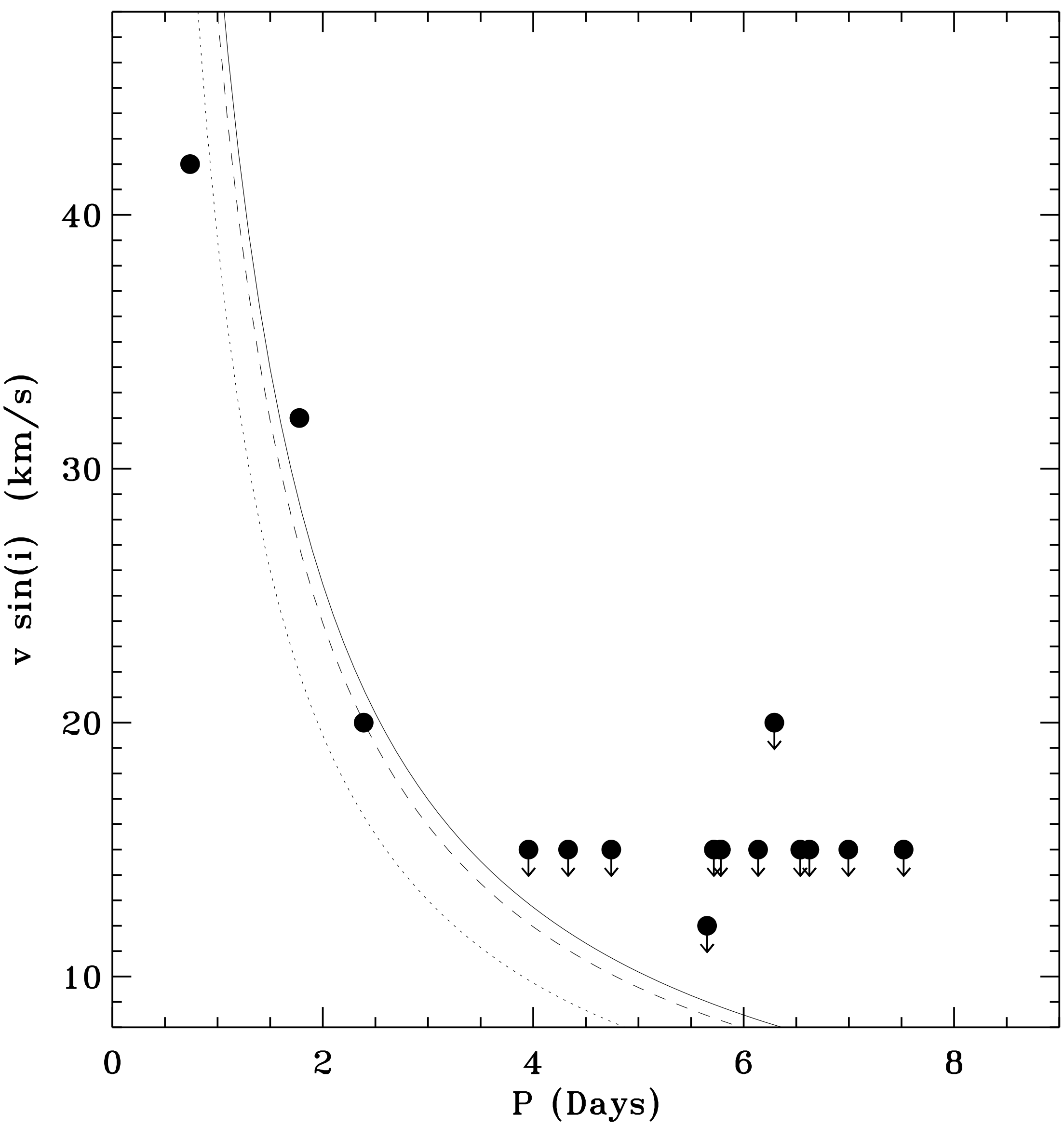

Fig. 4.— Projected rotation velocities (Barrado y Navascués et al. 2001) plotted against the measured rotation period for 16 stars in M35. All stars have $P_{RV} \geq 60\%$ and none of the 16 stars are spectroscopic binaries. For comparison, the solid, dashed, and dotted curves indicate the relation between rotation period and the projected rotational velocity for a solar-like star with a 90°, 70°, and 50° inclination of the rotational axis, respectively. The rotation periods and the projected rotation velocities are consistent for all 16 stars.

2.4. The Spectroscopic Survey

M35 has been included in the WIYN Open Cluster Study (WOCS; Mathieu (2000)) since 1997. As part of WOCS more than 6000 spectra has been obtained of approximately 1500 solar-type stars within a 1-degree field centered on M35. The selection of survey target stars was based on photometric (Deliyannis (2008), see Section 2.5) and proper-motion (McNamara & Sekiguchi 1986; Cudworth 1971) membership data. Stars on or less than $\sim 1\overset{m}{.}0$ above the cluster main sequence were selected, with brightness and color ranges corresponding to a range in mass from $\sim 0.7\ M_{\odot}$ to $\sim 1.4\ M_{\odot}$. All spectroscopic data were obtained using the WIYN 3.5m telescope equipped with a multi-object fiber optic positioner (Hydra) feeding a bench mounted spectrograph. Observations were done at central wavelengths of 5130Å or 6385Å with a wavelength range of ∼200Å providing many narrow absorption lines. Radial velocities with a precision of $\lesssim 0.5\ km\ s^{-1}$ (Geller et al. 2008; Meibom et al. 2001) were derived from the spectra via cross-correlation with a high S/N sky spectrum. From this extensive radial-velocity survey we have 1) calculated the cluster membership probability; 2) detected the cluster binary stars; and 3) determined the orbital parameters for the closest binaries.

Of the 441 stars with rotation periods presented in this study, 259 have one or more radial-velocity measurements (the remainder being below the faint limit of the spectroscopic survey or photometric non-members). The radial-velocity cluster membership probability of each star is calculated using the formalism by Vasilevskis et al. (1958). The mean or center-of-mass radial velocity of a single or binary star was used when calculating the membership probability. We have adopted 50% as the threshold for assigning radial-velocity and proper-motion cluster membership. Of the 259 rotators with one or more radial-velocity measurement, 203 are radial-velocity members of M35 and 20 of those 203 stars are also proper-motion members. More detailed descriptions of the radial-velocity survey and membership determination can be found in Meibom & Mathieu (2005), Meibom et al. (2006), and Braden et al. (2008).

2.5. The M35 Color-Magnitude Diagram and Photometric Membership

Figure 5 shows the (V-I) vs. V color-magnitude diagram (CMD) for M35. The photometry was kindly provided by Deliyannis (2008) who obtained UBVRI data in a $23' \times 23'$ central field and BVRI data in a 2×2 mosaic for a total of $\sim 40' \times 40'$ using the WIYN 0.9m telescope. In the CMD the 441 stars for which we have measured rotation periods are highlighted in black. The solid lines enclosing stars within or above the cluster sequence (allowing for inclusion of equal-mass binaries) show our criteria for photometric membership. The in-

sert in Figure 5 shows the location in the M35 CMD of only radial-velocity members (open symbols), and radial-velocity and proper-motion members (filled symbols), the location of which was used to define the criteria for photometric membership. There are 23 photometric members with 3 or more radial-velocity measurements and a radial-velocity membership probability of less than 50%. Those 23 stars were removed from the list of cluster members. The final number of stars with measured rotation periods selected as radial-velocity and/or photometric members of M35 is 310.

3. THE ROTATION-PERIOD DISTRIBUTION

The 310 members of M35 with determined rotation periods correspond to ∼12% of the photometric cluster population within the brightness and areal limits of our photometric survey. Figure 6a shows the distribution of rotation periods, which spans more than 2 orders of magnitude from ∼0.1 days to ∼15 days. The distribution peaks shortward of 1 day and has a broader and shallower peak centered at about 6 days.

Figure 6b displays with an increased resolution of 0.1 day the distribution of rotation periods shortward of 1 day. The dashed and grey histograms, respectively, represent all stars and all cluster members with detected rotation periods. The distribution shows that we are capable of detecting rotation periods down to the pseudo-Nyquist period-limit of about 2 hours (~ 0.08 day) resulting from our typical sampling cadence of about 1 hr^{-1} in December 2002. The distribution of rotation periods for cluster members falls off shortward of 0.3-0.4 days. Two member stars have rotation periods between 0.1 days and 0.2 days, corresponding to surface rotational velocities of 50% or more of their breakup velocities ($v_{br} = \sqrt{(GM_\star/R_\star)}$). We argue based on this inspection of the short-period tail of the distribution that the lower limit of 0.1 days for our period search was set appropriately for the stars in M35.

The long-period ends of the period distributions for members and non-members (Figure 16, Appendix C) show that the long time-span of the queue-scheduled data enable us to detect rotation periods beyond the ∼10 days typically found to be the upper limit in photometric surveys with durations similar to our short-term December 2002 observing run. We report the detection of 18 stars with rotation periods longer than 10 days, 7 of which are members of M35. The longest rotation period among members is 15.3 days, and among the field stars rotation periods of up to $\sim$ 17 and 23 days have been measured. In the M35 period distribution we see a drop-off at ∼10 days. If the ∼12% of the cluster's late-type population with measured rotation periods is a representative sample of the late-type stellar population in M35, then the ∼10 day cutoff may represent a physical upper limit on the

rotation-period distribution at 150 Myr. However, it is also possible that we are not capable of detecting the slowest rotators despite our long-baseline photometric survey. Indeed, the modest number of rotation periods longer than 10 days found in the much larger sample of field stars may reflect that the frequency and size of spots on stars rotating slower than ∼10 days is insufficient for detection with the photometric precision of our data. Indeed, X-ray observations in Orion (Stassun et al. 2004) indicate that rotation-period studies of young stars may in general be biased against very slow rotators because such stars likely do not generate strong activity, and thus are not sufficiently spotted to allow detection of photometric periods." Measuring the rotation for such slowly rotating stars will likely require either higher photometric precision or high resolution ($R \gtrsim 50,000$) spectroscopic observations to measure projected rotation velocities. The small sample of M35 member stars with periods above 10 days will be discussed in Section 5.5.

3.1. Long-term stability of the number, sizes, and configurations of stellar spots and spot-groups

We find that for almost all cluster and field stars with measured rotation periods, the long-term queue-scheduled data, spanning ∼5 months in time, phase up with and coincide with the short-term data (16 nights in December 2002) in the light curves. We tested further the agreement between the short-term and long-term photometric variability, by measuring the rotation period separately from the short- and long-term data for 20 randomly chosen stars. For all but one star we found a difference between the two rotation periods that was less than 1% of the period measured from the short-term data alone (in most cases the difference was less than 0.1%). We examined the 20 light curves with all data phased to the period derived from only the short-term data. For all but one star, the long-term data produced light curves of the same shape and phase as the light curves based only on the short-term data. Even for two light curves with clear signs of multiple spots (spot-groups), the short- and long-term data coincided very well. Because it is unlikely that the disappearance and recurrences of spots will result in a light curve with the same shape, amplitude, and phase, the agreement suggests stability of individual spots and/or spot-groups over the ∼5 month time-span of our photometric observations.

We find that the stability of the sizes and configurations of spots on young stars have recently been studied for e.g. the solar analog PMS star V410 Tau (Stelzer et al. 2003) and for stars in the PMS cluster IC348 (Nordhagen et al. 2006). For V410 Tau data has been collected for over two decades, showing changes in the shape of the light curve over the last decade. The authors suggest that the observed changes reflect variations of the structure of

the active regions over timescales of years. However, stability in the rotation period and the recurrence of the light curve minimum, suggest stability of the largest spots over years, and either a lack of latitudinal differential rotation in V410 Tau, or confinement of its spots to a narrow range of latitudes. Similarly, Nordhagen et al. (2006) finds a remarkable stability over 7 years in the rotations periods for stars in IC348, suggesting again that these PMS stars do not have significant differential rotation, or that their spots are constrained to a narrow range of stellar latitudes. However, contrary to what is observed over 5 months in M35, all periodic stars in IC348, as well as V410 Tau, do show changes in the light curve shape and amplitude from year to year.

4. THE M35 COLOR-PERIOD DIAGRAM - THE DEPENDENCE OF STELLAR ROTATION ON MASS

In Figure 7 we display the rotation periods for the 310 members plotted against their $B-V$ color indices, or equivalently their masses. The color indices derive from the deep multi-band photometry by Deliyannis (2008, Section 2.5) and the corresponding stellar mass estimates (upper x-axis) from a fit of a 150 Myr Yale stellar evolutionary model (Yi et al. 2003) to the M35 color-magnitude diagram. Dark blue symbols represent stars that are both photometric and radial-velocity members of M35. Light blue symbols are used for stars that are photometric members only. Proper-motion members are marked with additional squares.

The M35 color-period diagram shows striking structure. The coeval stars fall along two well-defined sequences apparently representing two different rotational states. One sequence displays clear dependence between period and color, starting at the blue end at $(B-V)_0 \simeq 0.5$ ($M_\star \simeq 1.2\ M_\odot$) and $P_{rot} \simeq 2$ days and forming a rich diagonal band of stars whose periods are increasing with increasing color index (decreasing mass). This sequence terminates at about $(B-V)_0 \simeq 1.2$ ($M_\star \simeq 0.65\ M_\odot$) and $P_{rot} \simeq 10$ days. The second sequence consists of rapidly rotating ($P_{rot} \lesssim 1$ day) stars and extends from $(B-V)_0 \simeq 0.7-0.8$ ($M_\star \simeq 0.9-1.0\ M_\odot$) to $(B-V)_0 \simeq 1.5$ ($M_\star \lesssim 0.5\ M_\odot$). This well defined sequence of rapidly rotating stars shows a small but steady decrease in rotation period with increasing color (decreasing mass). Finally, a subset of stars are distributed in between the two sequences, and 10 stars have rotation periods that are unusually long, placing them above the diagonal sequence in Figure 7.

The M35 color-period diagram gives a clear picture of preferred stellar rotation periods as a function of color for 150 Myr late-type dwarfs. With the added dimension of color, the diagram take us beyond the one-dimensional period distribution and shows which stars are responsible for the structure observed in Figure 6. The short-period peak at $\lesssim$1 day is due primarily to the rapidly rotating late G- and K-dwarfs ($M \lesssim 0.9\,M_\odot$), and the sharpness of

this peak is the result of little dependence of rotation on color within this group. The more slowly rotating mid to late G- and K-dwarfs give rise to the broader peak at ∼6 days, while the early to mid G-dwarfs and some cooler stars fill in the distribution between the peaks.

The two sequences of stars in the color-period diagram represent the most likely/stable rotation period(s) for a given stellar mass at the age of M35. Under the assumption that rotation periods increase with time for all stars, the more sparsely populated area between the two sequences must then represent a phase of rotational evolution of shorter duration. We will discuss the different loci in the color-period diagram in more detail in Section 5.

5. ANGULAR MOMENTUM EVOLUTION AND THE COLOR-PERIOD DIAGRAM

Sequences similar to those observed in the M35 color-period diagram were noted by Barnes (2003, hereinafter B03) from careful examination of compilations of rotation-period data from photometric monitoring campaigns on open clusters and field stars. B03 named the diagonal sequence of stars on which rotation periods increase with color the *interface* sequence (or I sequence), and the sequence of rapidly rotating stars the *convective* sequence (or C sequence). In what follows we will adopt these names for the two sequences in the M35 color-period diagram.

B03 argues that the rapidly rotating stars on the C sequence have radiative cores and convective envelopes that are decoupled. For these stars he suggests that the evolution of their surface rotation rates is governed primarily by the moments of inertia of the convective envelope and by inefficient wind-driven loss of angular momentum linked to small-scale convective magnetic fields. For stars on the I sequence, large-scale (sun-like) magnetic fields provided by an interface dynamo couple the core and envelope, and the rotational evolution of the I sequence stars is thus primarily governed by the moments of inertia of the entire star and more efficient angular momentum loss (i.e., a Skumanich (1972) style spin-down). Accordingly, B03 suggests that a late-type star, in which the core and envelope are decoupled as it settles on the ZAMS, will begin its main-sequence life on the C sequence and evolve onto the I sequence when rotational shear between the stellar core and envelope establish a large-scale dynamo field that couples the two zones and provide efficient magnetic wind loss. Higher mass stars have thinner convective envelopes with smaller moments of inertia than low mass stars and thus leave the C sequence sooner. Stars that are either fully radiative or fully convective will remain as rapid rotators.

Color-period diagrams for coeval populations of different ages allow us to examine the

rotational properties of late-type coeval stars as a function of their mass and age, and may bring us closer to understanding the physical mechanisms (internal and/or external) regulating their rotational evolution. The M35 color-period diagram, rich in stars and cleaned for spectroscopic and photometric non-members, reveals the morphology described by B03 more clearly than any published stellar populations. We therefore begin with a discussion of the M35 result in the context of the framework developed by B03.

5.1. Timescales for migration from the C to the I sequence

In Figure 8 we add M35 to Fig. 3 in B03 which shows the relative fractions of stars with $0.5 \leq (B-V)_0 \leq 1.5$ on the I and C sequences for stellar populations of distinct ages. With rotation periods measured over more than two orders of magnitude for confirmed spectroscopic and photometric cluster members, M35 adds the statistically most secure datapoints to this figure. M35 fit well with the evolutionary trends of increasing relative fractions of C sequence (and gap) stars and decreasing fractions of I sequence stars for younger cluster populations. The almost linear trends in Figure 8 suggest that the decrease and increase in the number of stars on the C and I sequences, respectively, are approximately exponential with time. Under the presumption of an exponential time dependence and that all stars start on the C sequence at the ZAMS, we can estimate the characteristic timescale for the rotational evolution of stars off the C sequence and onto the I sequence, by counting stars on both sequences and in the gap in the M35 color-period diagram. Such timescales may offer valuable constraints on the rates of internal and external angular momentum transport and on the evolution rates of stellar dynamos in late-type stars of different masses.

When counting the number of stars on the I and C sequences and in the gap, we use the following criteria. Stars located in the color-period diagram between the lines represented by $P_{rot} = 10(B-V)_0 - 2.5 \pm 2.0$ and with periods above 1.5 days were counted as I sequence stars (see dotted lines in Figure 11). Stars redder than $(B-V)_0 = 0.6$ and with periods between 0 and 1.5 days were counted as C sequence stars. Stars located below $P_{rot} = 10(B-V)_0 - 4.5$ and with periods above 1.5 days were counted as gap-stars. These selection criteria are subjective and although the sequences are well defined, the I sequence becomes broader redward of $(B-V)_0 \simeq 1.0$ making the distinction between I sequence and gap stars more difficult. However, due to the large number of rotation periods in M35, the small number of stars that might be moved from the gap to the I sequence or vice versa by using slightly different criteria will not influence the relative fractions and thus the timescales in any significant way.

The number of C sequence stars (N_c) at a time t can then be expressed by:

$$N_c = N_{c_0} e^{-t/\tau_c} \tag{1}$$

where N_{c_0} and τ_c are, respectively, the total number of stars on the I and C sequences and in the gap, and the characteristic exponential timescale. We use the B-V color index to divide the stars into G-dwarfs ($0.6 < B - V < 0.8$) and K-dwarfs ($0.8 < B - V < 1.3$) We count all stars within each color-interval in the color-period diagram as N_{c_0}, all C sequence stars within each color-interval as N_c, and adopt 150 Myr as the age of M35. We derive from equation [1] $\tau_c^G = 60$ Myr and $\tau_c^K = 140$ Myr as the characteristic exponential timescales for transition between the C and the I sequence for G and K dwarfs, respectively.

We can qualitatively verify these time scales by a comparison between the M35 color-period diagram and those of the younger Pleiades cluster and the older cluster NGC3532 presented in B03. In M35 only 7 G dwarfs ($0.6 \lesssim (B-V)_0 \lesssim 0.8$) are found on the C sequence and in the gap, while the G dwarf I sequence is well defined and rich. In contrast, In contrast, the M35 C sequence and gap are rich in K dwarfs ($0.8 \lesssim (B-V)_0 \lesssim 1.3$), whereas the K dwarf I sequence is less densely populated and less well defined. The lack of G dwarfs on the C sequence seen in M35 is already apparent at 100 Myr in the Pleiades color-period diagram, indicating that the characteristic timescale for G dwarfs to evolve off the C sequence and onto the I sequence is less than ∼100-150 Myr. The rich population of early and mid K dwarfs on the M35 C sequence have evolved off the C sequence and onto a well defined I sequence by the age of NGC 3532 (300 Myr). The NGC 3532 C sequence and gap, however, are populated by late K dwarfs, suggesting that early to mid K dwarfs evolve onto the I sequence on a timescale between 150 and 300 Myr, or approximately twice the time required for G dwarfs. Finally, by the age of the Hyades only 3 late K or early M dwarfs have been found off the I sequence, or in the gap (see Fig. 1 in B03 or Figure 9 below), suggesting that such stars evolve off the C sequence and possibly onto the I sequence on a timescale of ∼600 Myr, or approximately twice the time required for the early to mid K dwarfs.

There is thus good agreement between the exponential timescales derived from the M35 color-period diagram alone and the estimated timescales based on a comparison of color-period diagrams of different ages. We note that although the relative fractions displayed in Figure 8 represent all rotators with $0.5 \leq (B-V)_0 \leq 1.5$, a least-squares fit of an exponential function to the C sequence fractions in Figure 8, gives a timescale of 106 Myr for a decrease in the number of C sequence stars by a factor of e.

5.2. Testing the Skumanich $\sqrt{t}$ spin-down rate between M35 and Hyades

The color-period diagram for the Hyades contains 25 stars (Radick et al. 1987; Prosser et al. 1995), 22 of which form an I sequence of G and K dwarfs. Despite the smaller number of stars, the blue part of the Hyades I sequence, populated by G dwarfs, is well defined. By comparing the rotation periods for the I sequence G dwarfs in M35 to those of the I sequence G dwarfs in the $\sim$4 times older Hyades, we can directly test the Skumanich (1972) $\sqrt{t}$ time-dependence on the rotation-period evolution for stars in this mass-range. We follow B03 in assuming separate mass and time dependencies for stellar rotation, and that the same mass dependence can be applied to different stellar populations. Adopting an age of 625 Myr for the Hyades (Perryman et al. 1998) and of 150 Myr for M35, we decrease the Hyades rotation periods by $\sqrt{625/150} \simeq 2$. We show in Fig. 9 the color-period diagram with the 310 M35 members (all grey symbols) and with the locations of the 25 Hyades stars overplotted (black symbols). The spun-up Hyades I sequence G dwarfs coincide nicely with the M35 I sequence G dwarfs, in support of the Skumanich $\sqrt{t}$ time-dependence for such stars. Curiously, the Hyades K-dwarfs, also spun-up according to the Skumanich law, have rotation periods systematically shorter than the M35 K dwarfs. At face value, this suggests that the time-dependence for spin-down of K dwarfs is different and slower than for G dwarfs between 150 Myr and 625 Myr.

5.3. The gyro-age of M35

Arguing that the rotation of stars on the C and I sequences follow separate mass (M) and age (t) dependencies ($P(t, M) = g(t) \times f(M)$), B03 introduced heuristic functional forms to represent these separate dependencies of the I and C sequences. Barnes (2007, hereinafter B07) presents a modified functional form for the I sequence. These functions define one-parameter families, with that parameter being the age of the stellar population, and the resulting curves in the color-period plane represent a set of rotational isochrones. We note that B03 use $g(t) = \sqrt{t}$ (Skumanich), while B07 derive $g(t) = t^{0.52}$ by requiring that a solar-like star spin down to solar rotation at solar age.

Kawaler (1989) used his own calibrated angular momentum loss law (Kawaler 1988) and the assumption of solid body rotation after $\sim$100 Myr (Pinsonneault et al. 1989), to derive a relationship between stellar age, rotation period, and color. Kawaler's age-period-color relation is thus based on models calibrated to the sun, and the assumption that the Skumanich relationship is valid for all masses. He express the stellar mass, radius, and moment of inertia, in terms of observables such as stellar color, via stellar models.

We note that our result in Section 5.2, suggest that the time dependence of stellar rotation is not independent of stellar mass, as assumed by both B03, B07, and Kawaler (1989).

The well-defined sequences in the M35 color-period diagram make possible a test of the period-color relations proposed by B03, B07, and Kawaler (1989). We show in Figure 10 the M35 color-period diagram with the B03 and B07 rotational isochrones for the independently determined stellar-evolution age for M35 of 150 Myr (von Hippel et al. 2002; Deliyannis 2008). The rotational isochrones match the M35 I and C sequences well, suggesting that they can indeed provide a consistent age estimate (gyro-age) for a cluster based on a well populated color-period diagram cleaned for non-members. To illustrate the sensitivity to age, rotational isochrones for 130 Myr and 170 Myr are also displayed in Figure 10.

Assuming no prior knowledge about the age of M35 (thus letting age be a free parameter), we perform a non-linear least squares fit to the I sequence stars (enclosed by the dotted lines in Figure 11) of the functional form of the rotational I sequence isochrones from B03:

$$P(t,(B-V)) = \sqrt{t} \times (\sqrt{((B-V)-a)} - b((B-V)-a) \tag{2}$$

with $a = 0.50$, and $b = 0.15$, and from B07:

$$P(t,(B-V)) = t^{0.52} \times (c((B-V)-d)^{f}) \tag{3}$$

with $c = 0.77$, $d = 0.40$, and $f = 0.60$.

When fitting, the I sequence stars were weighted them according to their cluster membership, with most weight given to confirmed radial-velocity and proper motion members and least weight given to stars with only photometric membership. The weights given to individual stars are listed in Table 2 in Appendix B. Figure 11 shows the best fits of both eq. [2] and eq. [3] to the M35 I sequence. The derived age is 134 Myr for both functional forms, each with a formal $1-\sigma$ uncertainty of $\sim$3 Myr. The close agreement of the two ages likely reflects the similar shape of the two isochrones over the color interval from $\sim 0.5-1.0$ where the M35 I sequence is most densely populated. The small formal uncertainties reflect a well-defined I sequence rich in stars. However, the gyro-ages may still be affected by systematic errors in the stellar evolutionary ages for the young open clusters.

Alternatively, we show in Figure 12 the distribution of gyro-ages of the M35 I sequence stars, calculated using the age-period-color relations of B03 (left panel) and B07 (right panel). The mean gyro-ages of 137 Myr and 161 Myr, are both close to the 150 Myr derived

for the cluster using the isochrone method (see Section 1). Assuming that all I sequence stars are truely coeval, the standard errors of 3.8 Myr and 4.1 Myr give uncertainties on the calculated mean gyro-ages for M35 of 2.8% and 2.5%, close to the formal uncertainty on the least squares fits. The close agreement between the mean gyro-age (137 Myr) and the gyro-age determined from the least square fit (134 Myr), as well as a smaller standard deviation in the gyro-age distribution, suggest that the B03 I sequence isochrone (eq. [2]) provide a better match to the color dependence of stellar rotation on the I sequence than the B07 isochrone (eq. [3]).

In Figure 13 we show the corresponding distribution of gyro-ages calculated using the Kawaler (1989) age-period-color relation. The mean age is equal to that derived for the B07 relation, while the larger σ and standard error (3.3%) reflects primarily a poorer fit to the M35 I sequence for the late F and early G type stars, resulting in gyro-ages that are too low for those stars.

5.4. Improving the I sequence mass-rotation relation using M35

The method of gyro-chronology relies on fitting the I sequence rotational isochrone, with age as a free parameter, to populations of cluster stars or to individual field stars in the color-period plane B07. The functional dependence between stellar color and rotation period of the isochrone will thus directly affect the derived gyro-age, and will, if not accurately determined, introduce a systematic error. It is therefore important to constrain and test the mass-rotation relation for stars on the I sequence as new data of sufficiently high quality becomes available.

Our data for M35 are well suited for such a test because of the rich and well-defined I sequence, the extensive knowledge about cluster membership, and the independent stellar evolution age for the cluster. To constrain the color-period relation, we fit equations [2] and [3] to the M35 I sequence, using the same selection of stars and the same fitting weights as described in Section 5.3. We determine all coefficients in equations [2] and [3] for the fixed cluster age (t) of 150 Myr. The coefficients with 1σ uncertainties are listed in Table 1 and the corresponding rotational isochrones are shown in Figure 14. To illustrate how closely the isochrones trace the selected I sequence stars, Figure 14 also displays a dashed curve representing the moving average of the rotation periods along the I sequence.

We can compare the coefficients derived using the M35 data to those chosen and/or derived by B03 and B07. Our best fit of the B03 isochrone confirms the value of 0.5 for the a coefficient chosen (not fitted) by B03 to best represent the color-period data included in

his study. a is a translational term that determines the color for which the isochrone gives a period of zero days. For the b coefficient our best fit give a value of 0.20 compared to the choice of 0.15 by B03. Our larger value of the b coefficient results in an isochrone with slightly more curvature.

From our best fit of the B07 rotational isochrone to the M35 I sequence, we determined a c coefficient of 0.77, equal to the value used by B07, while our value 0.55 for the f coefficient is smaller than the value of 0.60 used by B07. In the case of the c and f coefficients, B07 also determined their values from least squares fitting to the I sequence stars of several young open clusters. However, for the translational term d, he chose a fixed value of 0.4 to allow for more blue stars to be fitted. We left the d coefficient as a free parameter when fitting to the M35 I sequence, and got a value of 0.47.

The new value of 0.47 for d is particularly interesting as it corresponds to the approximate $B-V$ color for F-type stars at the transition from a radiative to a convective envelope. This transition was noted from observations of stellar rotation (known as the break in the Kraft curve (Kraft 1967)), and is associated with the onset of effective magnetic wind breaking (e.g. Schatzman 1962). The value of 0.47 for the d coefficient therefore suggest that, for M35, the blue (high-mass) end of the I sequence begins at the break in the Kraft curve.

5.5. Prediction: Tidal Evolution is Responsible for the Unusually Slow Rotators

Ten stars fall above the M35 I sequence, and thus rotate unusually slowly in comparison to other members of M35 with similar masses. All 10 stars are photometric members of M35 and 2 are also spectroscopic members. We have no reason to believe that the rotation

Table 1. New coefficients for the I sequence rotational isochrones

Isochrone	Coefficient	Value	1σ error
B03	a	0.507	0.005
B03	b	0.204	0.013
B07	c	0.770	0.014
B07	d	0.472	0.027
B07	f	0.553	0.052

periods for these stars are due to aliases in the power spectra, and we note that a similar pattern is seen in NGC 3532 with 7 stars located above the I sequence B03 and in M34 with 6 stars above the I sequence (Meibom et al. 2008).

What causes the rotational evolution of these stars to deviate significantly from that of most similar-color stars in M35? We propose here that tidal interactions with a close stellar companion has acted to partially or fully synchronize the stellar spins of these stars to the orbital motions, and that such tidal synchronization is responsible for their slower-than-expected rotation. We thus predict that these 10 stars are the primary stars in binaries with periods of ∼10-15 days.

This proposition finds support from the star of M35 located in the color-period diagram at $(B-V)_0 = 0.68$ and $P_{rot} = 10.13$ days. This star is the primary in a circular binary with an orbital period of 10.33 days. The rotation of this star has been synchronized to the orbital motion of the companion (Meibom et al. 2006), forcing it to rotate more slowly than stars of similar mass. In addition to the spectroscopic binary, 3 of the remaining 9 slow rotators are photometric binaries. Spectroscopic observations has begun of those stars and of the remaining 5 stars as of fall 2007 to determine their status as binary or single stars, and in the case of binarity, the degree of tidal evolution.

5.6. Stellar angular momentum evolution near the ZAMS

The trend in Figure 8 of an increasing fraction of C sequence (and gap) stars for younger cluster populations leads naturally to the suggestion that most, if not all, late-type stars pass through a phase of rapid rotation (the C sequence) at the ZAMS. We note that even should this be the case, an *observed* C sequence fraction of 1 is not expected for even the youngest coeval populations, as stars of different masses will reach the ZAMS, and thus hypothetically the C sequence, at different times. For example, late-F stars will be the first to arrive at/on the ZAMS and C sequence, and leave it before the arrival of G and K type stars.

The color-period diagrams for the youngest stellar populations presented in Figure 8 (see also Figure 1 in B03) show that most stars lay either on the C sequence or in the gap. B03 finds only 25% of the stars at 30 Myr to be on the I sequence. In fact the I sequence is not clearly identifiable at this age, and the stars identified as being on the I sequence are early-type rapid rotators near the intersection of the two sequences.

By 30 Myr very few of the cluster members have rotation periods longer than 5 days. This is in marked contrast to fractions of ∼60% and ∼40%, respectively, for such slow rotators in the PMS populations of the Orion Nebula cluster (ONC) and NGC 2264 (see

Herbst et al. 2007). The difference in the numbers of slowly rotating stars pre- and post-ZAMS, suggests that most, if not all, of the stars rotating slowly at ∼1-3 Myr, spin up as they evolve onto the ZAMS. Such spin-up may have been observed. Comparison of the rotation period distributions for stars in the ∼1 Myr ONC and the ∼2-3 Myr NGC 2264 (Herbst et al. 2007, and references therein) shows a spin-up with time by a factor ∼2, presumably due to conservation of angular momentum as the stars contract on the PMS. On the other hand, the distribution of a smaller sample of rotation periods in the ∼2-3 Myr IC 348 (Nordhagen et al. 2006) does not show similar evidence for spin-up when compared to the ONC.

From the point of view of modeling stellar angular momentum evolution, we emphasize the narrowness of the C sequence, with all rotation periods between 0.5 days and 1.5 days. We suggest that the broad distribution of rotation period among solar-like stars in the PMS populations must collapse into a narrow C sequence of similar rotation periods independent of mass. Indeed, we suggest that in the two 30 Myr clusters of B03 (Figure 1), the gap stars with $(B-V)_0 \gtrsim 0.9$ may in fact be evolving *toward* the C sequence, and point out that in the 50 Myr clusters in B03, mostly C sequence stars are observed redward of $(B-V)_0 \simeq 0.9$.

6. SUMMARY AND CONCLUSIONS

We present the results of an extensive time-series photometric survey over ∼5 months of late-type members in the 150 Myr open cluster M35 (NGC 2168). We have obtained photometric light curves for 14022 stars with $12 \lesssim V \lesssim 19.5$ over a $40' \times 40'$ field centered on M35. We have determined the rotation periods for 441 stars. Cluster membership and binarity for stars with rotation periods are determined from the results of a decade long spectroscopic survey in M35. Of the 441 rotators 310 stars are radial-velocity and/or photometric members of M35.

With an age slightly older than the Pleiades but with a much larger population of late-type stars, M35 is particularly interesting for studying stellar rotational evolution during this active phase of angular momentum evolution between the ZAMS and the age of the Hyades. The rotation periods of the 310 late-type members span over two orders of magnitude from 0.1 day ($\gtrsim$ 50% of their breakup velocities), up to ∼15 days. A drop-off in the period distribution is found at ∼10 days, well below the upper limit of our period search. The ∼10-day cutoff may represent a physical upper limit on the rotation-period distribution at 150 Myr. However, it is also possible that detecting more slowly rotating stars in M35 will require higher photometric precision or higher resolution spectroscopic observations.

We find in the phased light curves for almost all stars with measured rotation peri-

ods that the long-baseline (∼5 months), low-frequency (1/night) photometric measurements match the short-baseline (16 nights), high-frequency (∼ 1/hours) measurements in both phase, shape, and amplitude. Further tests on a subset of stars show that the same rotation periods are derived from the short- and long-term data to within 1%. This stability in the modulation of the stellar brightness suggest a similar stability in the configuration, size, and number of starspots.

In the color-period plane, the 310 M35 rotators reveal striking dependencies between surface rotation period and stellar color (mass). More than 75% of the stars lay along two distinct sequences in the color-period diagram, apparently representing two different states in their rotational evolution. Similar sequences were identified by Barnes (2003) for stars in other clusters. Comparison between M35 and these clusters of the locations of the sequences in color-period diagram, as well as the relative numbers of stars on each, support for the idea (proposed by Barnes (2003)) that stars evolve from one sequence (C) to the other sequence (I) at a rate that is inversely proportional to the stellar mass.

We determine from the M35 color-period diagram that the characteristic exponential timescale for rotational evolution off the C sequence and onto the I sequence is ∼60 Myr and ∼140 Myr for G and K dwarfs, respectively. These timescales may offer valuable constraints on the rates of internal and external angular momentum transport and on the evolution rates of stellar dynamos in late-type stars of different masses.

From the emerging trend (supported by M35) of an increasing relative fraction of rapidly rotating C sequence stars with decreasing population age, we propose the hypothesis that most, if not all, late-type stars pass through a phase of rapid rotation (C sequence) on the ZAMS. By conjecture, there may not be a need for a direct connection between slowly rotating stars observed in the early PMS and slowly rotating stars at ∼100 Myr post the ZAMS. Such a connection has often been assumed and set as a constraint on models of stellar angular momentum evolution, motivating the introduction of mechanisms to prevent slowly rotating PMS stars from spinning up as they evolve onto the main-sequence.

By comparison with measured rotation periods in the Hyades, we put to the test the empirical Skumanich $\sqrt{t}$ time-dependence on the stellar rotation period for G dwarfs. By reducing the Hyades rotation periods by a factor $\sqrt{Age_{Hyades}/Age_{M35}}$ we find that the $\sqrt{t}$ law accounts very well for the rotational evolution of G dwarfs between M35 and the Hyades, whereas among the K dwarfs the $\sqrt{t}$ time-dependence predicts a spin-down rate that is faster than observed between M35 and the Hyades.

We find that the heuristic rotational isochrones proposed by Barnes (2003) and Barnes (2007) match the location of M35 I and C sequences using the independently determined

stellar evolution isochrone age for M35. A non-linear least-squares fit of the rotational isochrones to the M35 I sequence sets the cluster's gyro-age to 134 Myr with a formal 1σ uncertainty of 3 Myr. We use the age-period-color relations by Barnes (2003), Barnes (2007), and Kawaler (1989), to calculate the distributions of gyro-ages for the M35 I sequence stars. The mean gyro-ages have standard errors of order 3% and agree well with the $\sim$150 Myr age derived for the cluster using the isochrone method. These results suggest that a well-populated color-period diagram, cleaned for non-members, in combination with rotational isochrones, can provide a precise age estimate that is consistent with the age derived from isochrone fitting in the CMD. We also use the M35 I sequence to improve the coefficients for the color-dependence of the rotational isochrones.

Finally, to explain the ten M35 stars rotating with rates that are unusually slow compared to similar stars in the cluster, we propose that tidal synchronization in binary stars with orbital periods of order 10-15 days is responsible. Two of the 10 stars have already been found to be primary stars in tidally evolved spectroscopic binaries, while 3 other stars are photometric binaries. Accordingly, we predict that the remaining stars are also primary stars in spectroscopic binaries with orbital periods of $\sim$10-15 days.

We wish to thank the University of Wisconsin - Madison Astronomy Department and NOAO for the time granted on the WIYN 0.9m and 3.5m telescopes. We express our appreciation to the site managers and support staff at both telescopes for their exceptional and friendly support. We are thankful to all observers in the WIYN 0.9m consortium who provided us with high-quality data through the queue-scheduled observing program. This work has been supported by NSF grant AST-0406615 to the UW-Madison, a Ph.D fellowship from the Danish Research Academy to S.M., partial support to S.M. from the Kepler mission via NASA Cooperative Agreement NCC2-1390, and by the Cottrell Scholarship from the Research Corporation to K.G.S.

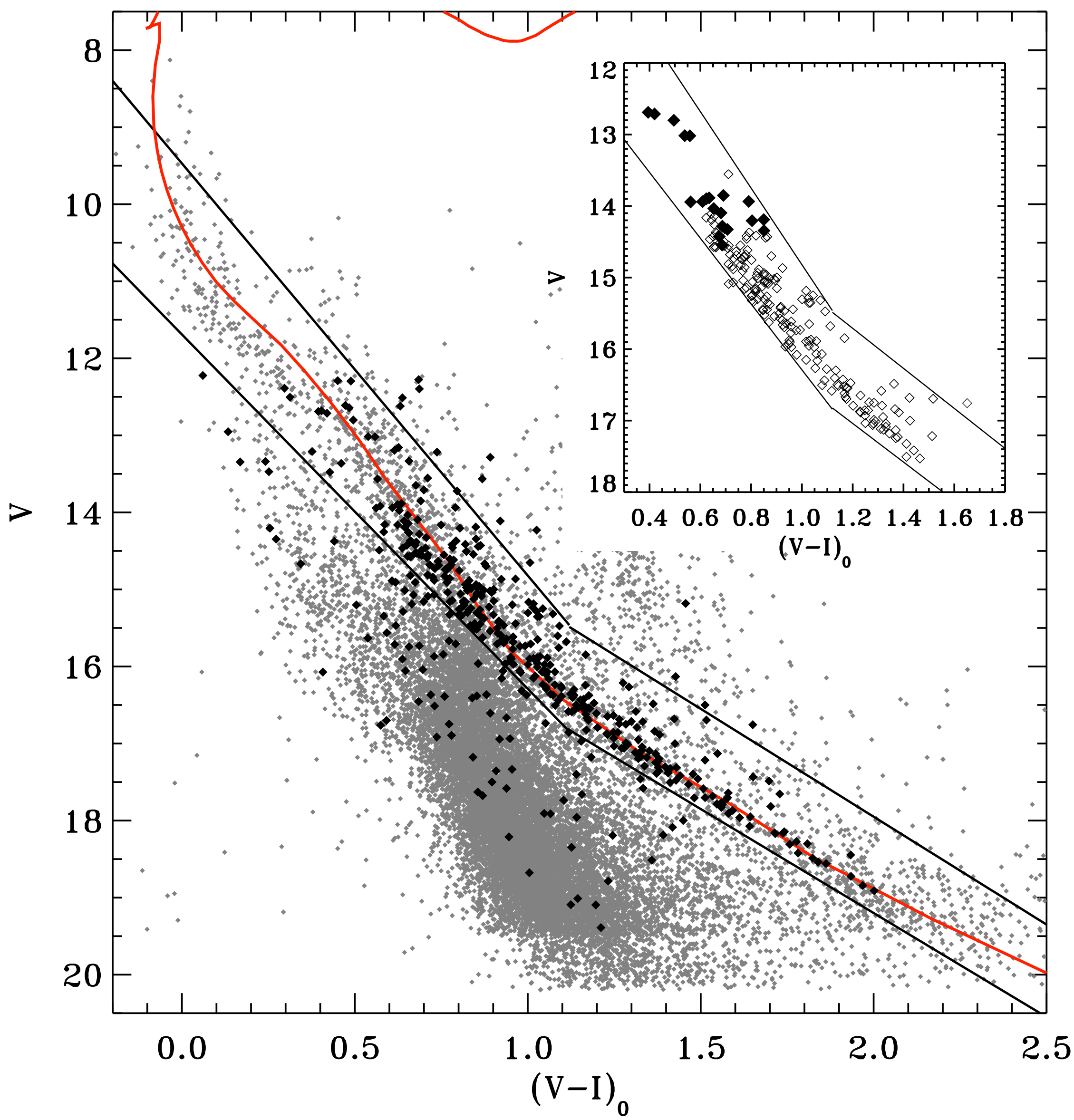

Fig. 5.— The M35 $(V - I)_0$ vs. V color-magnitude diagram. Photometry was provided by Deliyannis (2008). The 441 stars with rotation periods are highlighted in black. Stars located between the solid lines are considered photometric members of M35. Note that the faint limits for proper-motion and radial-velocity surveys are $V \simeq 14.5$ and $V \simeq 17.5$, respectively. The insert shows the location of stars that are radial-velocity members (open symbols), and radial-velocity and proper-motion members (filled symbols). These kinematic members of M35 were used to define the boundaries for photometric membership. The isochrone shown represents a 150 Myr Yale model (Yi et al. 2003).

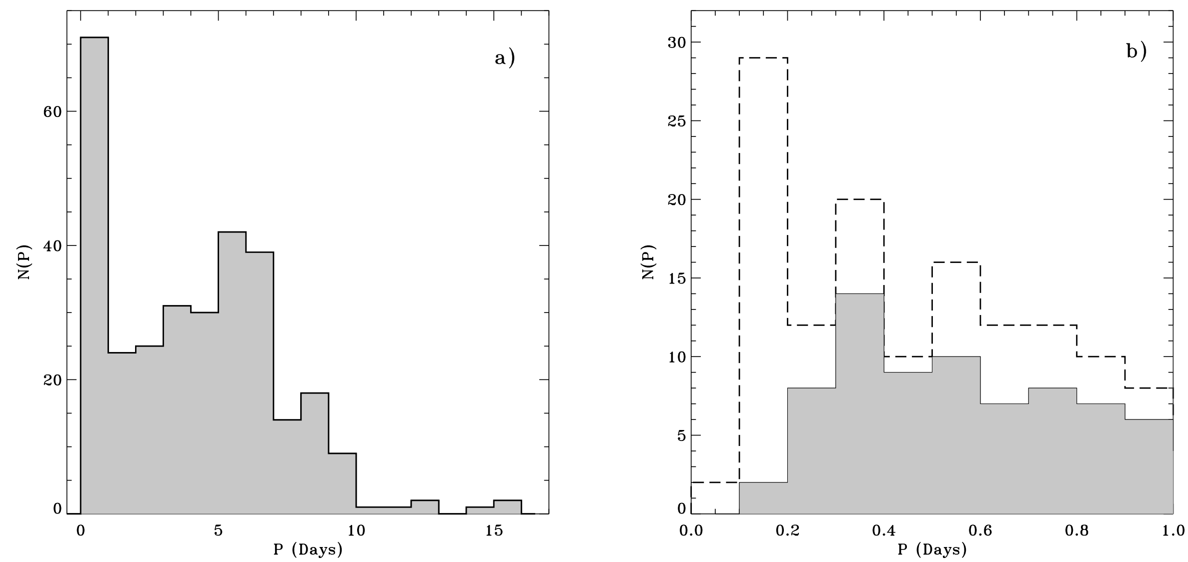

Fig. 6.— **a)** The distribution of rotation periods for the sample of 310 cluster members with masses from $\sim 0.6 - 1.4\ M_{\odot}$ (spectral type late K to mid F). The distribution show a large dispersion from ∼0.1 days to ∼15 days, and a distinct peak at ≤ 1 day and a shallower and broader peak centered at ∼6 days. **b)** The distribution of rotation periods shortward of 1 day binned in 0.1 day bins. The dashed line histogram represents member as well as non-member stars with measured rotation periods in our sample. The grey histogram represents only members of M35.

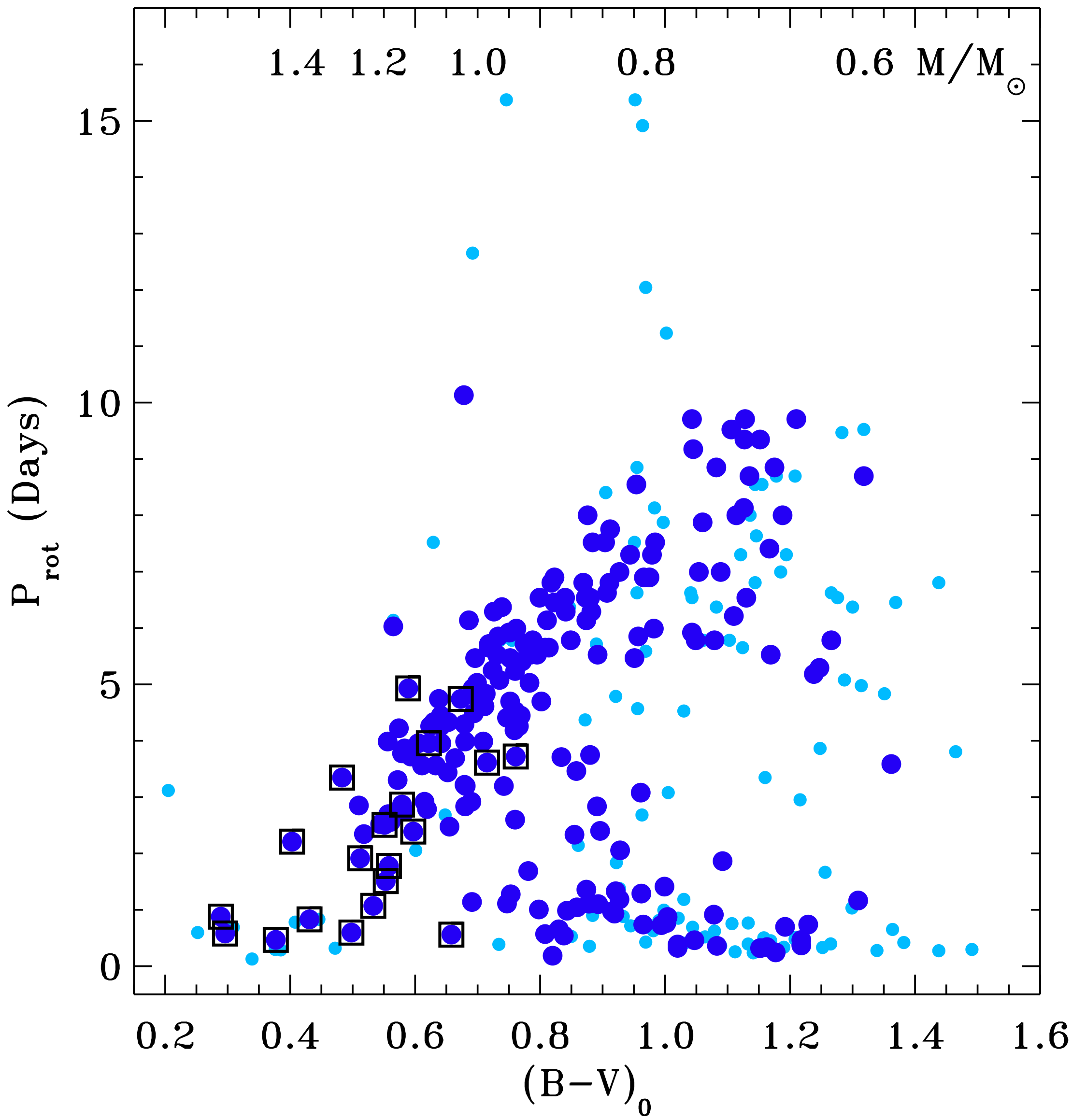

Fig. 7.— The distribution of stellar rotation periods with (B-V) color index for 310 members of M35. Dark blue symbols represent stars that are both photometric and radial-velocity members of M35. Light blue symbols are used for stars that are photometric members only. Proper-motion members are marked with additional squares. The upper x-axis gives a stellar mass estimate corresponding to the color on the lower axis. Masses are derived using a 150 Myr Yale isochrone.

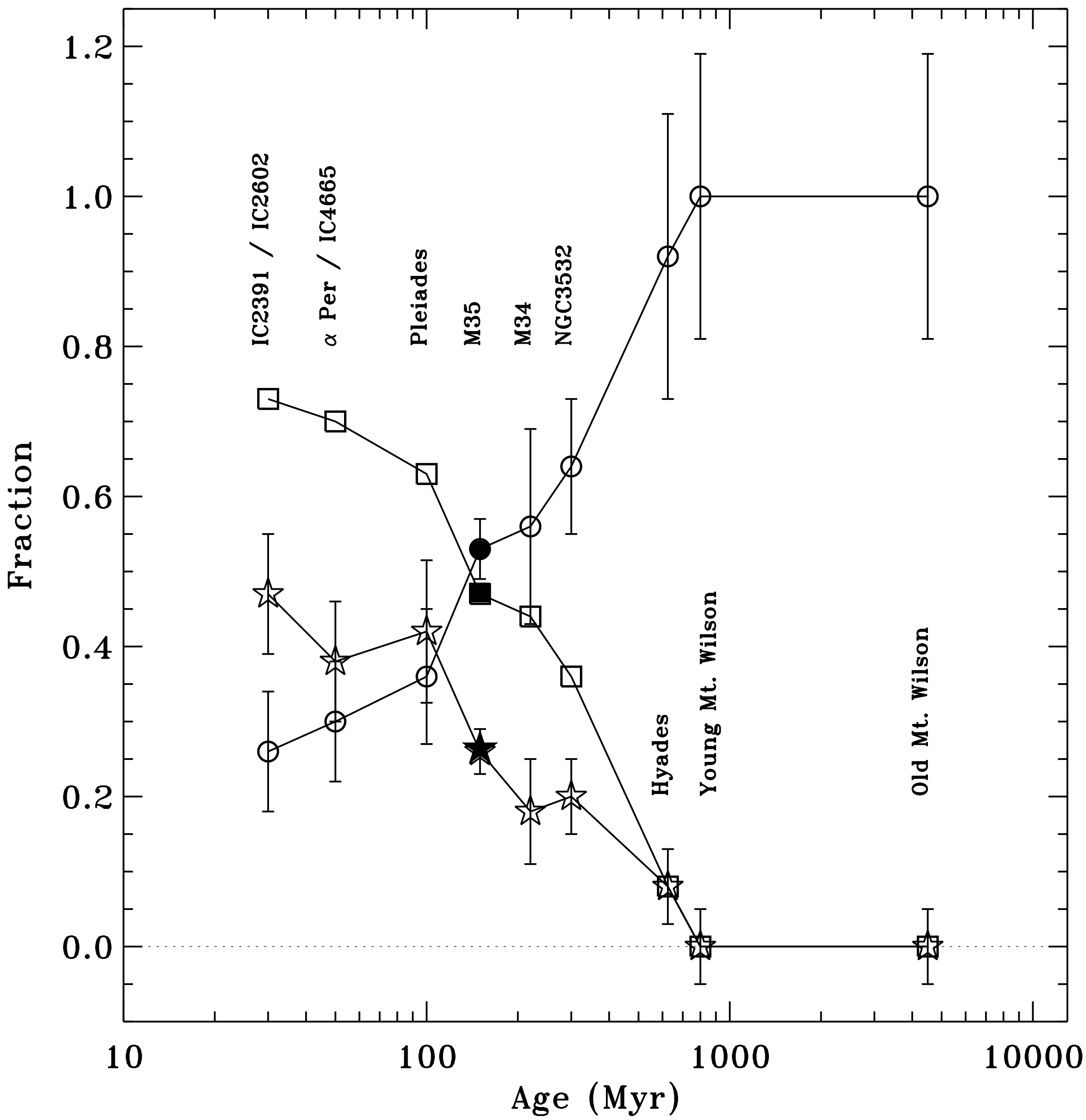

Fig. 8.— Figure 3 from B03 with M35 added. The figure shows the fractions of stars with $0.5 \leq (B-V)_0 \leq 1.5$ on the I sequence (circles) and the C sequence (stars) for clusters of different ages. The squares represent the relative fraction of the sum of C sequence and gap stars. The filled symbols show the relative fractions for M35. We follow B03 in estimating the uncertainties in the fractions by the square root of the number of stars.

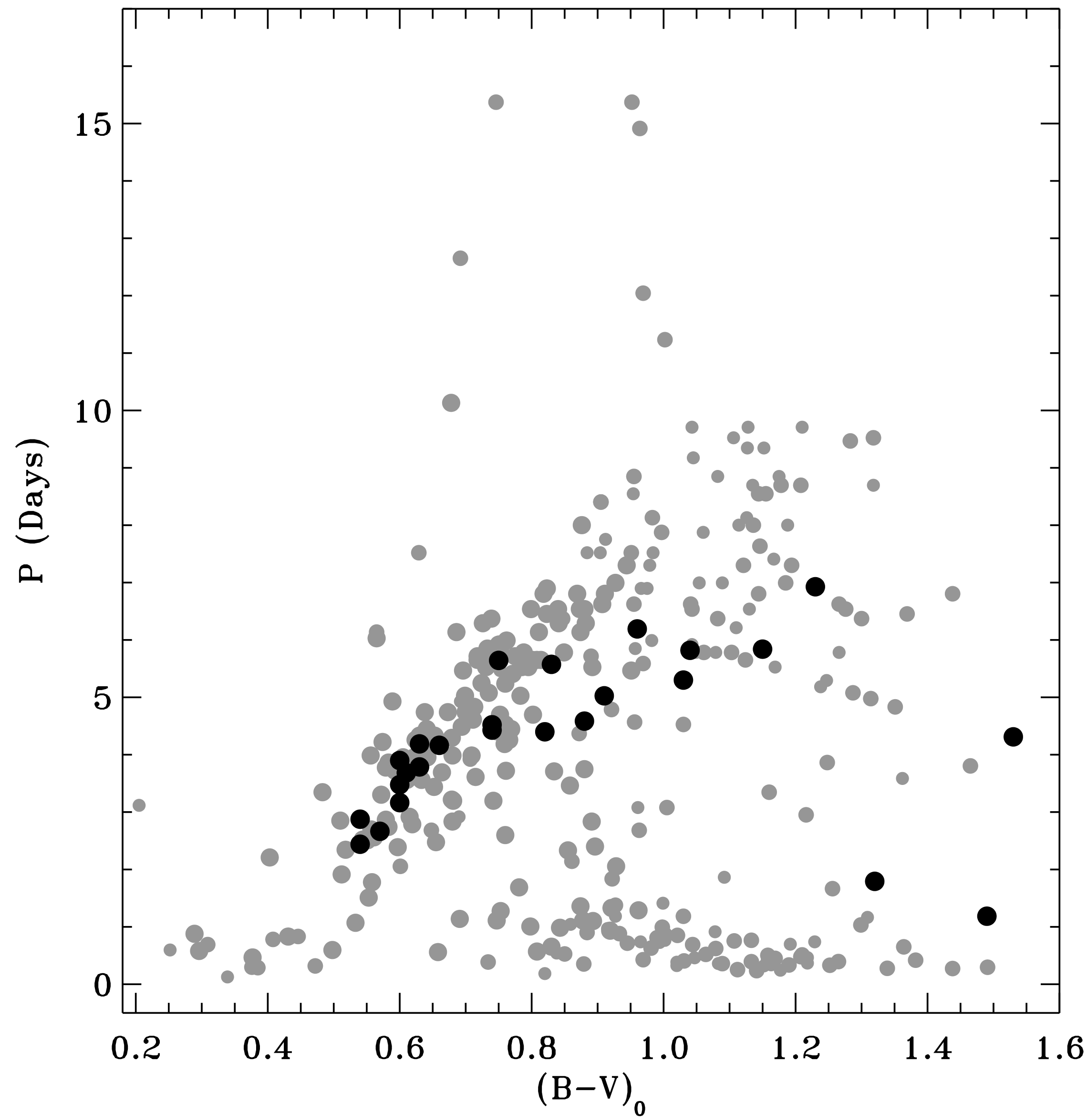

Fig. 9.— The M35 color-period diagram (grey symbols) with 25 Hyades stars overplotted (black; Radick et al. 1987; Prosser et al. 1995). All but the 3 reddest Hyades stars fall on a sequence similar to the M35 I sequence. All Hyades rotation periods were spun-up by a factor $\sqrt{625/150} \simeq 2$ in accordance with the Skumanich $\sqrt{t}$ time-dependence on stellar rotation evolution, assuming ages of 625 Myr and 150 Myr for the Hyades and M35, respectively.

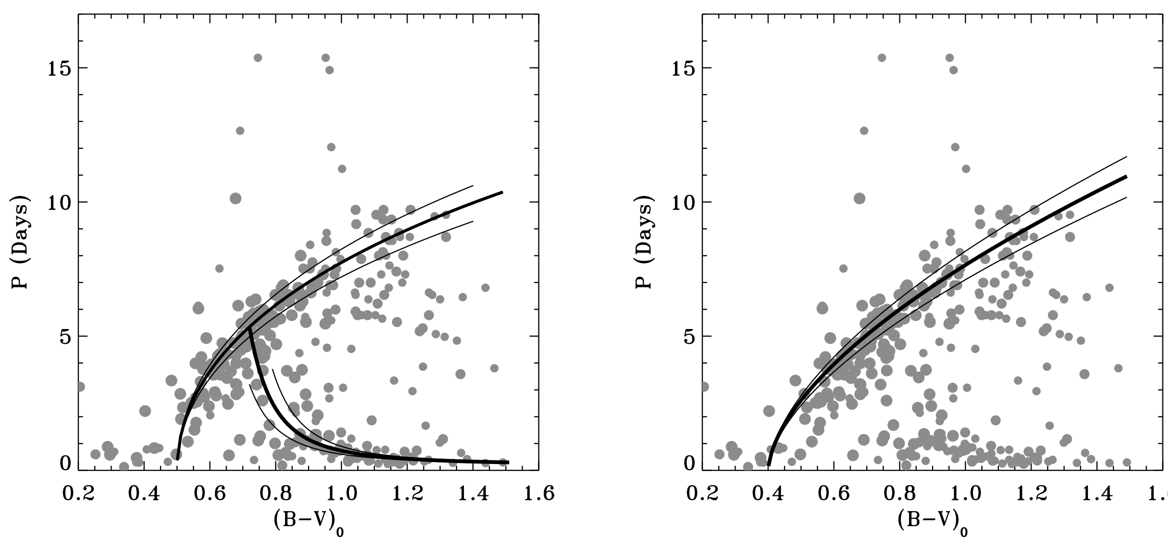

Fig. 10.— The M35 color-period diagram with the 150 Myr rotational isochrones from B03 (left) and B07 (right) overplotted as a thick black solid curves. To illustrate the sensitivity to age we show the 130 Myr and the 170 Myr isochrones as thinner curves flanking the 150 Myr isochrones.

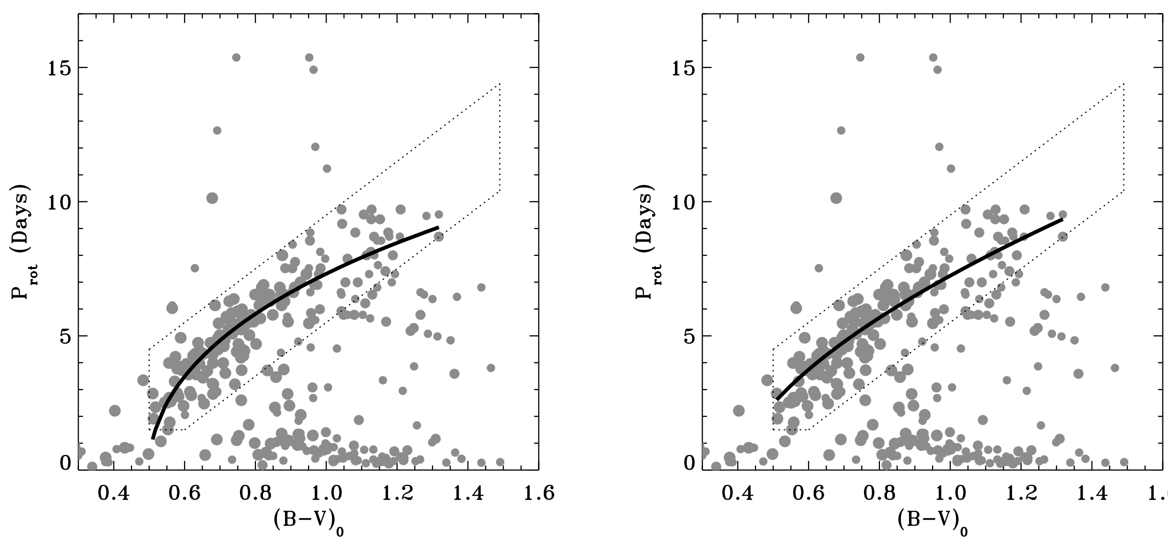

Fig. 11.— The least squares fit of the B03 I sequence isochrone (left; eq. [2]) and the B07 I sequence isochrone (right; eq. [3]) to the M35 I sequence with age (t) as a free parameter. The gyro-ages corresponding to the fits are 133.9 ± 3Myr and 133.5 ± 3Myr, respectively. The I sequence stars to which the isochrones were fitted are enclosed by the dotted lines in both figures.

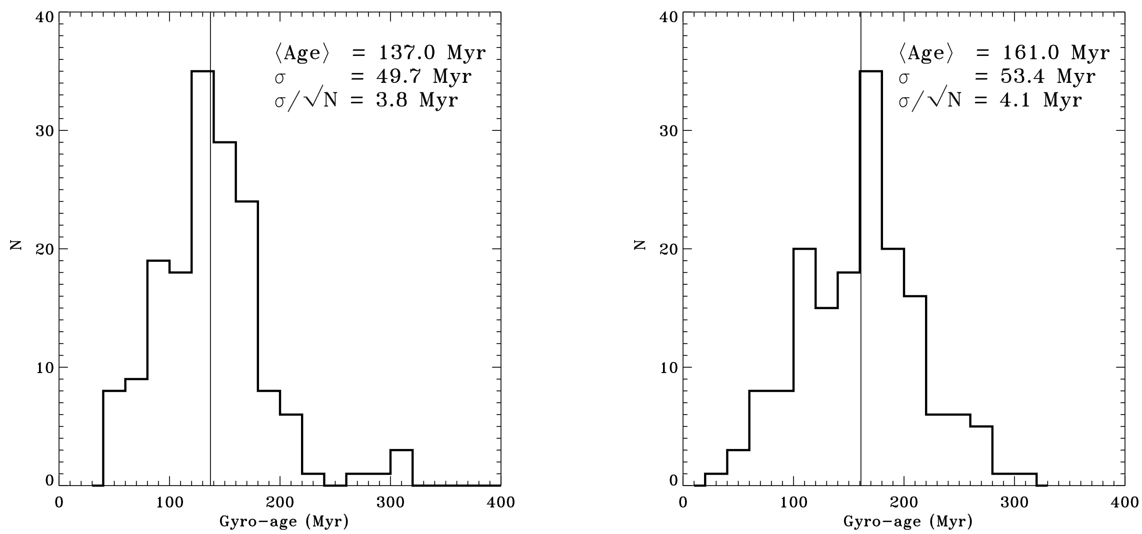

Fig. 12.— The distribution of gyro-ages for M35 I sequence stars. The panels show the distributions of M35 gyro-ages calculated using the B03 (left panel) and B07 (right panel) age-rotation-color relations. The distribution mean, standard deviation, and standard error on the mean, are given in the upper right corner of each panel.

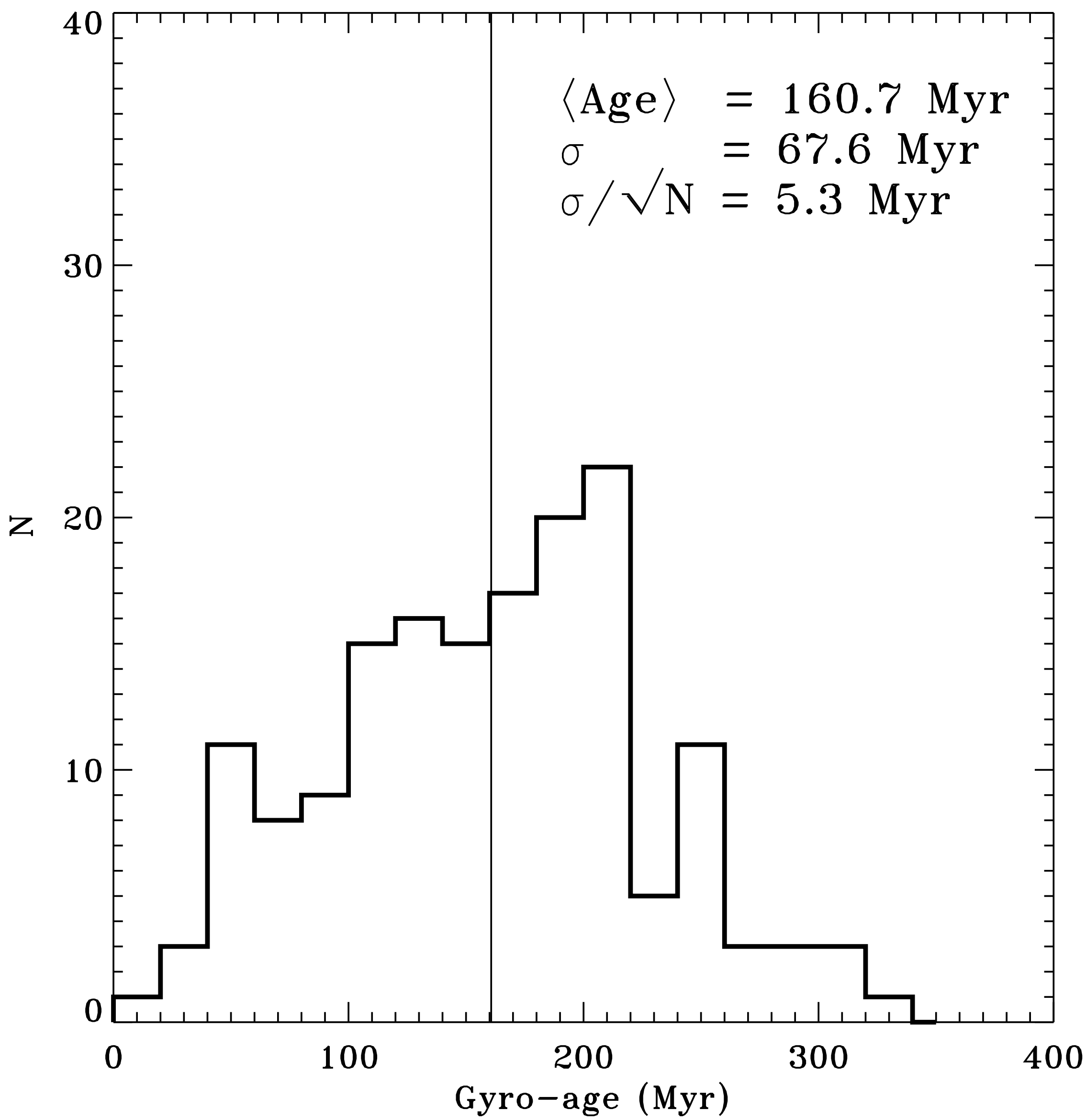

Fig. 13.— The distribution of gyro-ages for M35 I sequence stars calculated using the Kawaler (1989) age-rotation-color relation. The distribution mean, standard deviation, and standard error on the mean, are given in the upper right corner of each panel.

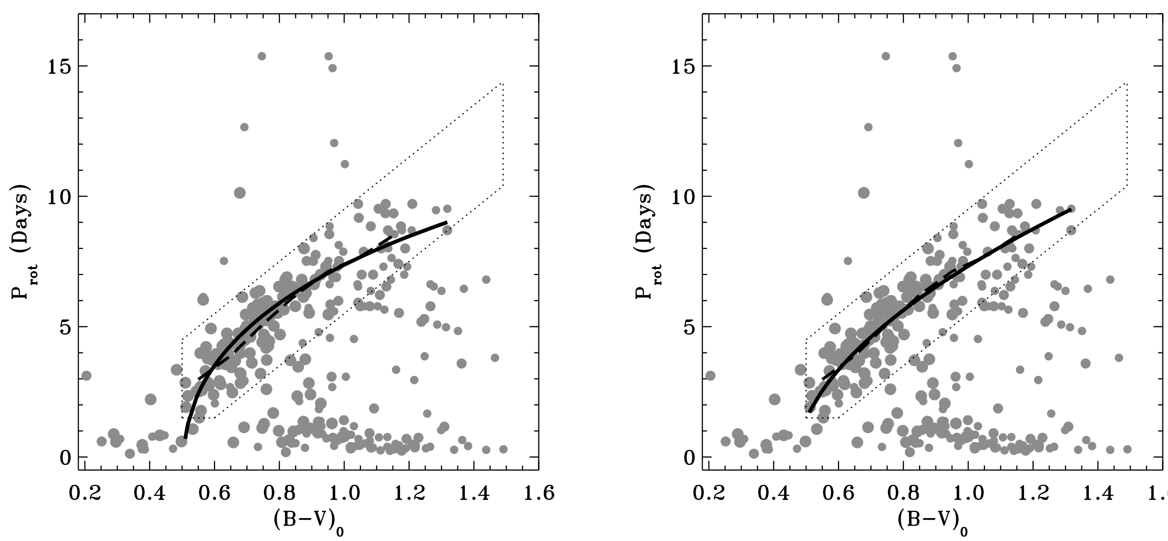

Fig. 14.— The least squares fits (solid curves) of 150 Myr B03 (left) and B07 (right) I sequence isochrones (eq. [2] and eq. [3]) to the M35 I sequence. The corresponding new values for the isochrone coefficients a, b, c, d, and f were determined from the fits and are listed in Table 1. The moving average of the rotation periods for the I sequence stars is also shown as a dashed curve for comparison.

A. PHASED LIGHT CURVES

This appendix presents the light curves for the stars in the field of M35 for which we measured rotation periods. In the printed journal, Figure 15 below show examples of our light curves and light curve plots. Phased light curves for all 441 stars can be found in the electronic edition of the Journal. The light curves have been divided into 3 groups according to the amplitude of the photometric variation. For each group the light curves are sorted by the rotation period and are presented with the same δV range on the ordinate. The group of stars with the largest photometric variability are shown first.

For each star we plot the data from the high-frequency survey (December 2002) as black symbols and data from the low-frequency survey (October 2002 through March 2003) as grey symbols. A running ID number corresponding to the ID number in Table 1 Appendix B is given in the upper left hand corner in each plot. The period to which the data are phased (the rotation period listed in Table 1 as P_{rot}) is given in the upper right corner. The 2-5 letter code in the lower right corner informs about the stars membership status. The codes have the following meaning: Photometric Member (PM; described in Section 2.5), Photometric Non-Member (PNM), Photometric and Spectroscopic Member (PSM), Photometric and Proper-motion Member (PPM), and Photometric Member but Spectroscopic Non-Member (PMSNM). For each star a horizontal grey line in each plot mark $\delta V = 0.0$ and a vertical grey line marks a phase of 1.0.

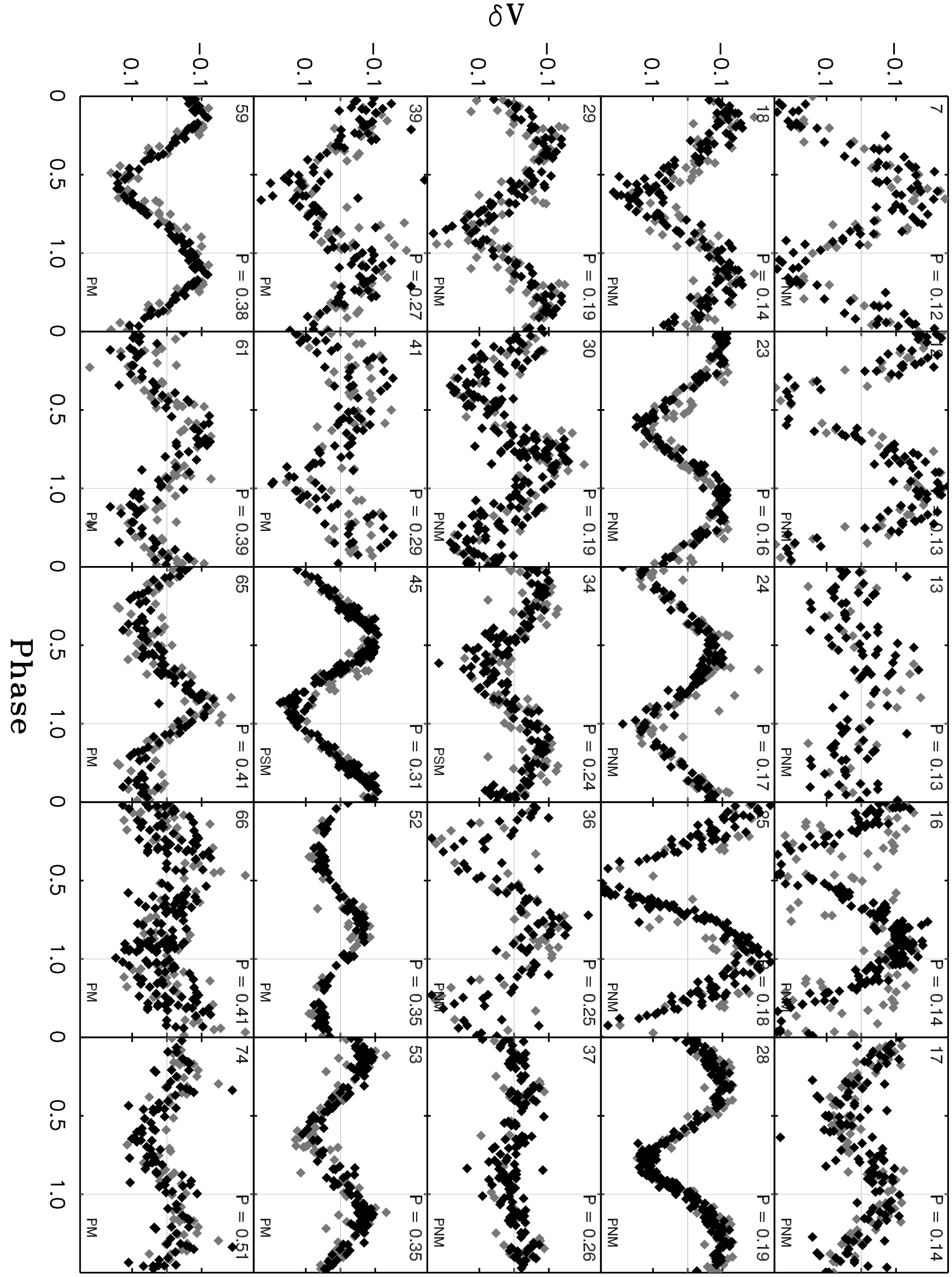

Fig. 15.— Phased light curves for stars with measured rotation periods.

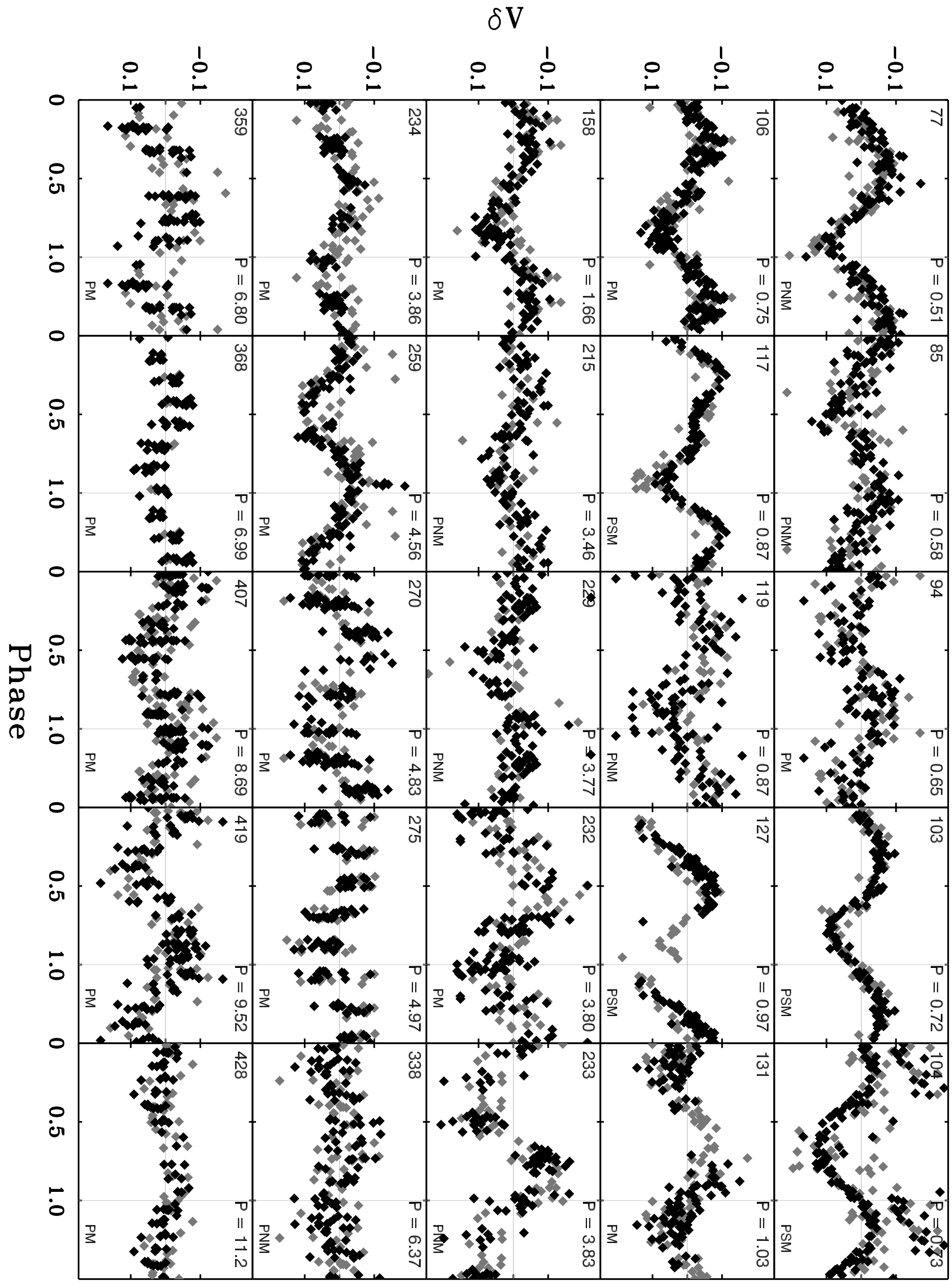

Fig. 14. — Continued.

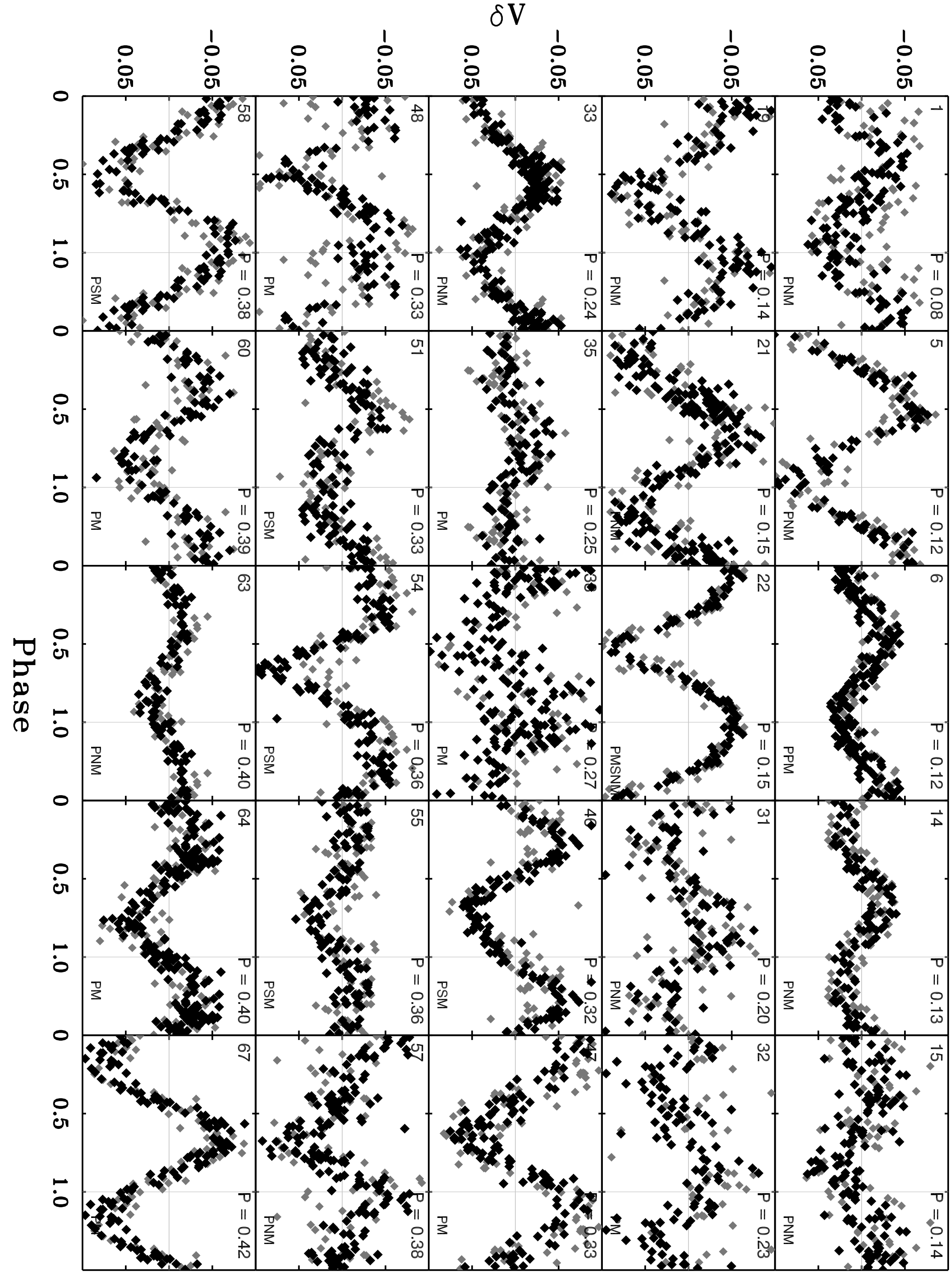

Fig. 14. — Continued.

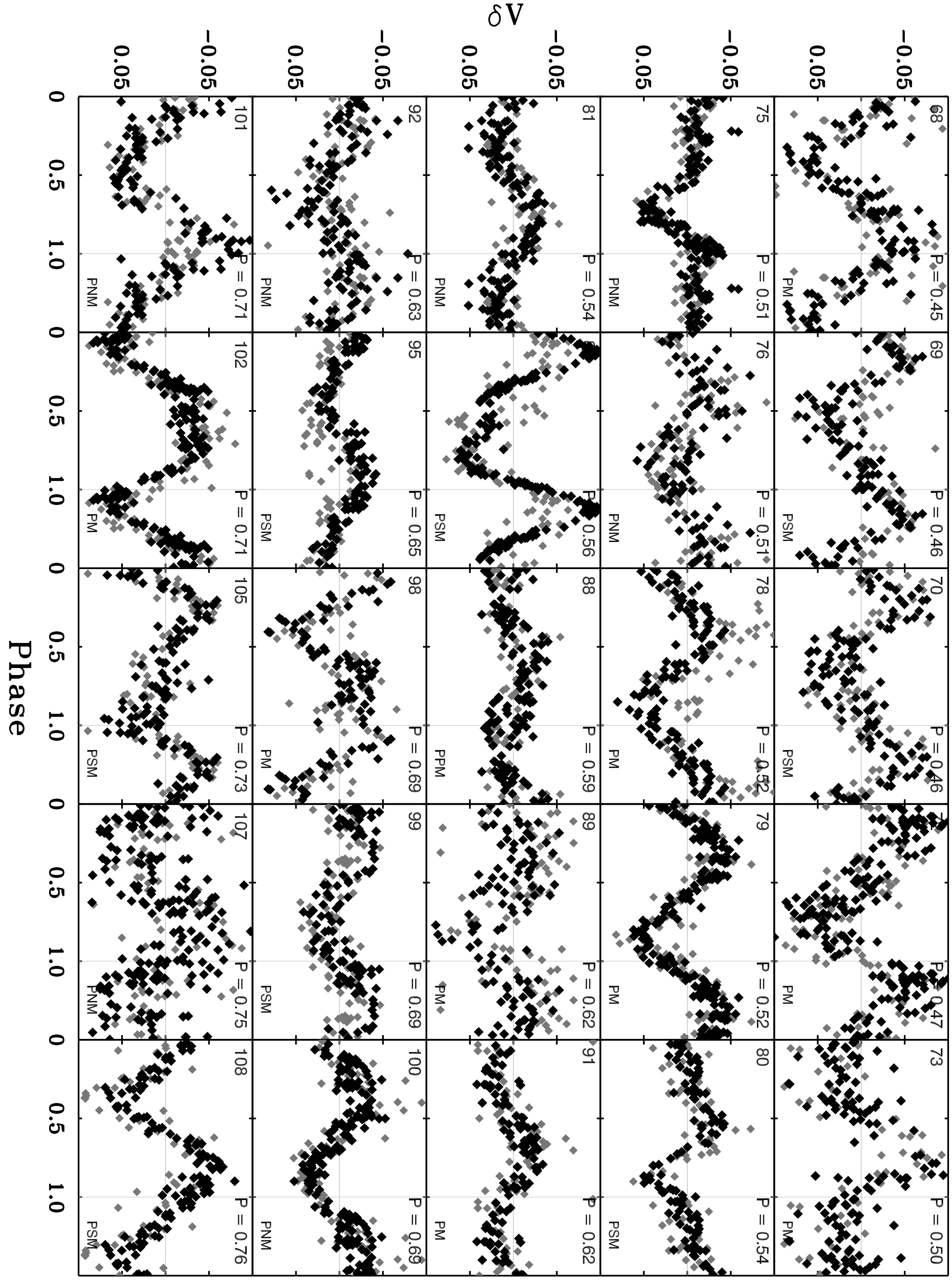

Fig. 14. — Continued.

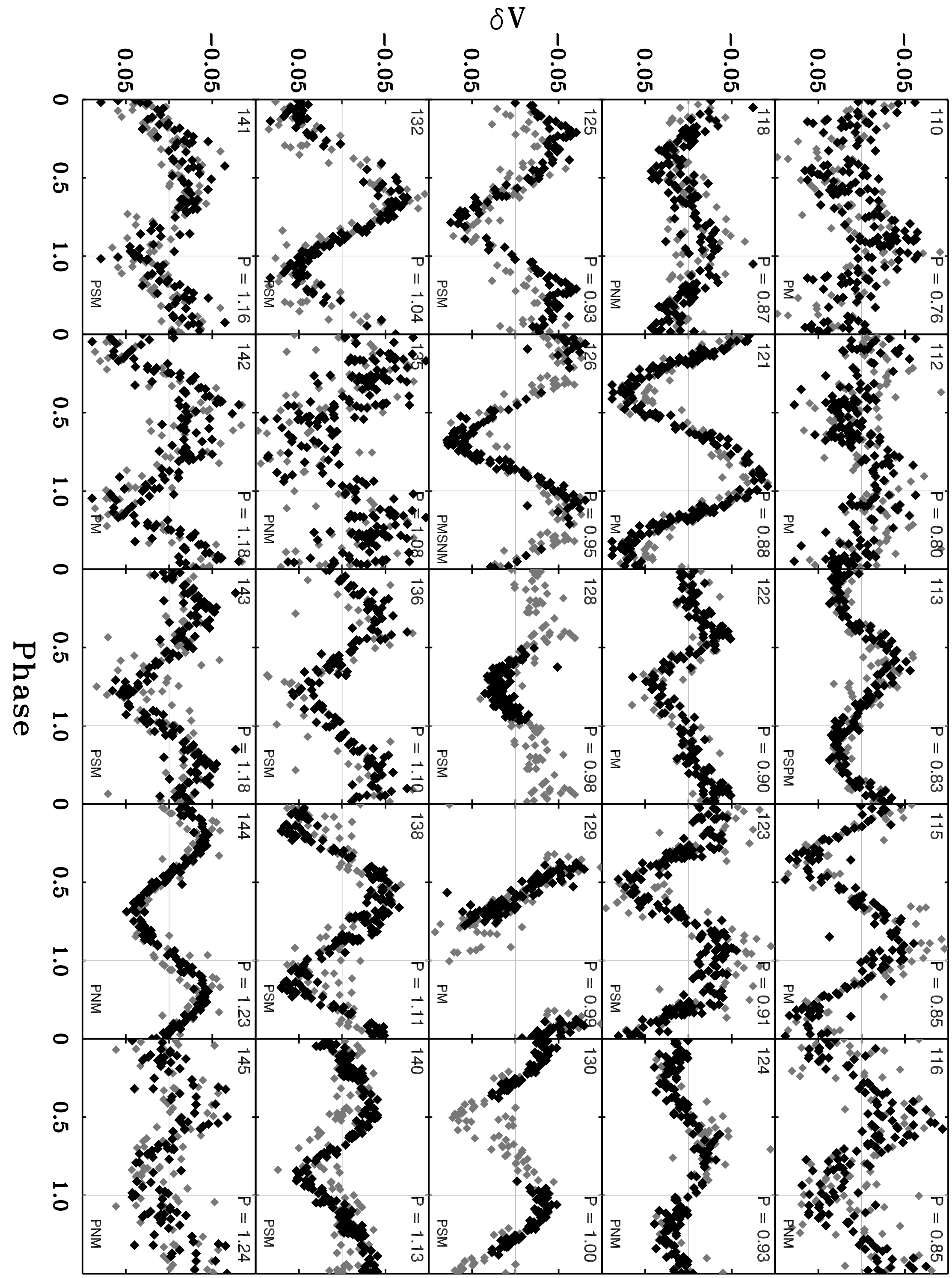

Fig. 14. — Continued.

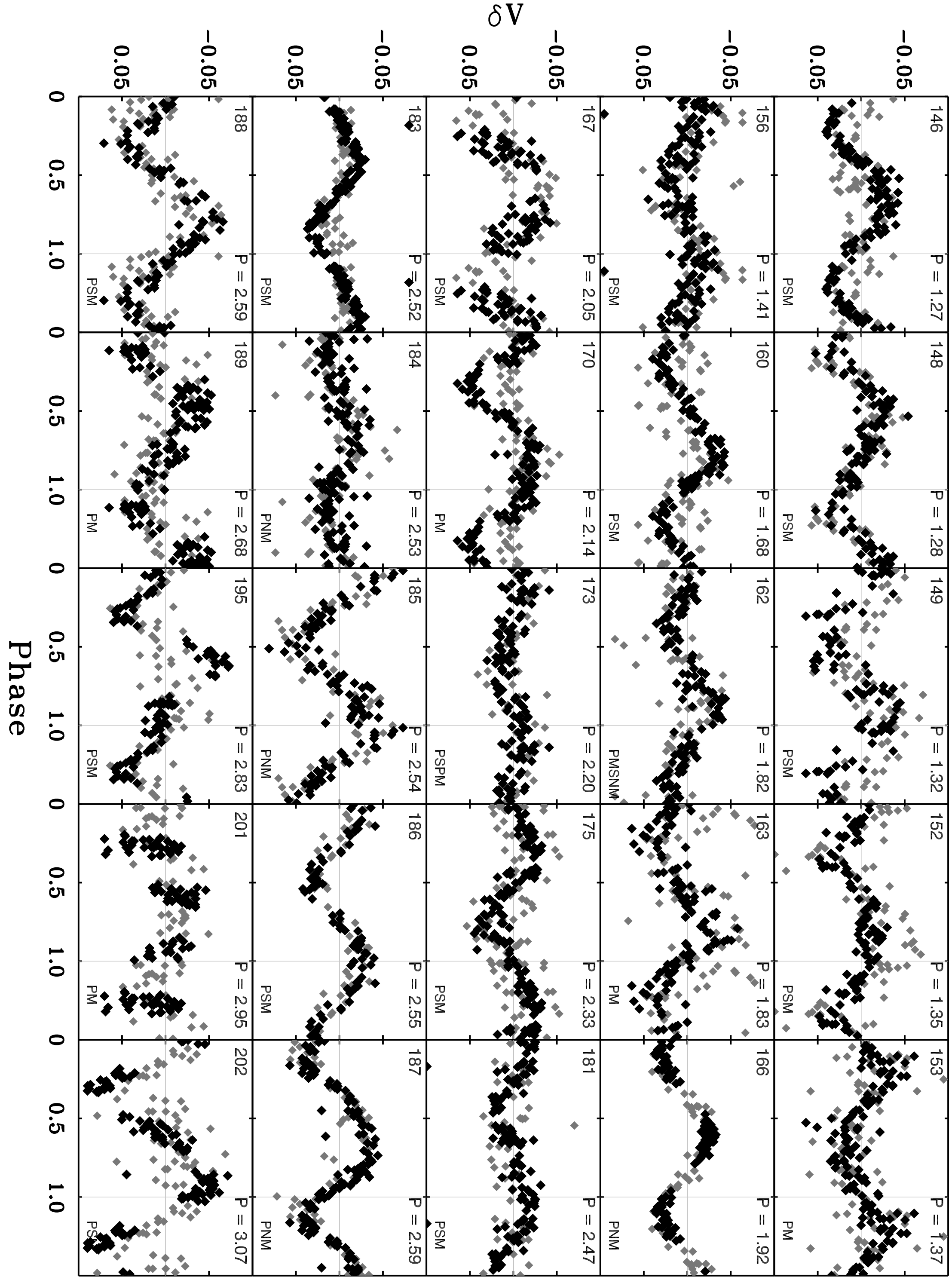

Fig. 14. — Continued.

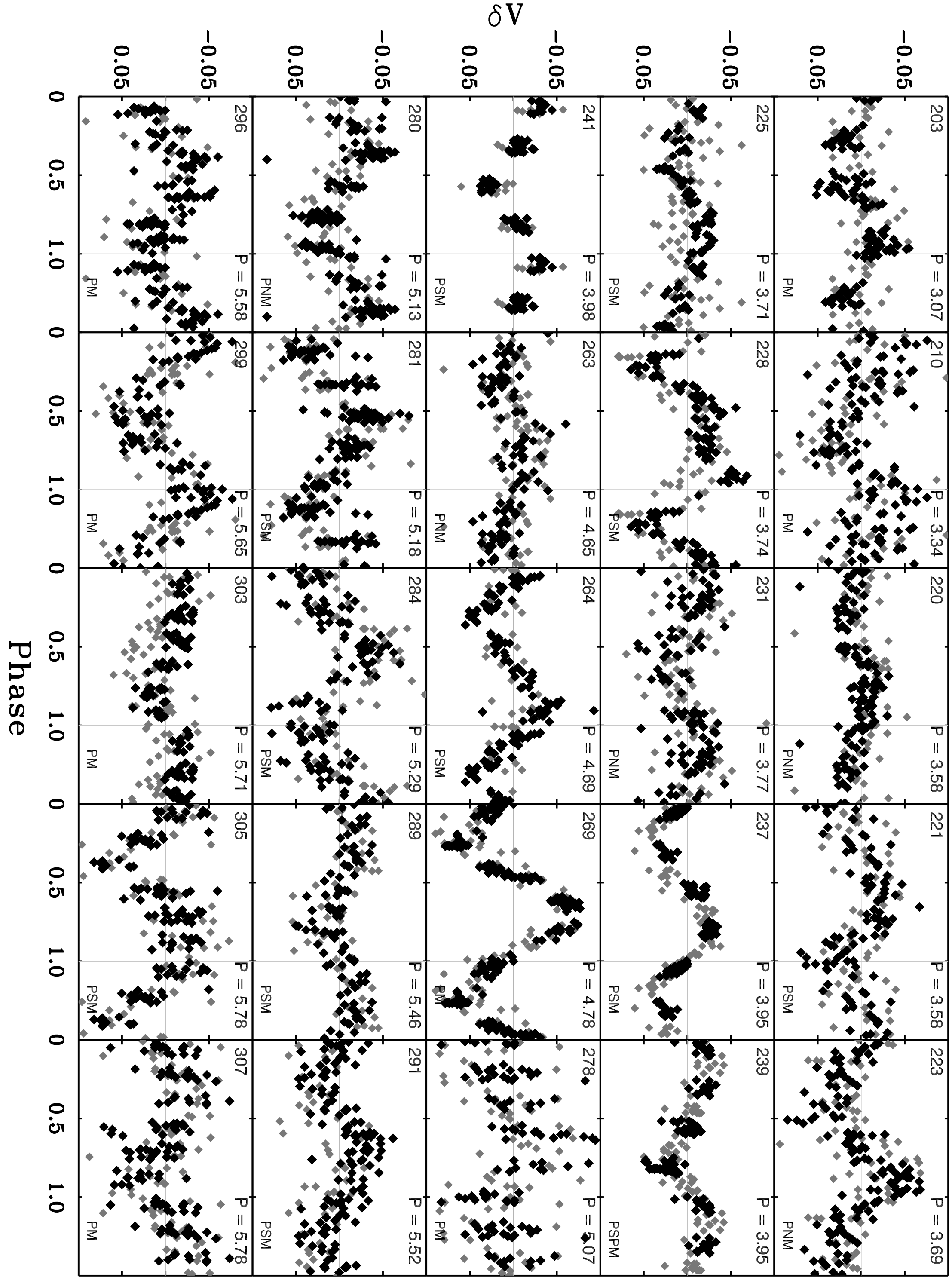

Fig. 14. — Continued.

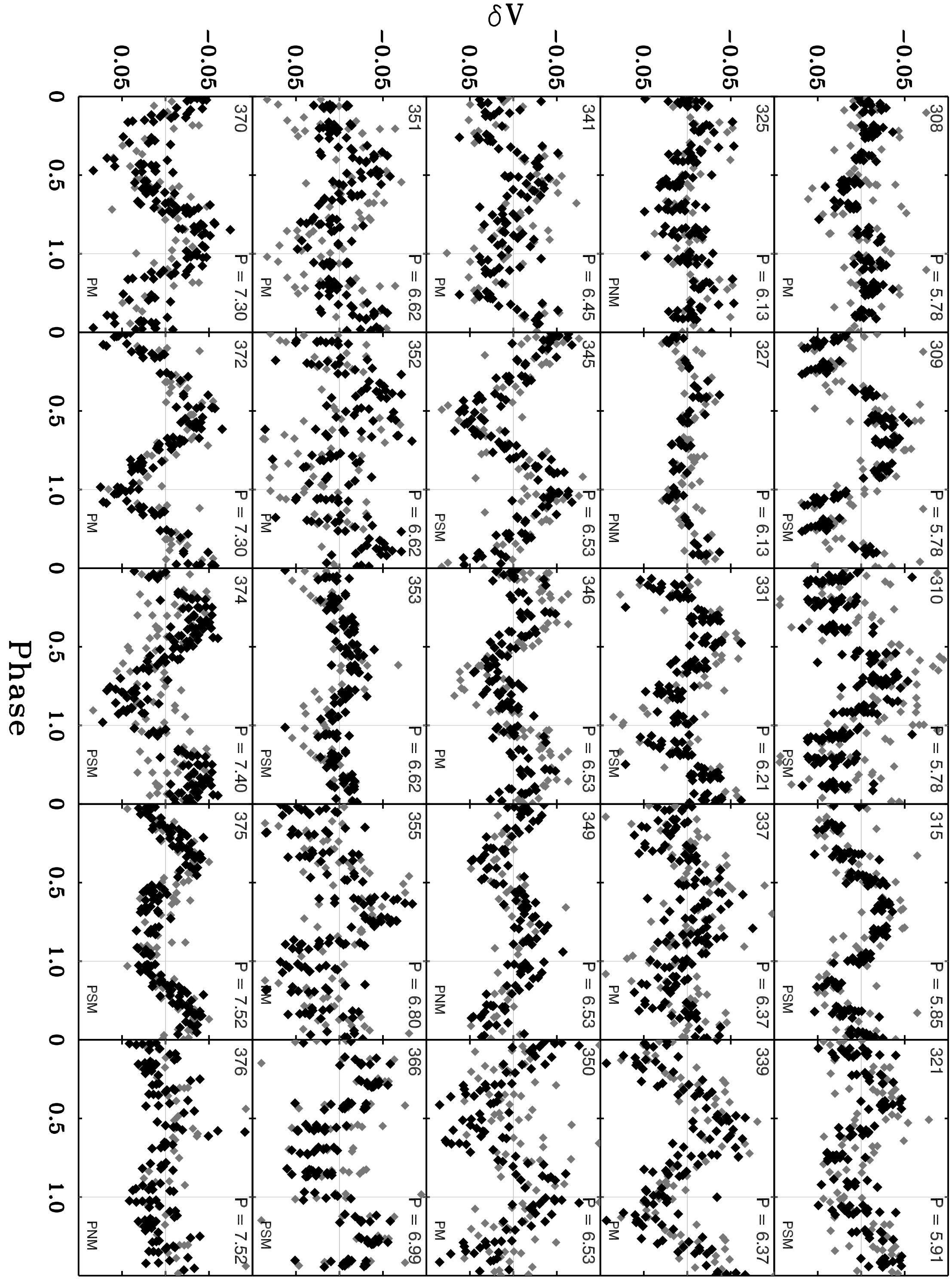

Fig. 14. — Continued.

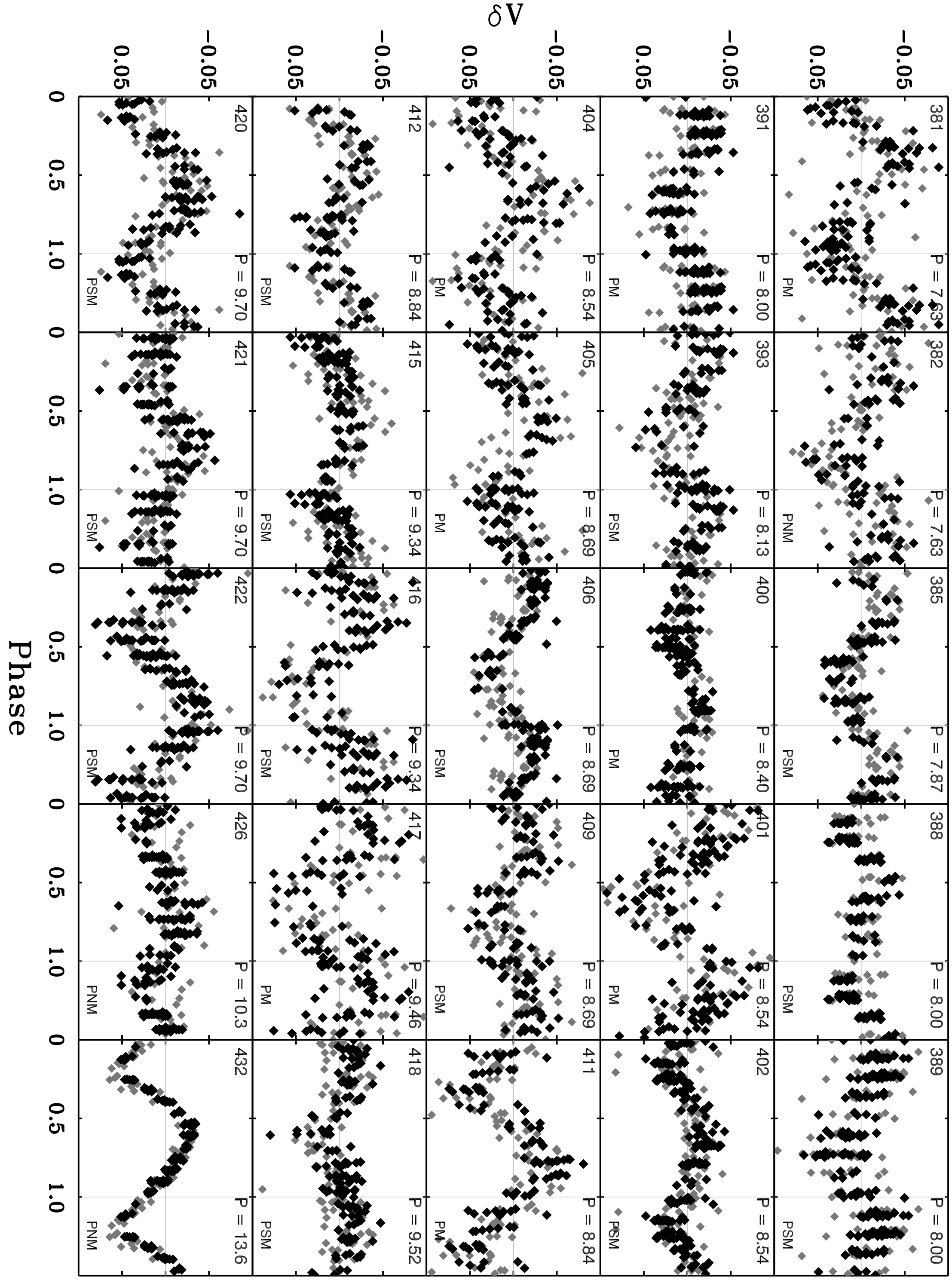

Fig. 14. — Continued.

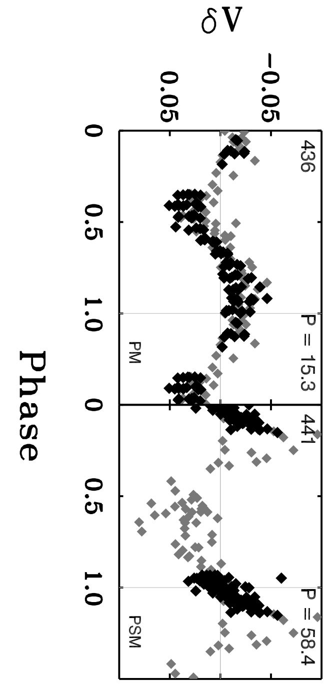

Fig. 14. — Continued.

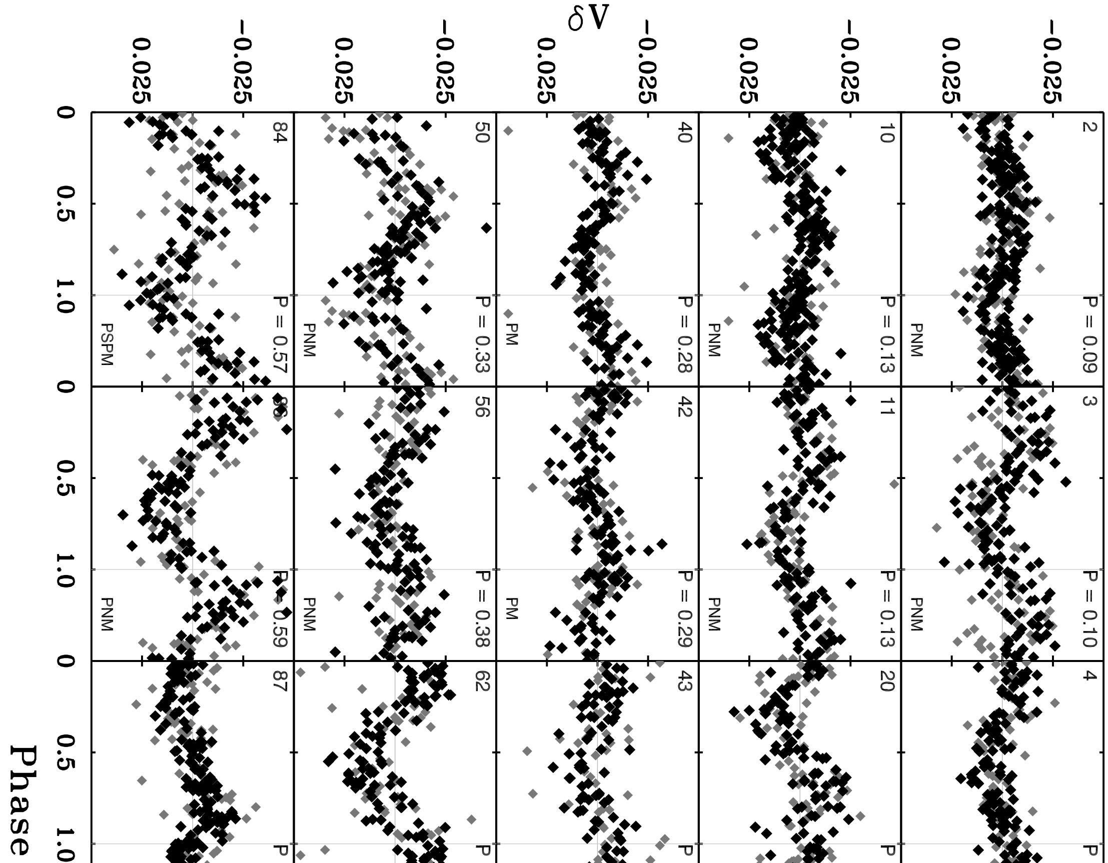

Fig. 14. — Continued.

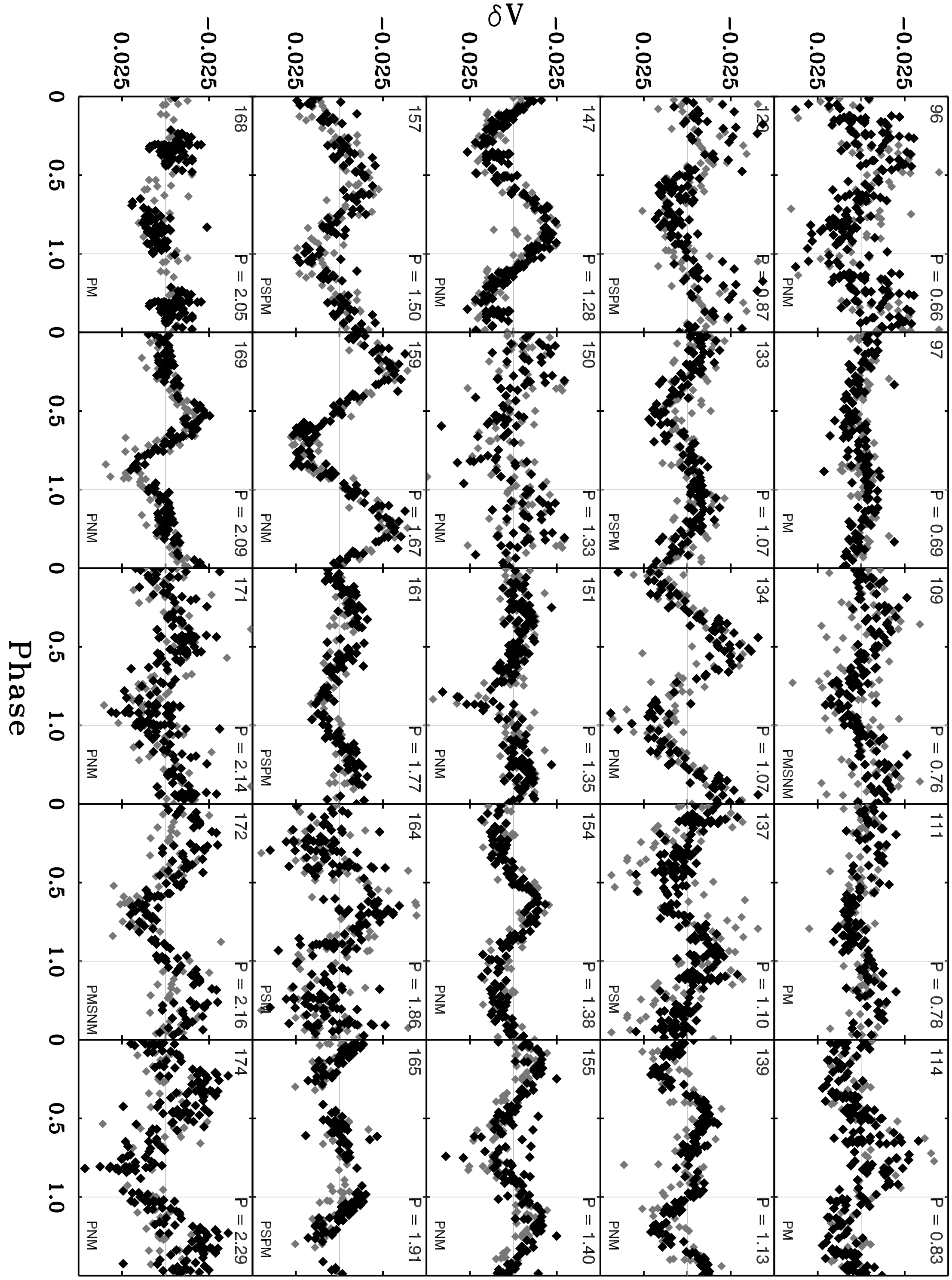

Fig. 14. — Continued.

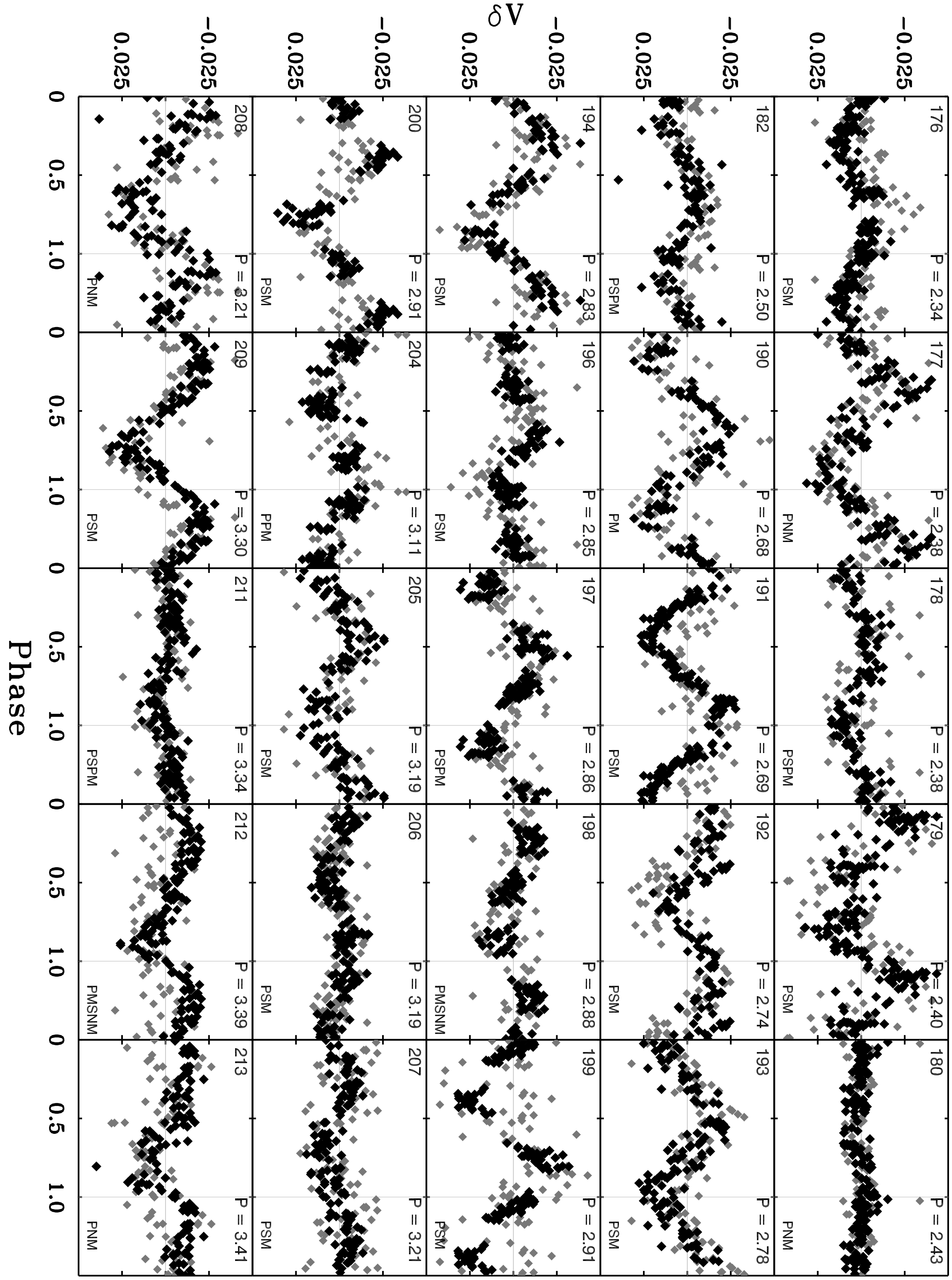

Fig. 14. — Continued.

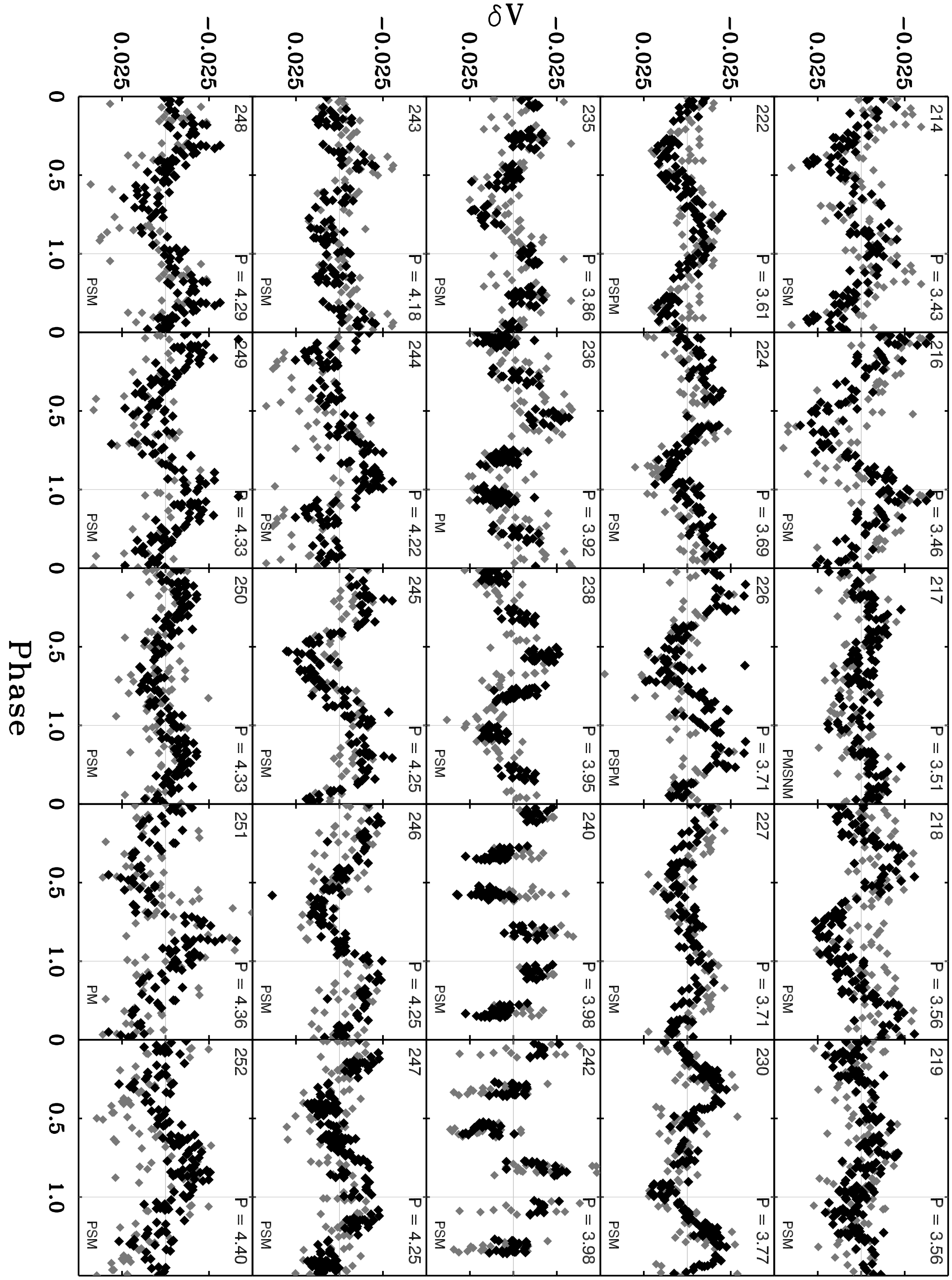

Fig. 14. — Continued.

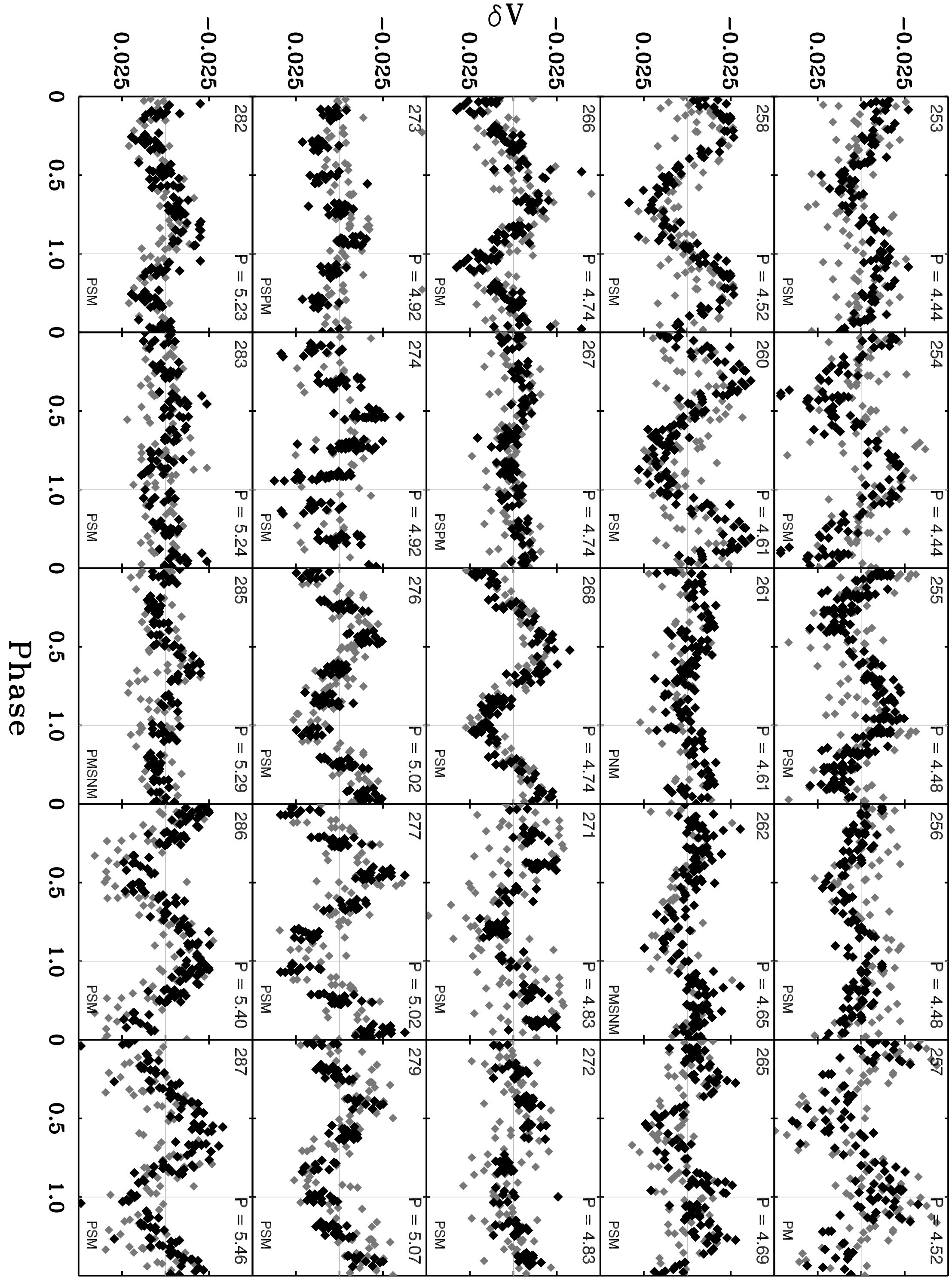

Fig. 14. — Continued.

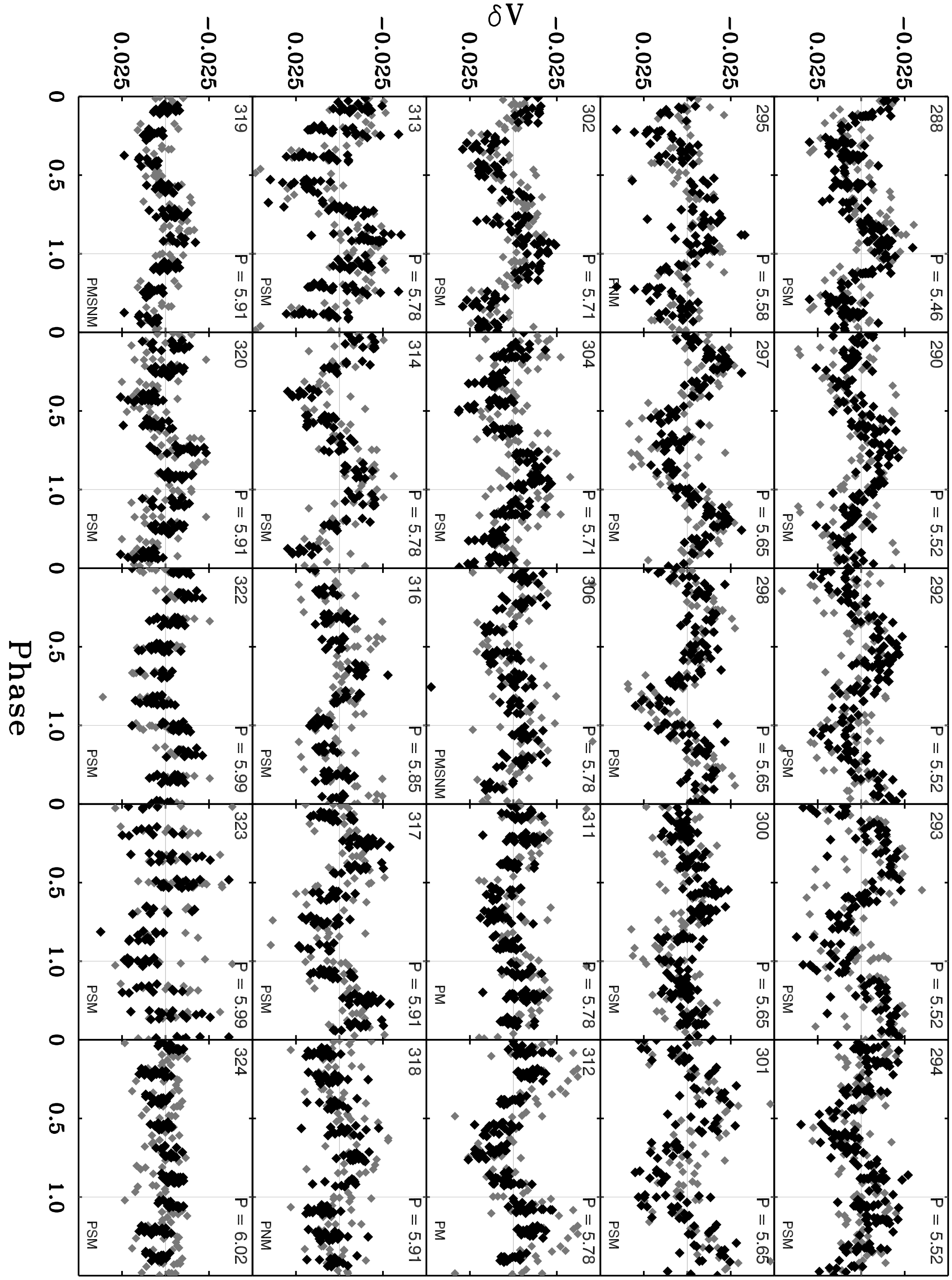

Fig. 14. — Continued.

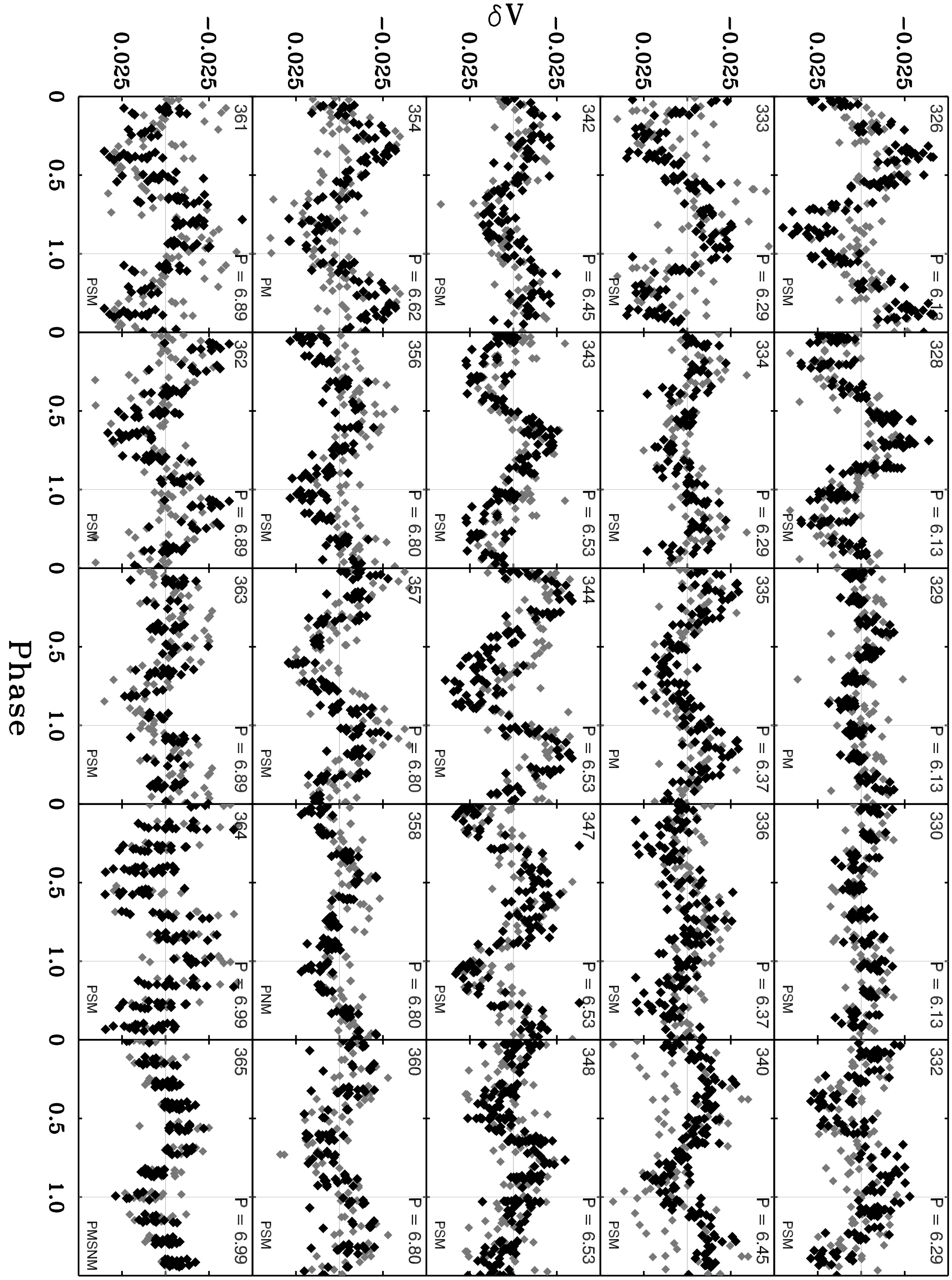

Fig. 14. — Continued.

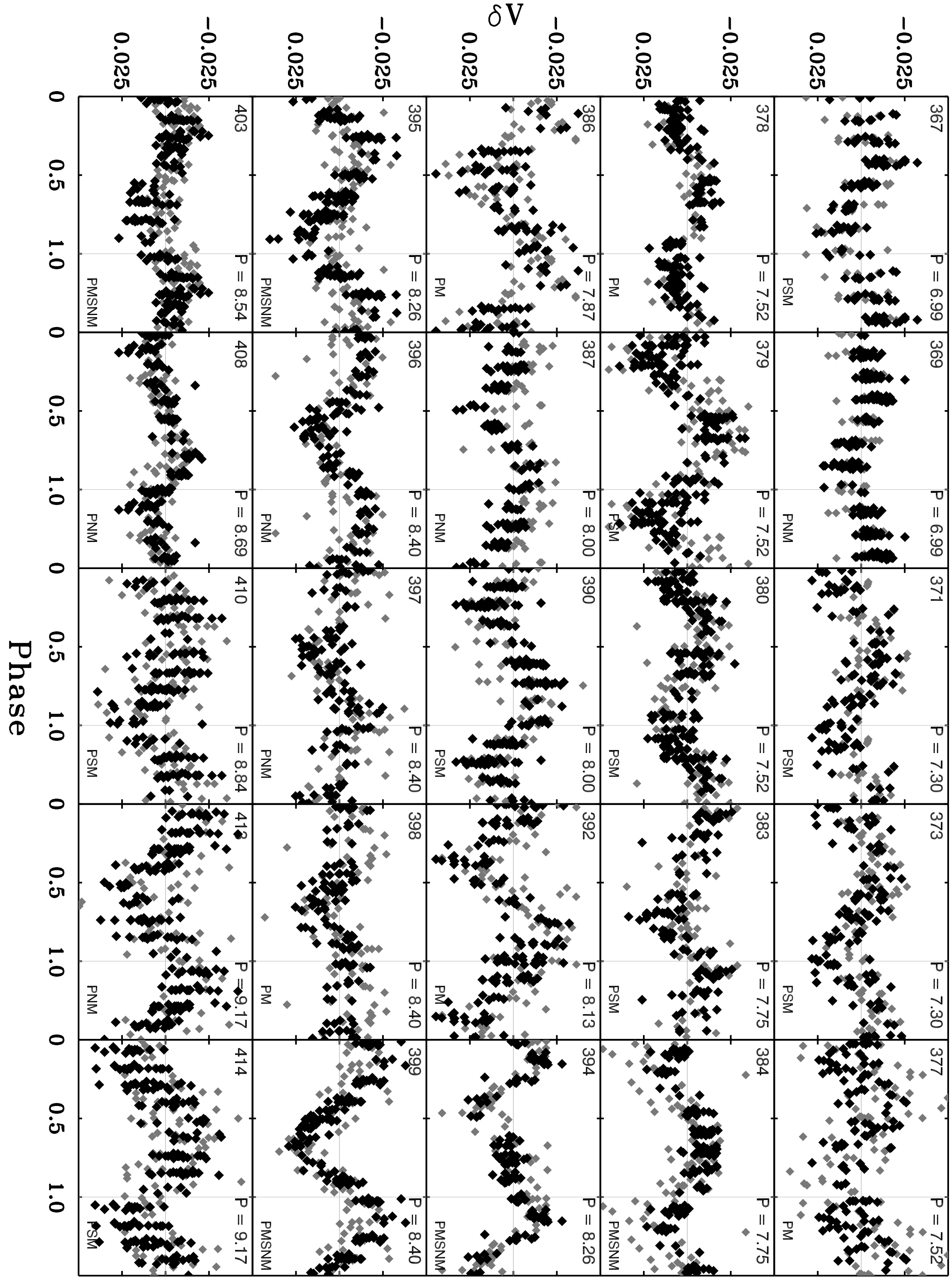

Fig. 14. — Continued.

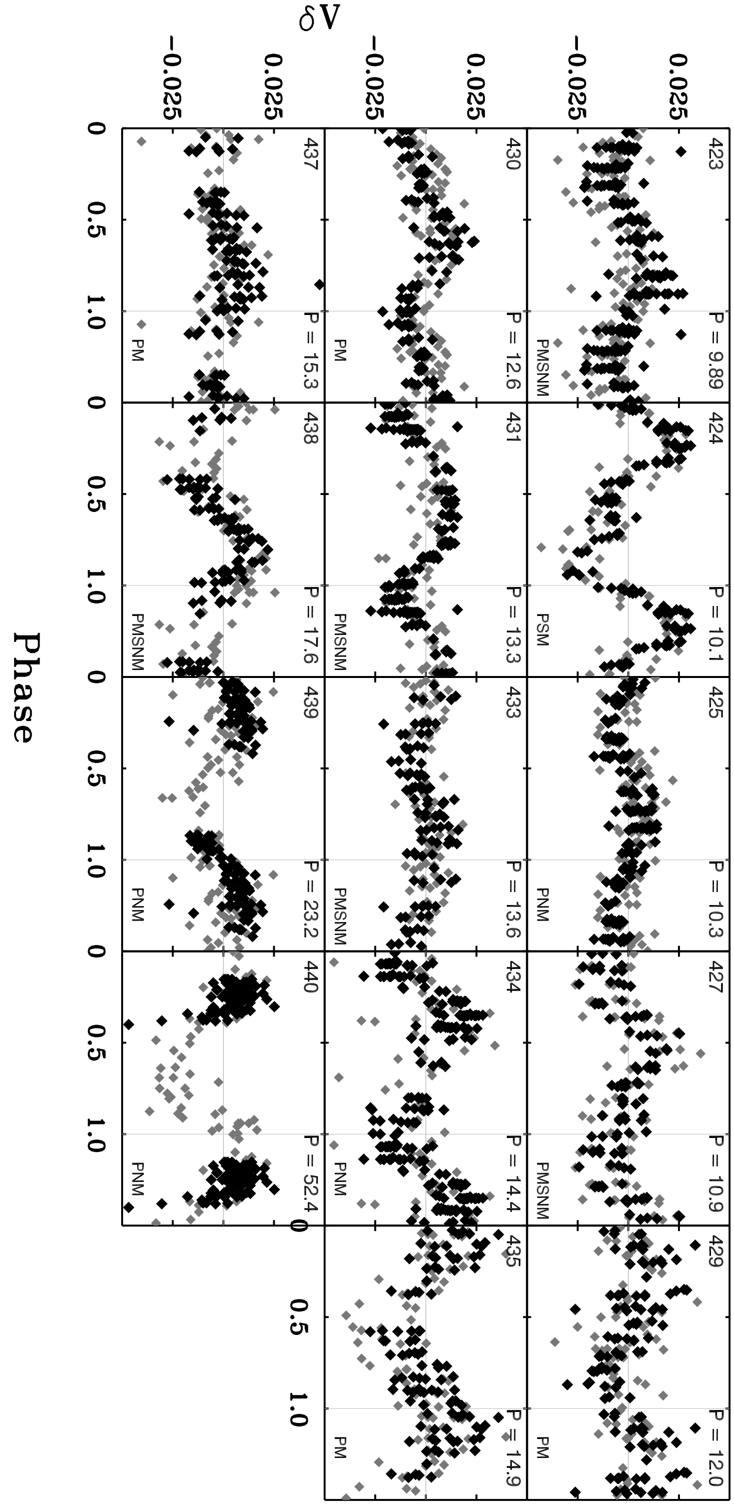

Fig. 14. — Continued.

B. DATA FOR THE 441 STARS WITH MEASURED ROTATION PERIODS IN THE FIELD OF M35

Table 2 presents the results from this study together with information relevant to this paper for 441 stars in the field of M35. In the printed journal a stub version of Table 2 show the form of the full table and a sample the first 5 lines of its contents. The full version of the table can be found online. The stars appear in order of increasing rotation period, and the running number in the first column corresponds to the number in the upper left hand corner of the stars light curve in Appendix A. Columns 2 and 3 give the stellar equatorial coordinates (equinox 2000). Column 4 lists the measured stellar rotation period in decimal days. Columns 5, 6, and 7 gives the stellar V magnitude and B-V and V-I color indices, respectively, corrected for extinction and reddening. Column 8 presents the number of radial-velocity measurements for the star and columns 9 and 10 give the mean radial-velocity and the velocity standard deviation, respectively. Column 11 list the radial-velocity cluster membership probability calculated using the formalism by Vasilevskis et al. (1958). Column 12 contains a proper-motion cluster membership probability from either Cudworth (1971) or McNamara & Sekiguchi (1986). In column 13 we give the abbreviated membership codes (initialisms) also found in the light curves in Appendix A. The codes denote the type of membership information available for the star and have the following meaning: Photometric Member (PM; described in Section 2.5), Photometric Non-Member (PNM), Photometric and Spectroscopic Member (PSM), Photometric and Proper-motion Member (PPM), and Photometric Member but Spectroscopic Non-Member (PMSNM). In column 14 we give the weights used for each star when fitting the rotational isochrones in Section 5.3 and Section 5.4. Finally, in column 15 the rotational state of the star is indicated by a 1-letter code representing, respectively, the I sequence ("i"), the C sequence ("c"), and the gap ("g"). Stars with a "-" in column 15 have locations in the color-period diagram that do not correspond to either of the sequences or the gap.

Table 2. Data for the 441 stars with measured rotation periods in the field of M35

No. [a]	RA $h\ m\ s$	DEC $^\circ\ '\ ''$	P_{rot} Days	V_0	$(B-V)_0$	$(V-I)_0$	N_{RV}	$\bar{RV}$ $km\ s^{-1}$	σ_{RV} $km\ s^{-1}$	P_{RV} %	P_{PM} %	mcode [b]	Weight	Sequence [c]
1	6 08 27.136	24 21 16.131	0.088	15.20	0.42	0.50	...	...	...	...	0	PNM	0.0	–
2	6 08 32.183	24 15 33.227	0.096	15.01	0.47	0.64	...	...	...	...	0	PNM	0.0	–
3	6 08 43.198	24 30 01.147	0.107	15.90	0.45	0.64	...	...	...	...	0	PNM	0.0	–
4	6 08 43.282	24 37 24.589	0.112	14.89	0.45	0.61	...	...	...	...	0	PNM	0.0	–
5	6 10 18.959	24 03 17.857	0.126	16.74	0.73	1.05	...	...	...	...	0	PNM	0.0	c
6	6 08 23.684	24 05 52.352	0.127	12.29	0.34	0.45	1	7.2	0.0	0	95	PPM	0.75	–
7	6 08 44.048	24 36 34.265	0.128	19.01	...	1.14	...	...	...	...	0	PNM	0.0	c
8	6 09 07.521	24 23 49.424	0.128	14.82	0.47	0.66	...	...	...	...	0	PNM	0.0	–
9	6 08 14.550	24 03 08.889	0.130	14.16	0.43	0.59	3	15.3	0.1	0	0	PMSNM	0.0	–
10	6 08 18.086	24 00 46.747	0.132	14.91	0.43	0.62	...	...	...	...	0	PNM	0.0	–
11	6 09 55.739	24 34 23.644	0.133	15.19	0.48	0.66	...	...	...	...	0	PNM	0.0	–
12	6 10 15.035	24 33 02.277	0.134	19.09	...	1.20	...	...	...	...	0	PNM	0.0	c
13	6 10 21.493	24 26 52.779	0.138	19.39	...	1.21	...	...	...	...	0	PNM	0.0	c
14	6 10 15.118	24 10 24.429	0.139	12.51	0.50	0.64	...	...	...	...	0	PNM	0.0	–
15	6 08 15.724	24 31 23.826	0.141	16.92	0.54	0.74	...	...	...	...	0	PNM	0.0	–
16	6 08 47.778	24 16 09.715	0.143	17.96	0.83	1.14	...	...	...	...	0	PNM	0.0	c
17	6 09 39.805	24 37 21.197	0.148	18.19	...	1.25	...	...	...	...	0	PNM	0.0	c
18	6 08 56.181	24 36 58.469	0.148	17.91	...	1.05	...	...	...	...	0	PNM	0.0	c
19	6 09 16.066	24 36 30.742	0.149	17.63	0.60	0.86	...	...	...	...	0	PNM	0.0	c
20	6 09 55.538	24 32 42.817	0.154	15.07	0.50	0.67	...	...	...	...	0	PNM	0.0	–
21	6 08 59.666	24 06 27.309	0.158	17.74	...	1.10	...	...	...	...	0	PNM	0.0	c
22	6 10 01.862	24 05 49.873	0.158	15.33	0.61	0.90	3	0.9	1.4	0	0	PMSNM	0.0	c
23	6 10 10.859	24 25 28.741	0.164	16.38	0.76	0.85	...	...	...	...	0	PNM	0.0	c
24	6 10 16.427	24 16 03.158	0.179	17.34	0.58	0.95	...	...	...	...	0	PNM	0.0	–
25	6 07 40.588	24 05 03.676	0.182	17.68	0.60	0.87	...	...	...	...	0	PNM	0.0	c
26	6 10 02.870	24 25 51.469	0.186	15.96	0.82	1.03	1	1.5	0.0	60	0	PSM	0.75	c
27	6 09 23.846	24 28 07.500	0.187	13.48	0.26	0.43	...	...	...	...	0	PNM	0.0	–
28	6 08 27.395	24 12 15.287	0.195	17.36	0.66	0.91	...	...	...	...	0	PNM	0.0	c
29	6 09 57.412	24 04 38.922	0.195	17.40	...	1.14	...	...	...	...	0	PNM	0.0	c
30	6 08 15.792	24 02 59.160	0.198	18.68	...	1.00	...	...	...	...	0	PNM	0.0	c
31	6 09 57.503	24 13 29.995	0.203	17.66	0.72	1.16	...	...	...	...	0	PNM	0.0	c
32	6 09 01.138	24 18 00.567	0.237	17.31	1.14	1.38	1	133.0	0.0	10	0	PM	0.5	c
33	6 08 12.934	24 15 37.264	0.241	16.70	0.38	0.59	...	...	...	...	0	PNM	0.0	–
34	6 08 31.862	24 27 02.660	0.244	17.32	1.18	1.41	1	-12.9	0.0	60	0	PSM	0.75	c
35	6 10 02.629	24 15 38.466	0.254	16.27	1.11	1.29	...	...	...	...	0	PM	0.5	c
36	6 09 10.897	24 28 50.759	0.259	19.09	...	1.12	...	...	...	...	0	PNM	0.0	c
37	6 09 06.573	23 59 45.457	0.263	17.50	...	0.90	...	...	...	...	0	PNM	0.0	c
38	6 08 18.503	24 04 40.632	0.274	18.45	1.44	1.93	...	...	...	...	0	PM	0.5	c
39	6 09 34.715	24 29 22.543	0.278	18.30	1.34	1.81	...	...	...	...	0	PM	0.5	c
40	6 09 10.753	24 31 23.434	0.289	12.64	0.39	0.48	...	...	...	...	0	PM	0.5	–
41	6 10 05.826	24 03 21.407	0.296	18.91	1.49	2.00	...	...	...	...	0	PM	0.5	c
42	6 09 21.377	24 35 02.536	0.297	12.61	0.38	0.47	...	...	...	...	0	PM	0.5	–
43	6 09 05.536	24 13 38.681	0.303	15.47	0.49	0.62	...	...	...	...	0	PNM	0.0	–
44	6 09 48.244	24 03 38.889	0.319	13.98	0.47	0.63	1	15.0	0.0	0	0	PM	0.5	–
45	6 07 46.981	24 12 08.854	0.320	17.04	1.15	1.33	1	-2.1	0.0	60	0	PSM	0.75	c

Table 2—Continued

No. [a]	RA $h\ m\ s$	DEC $^\circ\ '\ ''$	P_{rot} Days	V_0	$(B-V)_0$	$(V-I)_0$	N_{RV}	$\bar{RV}$ $km\ s^{-1}$	σ_{RV} $km\ s^{-1}$	P_{RV} %	P_{PM} %	mcode [b]	Weight	Sequence [c]
46	6 08 38.944	24 33 18.489	0.325	16.43	1.02	1.16	1	-6.5	0.0	60	0	PSM	0.75	c
47	6 08 15.195	24 23 49.397	0.331	17.49	1.25	1.70	...	...	...	...	0	PM	0.5	c
48	6 09 53.639	24 25 28.542	0.336	17.31	1.19	1.43	...	...	...	...	0	PM	0.5	c
49	6 08 03.934	24 05 21.261	0.337	15.29	0.55	0.64	...	...	...	...	0	PNM	0.0	–
50	6 08 56.177	24 23 37.408	0.337	14.49	0.43	0.57	...	...	...	...	0	PNM	0.0	–
51	6 09 20.505	24 36 38.625	0.338	17.00	1.16	1.43	1	-6.6	0.0	60	0	PSM	0.75	c
52	6 08 12.912	24 17 47.899	0.353	15.97	0.88	1.00	...	...	...	...	0	PM	0.5	c
53	6 08 51.093	24 18 57.339	0.359	17.46	1.09	1.49	...	...	...	...	0	PM	0.5	c
54	6 08 37.410	24 20 43.439	0.360	16.79	1.08	1.32	1	-12.5	0.0	60	0	PSM	0.75	c
55	6 09 43.014	24 27 24.955	0.368	16.68	1.22	1.42	1	-2.5	0.0	60	0	PSM	0.75	c
56	6 09 26.546	24 32 07.620	0.382	15.67	0.56	0.77	...	...	...	...	0	PNM	0.0	–
57	6 09 05.615	24 01 42.585	0.382	16.39	0.53	0.76	...	...	...	...	0	PNM	0.0	–
58	6 10 03.393	24 02 06.707	0.384	16.84	1.02	1.37	1	-9.2	0.0	60	0	PSM	0.75	c
59	6 09 14.271	24 06 27.481	0.387	16.68	0.73	1.26	...	...	...	...	0	PM	0.5	c
60	6 10 10.390	24 01 05.025	0.393	16.71	1.13	1.30	...	...	...	...	0	PM	0.5	c
61	6 08 32.665	24 38 40.889	0.395	18.16	1.26	1.71	...	...	...	...	0	PM	0.5	c
62	6 08 01.021	24 20 16.564	0.398	15.63	0.43	0.54	...	...	...	...	0	PNM	0.0	–
63	6 09 05.047	24 05 22.428	0.404	15.74	0.42	0.66	...	...	...	...	0	PNM	0.0	–
64	6 08 41.918	24 13 06.889	0.406	16.64	1.03	1.25	...	...	...	...	0	PM	0.5	c
65	6 10 23.340	24 10 56.529	0.413	17.64	1.16	1.58	...	...	...	...	0	PM	0.5	c
66	6 09 04.208	24 16 47.165	0.419	18.56	1.38	1.86	...	...	...	...	0	PM	0.5	c
67	6 08 16.580	24 23 25.508	0.427	16.43	0.97	1.15	...	...	...	...	0	PM	0.5	c
68	6 07 51.880	24 25 01.982	0.451	17.87	1.17	1.59	...	...	...	...	0	PM	0.5	c
69	6 09 11.466	24 25 24.078	0.460	16.86	1.05	1.26	1	-10.2	0.0	60	0	PSM	0.75	c
70	6 09 22.723	24 26 30.079	0.464	17.42	1.22	1.44	1	-13.6	0.0	60	0	PSM	0.75	c
71	6 08 50.374	24 32 13.539	0.467	12.80	0.38	0.50	2	-6.4	1.0	82	99	PSPM	1.0	–
72	6 08 33.745	24 07 23.353	0.480	18.07	1.21	1.64	...	...	...	...	0	PM	0.5	c
73	6 09 00.191	24 33 42.343	0.503	17.70	1.16	1.58	...	...	...	...	0	PM	0.5	c
74	6 09 05.004	24 11 46.380	0.511	17.95	1.21	1.64	...	...	...	...	0	PM	0.5	c
75	6 08 48.199	24 11 47.025	0.513	16.50	1.25	1.51	1	-28.8	0.0	10	0	PNM	0.0	c
76	6 10 05.228	24 12 02.907	0.513	16.51	0.60	0.73	...	...	...	...	0	PNM	0.0	–
77	6 08 59.745	24 23 52.652	0.517	17.58	...	1.33	...	...	...	...	0	PNM	0.0	c
78	6 09 29.279	24 28 20.182	0.520	16.82	1.06	1.17	1	30.6	0.0	10	0	PM	0.5	c
79	6 08 20.594	24 01 29.339	0.528	16.53	0.85	1.15	...	...	...	...	0	PM	0.5	c
80	6 09 07.462	24 08 11.103	0.543	15.89	0.84	1.03	1	-9.1	0.0	92	0	PSM	0.75	c
81	6 10 00.358	24 30 32.890	0.548	15.84	0.58	0.76	...	...	...	...	0	PNM	0.0	–
82	6 09 00.496	24 11 59.907	0.560	13.94	0.66	0.79	3	-7.9	0.2	94	91	PSPM	1.0	c
83	6 08 25.414	24 13 49.811	0.570	15.50	0.81	0.91	5	-9.8	4.7	84	0	PSM	1.0	c
84	6 09 17.063	24 17 12.536	0.580	12.71	0.30	0.42	1	-9.2	0.0	91	99	PSPM	1.0	–
85	6 08 38.299	24 20 30.984	0.582	18.19	...	1.39	...	...	...	...	0	PNM	0.0	c
86	6 09 15.840	24 23 05.877	0.596	15.35	0.44	0.58	...	...	...	...	0	PNM	0.0	–
87	6 08 04.696	24 08 26.277	0.596	13.89	0.50	0.63	4	-10.4	0.5	65	91	PSPM	1.0	–
88	6 07 53.169	24 21 12.945	0.597	12.51	0.25	0.31	1	-5.5	0.0	48	94	PPM	0.75	–
89	6 09 13.756	24 15 47.784	0.623	17.40	1.08	1.48	...	...	...	...	0	PM	0.5	c
90	6 08 05.670	24 09 05.890	0.624	16.04	0.56	0.70	...	...	...	...	0	PNM	0.0	–

Table 2—Continued

No. [a]	RA h m s	DEC ° ′ ″	P_{rot} Days	V_0	$(B-V)_0$	$(V-I)_0$	N_{RV}	$\bar{RV}$ $km\ s^{-1}$	σ_{RV} $km\ s^{-1}$	P_{RV} %	P_{PM} %	mcode [b]	Weight	Sequence [c]
91	6 09 37.594	24 14 58.386	0.629	16.24	0.98	1.17	1	-12.0	0.0	3	0	PM	0.5	c
92	6 09 45.458	24 31 29.690	0.631	16.89	0.48	0.78	...	...	...	...	0	PNM	0.0	–
93	6 07 48.950	24 05 25.539	0.636	16.75	0.54	0.77	...	...	...	...	0	PNM	0.0	–
94	6 09 08.647	24 29 47.070	0.651	18.54	1.36	1.84	...	...	...	...	0	PM	0.5	c
95	6 10 03.076	24 24 38.279	0.654	15.65	0.83	1.03	3	-7.3	0.4	93	0	PSM	1.0	c
96	6 07 54.228	24 08 29.656	0.662	16.45	0.50	0.68	...	...	...	...	0	PNM	0.0	–
97	6 08 38.004	24 35 44.559	0.691	12.68	0.31	0.40	1	-3.1	0.0	0	40	PM	0.5	–
98	6 09 07.420	24 15 24.390	0.691	16.21	1.04	1.28	...	...	...	...	0	PM	0.5	c
99	6 09 24.823	24 08 08.239	0.698	16.89	1.19	1.38	1	-5.2	0.0	60	0	PSM	0.75	c
100	6 08 33.824	24 03 45.110	0.699	15.71	0.47	0.62	...	...	...	...	0	PNM	0.0	–
101	6 09 40.018	24 33 09.974	0.716	16.37	0.54	0.72	...	...	...	...	0	PNM	0.0	–
102	6 08 54.255	24 09 01.386	0.716	16.36	0.94	1.12	...	...	...	...	0	PM	0.5	c
103	6 09 05.677	24 11 35.496	0.728	16.67	0.99	1.17	1	-12.8	0.0	60	0	PSM	0.75	c
104	6 08 15.234	24 28 05.344	0.739	16.79	0.96	1.20	1	-6.0	0.0	60	0	PSM	0.75	c
105	6 09 18.519	24 21 34.032	0.739	17.18	1.23	1.34	1	-2.7	0.0	60	0	PSM	0.75	c
106	6 08 53.797	24 10 28.054	0.754	17.70	1.11	1.51	...	...	...	...	0	PM	0.5	c
107	6 07 51.777	24 13 33.558	0.755	18.35	...	1.13	...	...	...	...	0	PNM	0.0	c
108	6 08 12.836	24 19 48.810	0.765	16.54	1.00	1.18	1	-7.7	0.0	60	0	PSM	0.75	c
109	6 08 42.403	24 29 19.735	0.766	13.57	0.45	0.57	3	6.0	0.8	0	98	PMSNM	0.0	–
110	6 08 59.518	24 18 00.011	0.766	17.79	1.13	1.55	...	...	...	...	0	PM	0.5	c
111	6 09 20.534	24 31 50.790	0.781	12.30	0.41	0.49	1	14.2	0.0	0	0	PM	0.5	–
112	6 08 30.650	24 03 08.642	0.809	17.48	0.99	1.43	...	...	...	...	0	PM	0.5	c
113	6 08 45.639	24 31 56.826	0.831	13.02	0.43	0.56	3	-8.7	0.3	94	98	PSPM	1.0	–
114	6 07 48.883	24 01 50.488	0.832	14.25	0.45	0.58	...	...	...	...	0	PM	0.5	–
115	6 10 18.894	24 29 10.280	0.852	16.72	1.02	1.33	...	...	...	...	0	PM	0.5	c
116	6 08 21.905	24 33 50.397	0.859	17.18	0.61	0.84	...	...	...	...	0	PNM	0.0	c
117	6 09 52.257	24 19 42.767	0.873	16.65	1.00	1.23	1	-7.2	0.0	60	0	PSM	0.75	c
118	6 08 28.792	24 32 32.119	0.874	15.87	0.49	0.73	...	...	...	...	0	PNM	0.0	–
119	6 09 09.651	24 20 46.825	0.877	18.79	...	1.23	...	...	...	...	0	PNM	0.0	c
120	6 08 39.870	24 27 11.593	0.879	12.69	0.29	0.39	1	-6.9	0.0	90	98	PSPM	1.0	–
121	6 09 01.920	24 16 34.798	0.882	15.76	0.93	1.09	1	12.1	0.0	0	0	PM	0.5	c
122	6 08 18.776	24 19 49.119	0.901	16.23	0.88	1.04	1	-11.4	0.0	13	0	PM	0.5	c
123	6 08 04.574	24 10 57.642	0.914	16.87	1.08	1.23	1	-9.9	0.0	60	0	PSM	0.75	c
124	6 09 09.004	24 31 18.353	0.933	16.13	1.27	1.43	...	...	...	...	0	PNM	0.0	c
125	6 09 54.529	24 18 19.663	0.933	15.97	0.92	1.05	3	-8.5	0.9	94	0	PSM	1.0	c
126	6 08 02.044	24 26 47.478	0.952	15.90	0.84	1.01	3	-4.2	2.2	2	0	PMSNM	0.0	c
127	6 09 08.805	24 20 05.537	0.971	16.30	0.92	1.13	1	-9.0	0.0	60	0	PSM	0.75	c
128	6 08 42.867	24 29 38.975	0.984	15.19	0.84	1.02	3	-9.1	0.5	92	0	PSM	1.0	c
129	6 08 53.649	24 27 16.702	0.994	16.38	1.00	1.18	1	-2.4	0.0	0	0	PM	0.5	c
130	6 10 14.311	24 15 23.669	1.006	15.43	0.80	0.92	3	-7.9	0.9	94	0	PSM	1.0	c
131	6 09 55.516	24 08 18.436	1.033	18.31	1.30	1.76	...	...	...	...	0	PM	0.5	c
132	6 08 59.410	24 34 35.496	1.044	16.28	0.86	1.10	1	-10.0	0.0	79	0	PSM	0.75	c
133	6 08 29.342	24 29 00.221	1.071	13.85	0.53	0.69	15	-8.7	4.4	94	99	PSPM	1.0	–
134	6 09 29.653	24 02 24.759	1.077	15.73	0.43	0.69	...	...	...	...	0	PNM	0.0	–
135	6 08 58.013	24 15 06.118	1.087	18.09	...	1.42	...	...	...	...	0	PNM	0.0	c

Table 2—Continued

No. [a]	RA h m s	DEC ° ′ ″	P_{rot} Days	V_0	$(B-V)_0$	$(V-I)_0$	N_{RV}	$\bar{RV}$ $km\ s^{-1}$	σ_{RV} $km\ s^{-1}$	P_{RV} %	P_{PM} %	mcode [b]	Weight	Sequence [c]
136	6 09 02.517	24 19 51.886	1.101	15.68	0.89	1.11	11	-8.4	5.5	94	0	PSM	1.0	c
137	6 08 27.628	24 12 37.267	1.109	15.74	0.88	0.98	3	-5.8	0.5	64	0	PSM	1.0	c
138	6 08 17.742	24 12 25.491	1.111	14.70	0.75	0.88	3	-7.3	1.8	92	0	PSM	1.0	c
139	6 07 50.938	24 07 32.039	1.134	13.35	0.09	0.17	...	...	...	...	0	PNM	0.0	–
140	6 08 19.832	24 05 02.460	1.139	15.04	0.69	0.77	3	-7.6	0.6	94	0	PSM	1.0	c
141	6 09 32.638	24 17 22.898	1.165	16.70	1.31	1.52	1	-10.7	0.0	60	0	PSM	0.75	c
142	6 08 13.496	24 36 04.114	1.185	17.39	1.03	1.37	...	...	...	...	0	PM	0.5	c
143	6 08 34.869	24 26 58.897	1.185	16.15	0.93	1.02	1	-8.4	0.0	94	0	PSM	0.75	c
144	6 08 09.971	24 21 00.626	1.231	14.11	0.81	0.92	1	46.6	0.0	0	0	PNM	0.0	c
145	6 10 14.884	24 18 08.642	1.240	16.76	0.53	0.57	...	...	...	...	0	PNM	0.0	–
146	6 09 28.786	24 25 33.080	1.275	15.07	0.75	0.85	3	-8.9	0.8	93	0	PSM	1.0	c
147	6 08 38.011	24 06 48.300	1.282	13.34	0.21	0.24	...	...	...	...	0	PNM	0.0	–
148	6 09 23.563	24 31 15.538	1.288	15.32	0.96	1.07	4	-9.0	2.3	92	0	PSM	1.0	c
149	6 09 21.985	24 18 49.889	1.329	15.25	0.92	1.04	4	-5.6	0.7	53	0	PSM	1.0	c
150	6 09 58.918	24 09 02.690	1.336	16.37	0.61	0.88	...	...	...	...	0	PNM	0.0	c
151	6 08 55.299	24 13 49.591	1.351	14.38	0.31	0.44	...	...	...	...	0	PNM	0.0	–
152	6 09 09.136	24 06 02.954	1.358	15.62	0.87	0.96	3	-10.0	0.6	78	0	PSM	1.0	c
153	6 08 45.615	24 29 00.331	1.377	16.07	0.93	1.04	1	-11.5	0.0	12	0	PM	0.5	c
154	6 09 16.732	24 31 14.048	1.381	14.21	0.17	0.25	...	...	...	...	0	PNM	0.0	–
155	6 09 00.867	24 37 30.700	1.404	12.95	0.08	0.13	...	...	...	...	0	PNM	0.0	–
156	6 08 53.304	24 36 36.380	1.412	17.06	1.00	1.28	1	-11.0	0.0	60	0	PSM	0.75	c
157	6 10 01.754	24 16 52.809	1.510	13.90	0.55	0.62	3	-9.6	0.9	87	79	PSPM	1.0	i
158	6 09 12.341	24 22 51.911	1.665	17.82	1.26	1.70	...	...	...	...	0	PM	0.5	g
159	6 09 50.810	24 34 58.334	1.671	14.67	0.18	0.34	...	...	...	...	0	PNM	0.0	–
160	6 09 33.124	24 30 41.171	1.688	15.01	0.78	0.87	8	-9.5	1.5	88	0	PSM	1.0	g
161	6 09 10.271	24 31 44.336	1.778	14.04	0.56	0.65	4	-7.4	0.3	93	95	PSPM	1.0	i
162	6 10 11.791	24 21 41.509	1.830	13.92	0.45	0.57	4	8.9	0.9	0	58	PMSNM	0.0	–
163	6 09 52.027	24 25 07.949	1.837	16.56	0.92	1.14	...	...	...	...	0	PM	0.5	g
164	6 08 25.007	24 06 06.264	1.864	16.70	1.09	1.18	1	-9.3	0.0	60	0	PSM	0.75	g
165	6 09 07.643	24 27 53.650	1.914	13.94	0.51	0.61	6	-8.6	0.9	94	91	PSPM	1.0	i
166	6 10 02.071	24 07 27.535	1.929	14.35	0.15	0.27	...	...	...	...	0	PNM	0.0	–
167	6 09 21.923	24 35 58.669	2.055	15.47	0.93	1.09	3	-8.3	1.4	94	0	PSM	1.0	g
168	6 07 44.332	24 08 03.680	2.055	14.53	0.60	0.68	2	25.4	106.5	0	0	PM	0.5	i
169	6 08 36.747	24 25 47.980	2.098	13.47	0.10	0.25	...	...	...	...	0	PNM	0.0	–
170	6 08 47.385	24 30 24.946	2.143	16.05	0.86	1.05	1	-11.1	0.0	25	0	PM	0.5	g
171	6 08 55.062	24 14 25.475	2.143	15.56	0.57	0.59	...	...	...	...	0	PNM	0.0	i
172	6 09 52.536	24 20 44.497	2.162	15.15	0.67	0.81	3	21.8	0.5	0	0	PMSNM	0.0	i
173	6 09 02.586	24 20 44.717	2.209	13.02	0.40	0.54	32	-8.3	21.4	94	99	PSPM	1.0	–
174	6 08 26.059	24 00 56.607	2.290	16.06	0.78	0.93	...	...	...	...	0	PNM	0.0	g
175	6 08 37.885	24 31 45.510	2.333	15.35	0.85	1.03	14	-8.1	34.5	94	0	PSM	1.0	g
176	6 08 03.278	24 13 25.538	2.344	14.11	0.52	0.64	4	-9.3	0.6	91	0	PSM	1.0	i
177	6 08 44.989	24 36 06.634	2.389	13.36	0.39	0.46	1	24.2	0.0	0	5	PNM	0.0	–
178	6 09 14.851	24 31 23.187	2.389	14.33	0.60	0.71	1	-7.9	0.0	94	94	PSPM	1.0	i
179	6 09 03.525	24 17 23.502	2.400	15.35	0.90	1.03	19	-7.1	13.3	91	0	PSM	1.0	g
180	6 08 27.802	24 04 18.563	2.435	12.39	1.49	1.57	...	...	...	...	0	PNM	0.0	g

Table 2—Continued

No. [a]	RA $h\ m\ s$	DEC $^\circ\ '\ ''$	P_{rot} Days	V_0	$(B-V)_0$	$(V-I)_0$	N_{RV}	$\bar{RV}$ $km\ s^{-1}$	σ_{RV} $km\ s^{-1}$	P_{RV} %	P_{PM} %	mcode [b]	Weight	Sequence [c]
181	6 09 03.068	24 20 09.567	2.476	14.37	0.66	0.79	11	-6.9	1.6	90	0	PSM	1.0	i
182	6 09 08.831	24 22 55.516	2.508	14.10	0.55	0.68	4	-9.1	0.2	92	96	PSPM	1.0	i
183	6 08 20.177	24 21 51.514	2.521	14.26	0.54	0.65	15	-8.2	2.1	94	0	PSM	1.0	i
184	6 08 39.646	24 27 51.652	2.534	16.61	0.75	0.89	...	...	...	...	0	PNM	0.0	g
185	6 10 09.116	24 21 38.351	2.547	16.97	0.97	1.15	...	...	...	...	0	PNM	0.0	g
186	6 07 39.270	24 24 08.451	2.560	14.14	0.56	0.65	3	-7.8	0.6	94	0	PSM	1.0	i
187	6 07 51.945	24 34 07.920	2.599	12.22	-0.0	0.06	...	...	...	...	0	PNM	0.0	–
188	6 10 23.508	24 14 57.610	2.599	14.75	0.76	0.80	4	-9.1	0.0	92	0	PSM	1.0	g
189	6 08 52.566	24 22 00.117	2.683	16.61	0.96	1.20	1	11.2	0.0	10	0	PM	0.5	g
190	6 09 24.131	24 12 59.892	2.683	14.60	0.65	0.77	...	...	...	...	0	PM	0.5	i
191	6 08 10.526	24 15 49.713	2.697	14.19	0.56	0.64	3	-6.8	0.7	89	0	PSM	1.0	i
192	6 10 14.203	24 25 23.529	2.742	14.38	0.58	0.66	14	-9.8	1.3	83	0	PSM	1.0	i
193	6 08 51.266	24 35 31.245	2.788	13.55	0.62	0.71	3	-8.2	0.9	94	0	PSM	1.0	i
194	6 09 55.631	24 17 45.379	2.835	14.42	0.68	0.78	18	-7.5	17.8	94	0	PSM	1.0	i
195	6 09 33.109	24 01 08.905	2.835	15.73	0.89	0.99	3	-8.8	2.0	93	0	PSM	1.0	g
196	6 08 24.738	24 04 41.291	2.851	14.16	0.51	0.62	3	-8.6	0.5	94	0	PSM	1.0	i
197	6 08 41.806	24 17 04.173	2.868	14.28	0.58	0.69	5	-7.4	0.2	93	90	PSPM	1.0	i
198	6 08 41.384	24 23 21.643	2.884	14.16	0.65	0.75	3	5.7	0.4	0	0	PMSNM	0.0	i
199	6 08 15.418	24 25 26.990	2.918	14.52	0.61	0.68	15	-6.0	1.8	70	0	PSM	1.0	i
200	6 09 57.327	24 09 32.092	2.918	14.44	0.69	0.86	1	-9.8	0.0	84	0	PSM	0.75	i
201	6 09 08.359	24 29 48.904	2.952	17.43	1.22	1.65	...	...	...	...	0	PM	0.5	g
202	6 08 15.080	24 23 16.136	3.079	16.51	0.96	1.14	1	-15.9	0.0	60	0	PSM	0.75	g
203	6 07 57.284	24 31 51.511	3.079	16.59	1.00	1.13	1	73.7	0.0	10	0	PM	0.5	g
204	6 08 36.783	24 02 12.399	3.118	12.39	0.20	0.30	1	-2.6	0.0	0	72	PPM	0.75	–
205	6 09 39.179	24 19 46.922	3.197	14.46	0.68	0.78	3	-7.2	0.4	92	0	PSM	1.0	i
206	6 09 01.267	24 11 45.624	3.197	14.43	0.74	0.86	3	-7.9	0.3	94	0	PSM	1.0	i
207	6 08 27.297	24 29 30.316	3.218	14.62	0.68	0.79	3	-8.5	0.2	94	0	PSM	1.0	i
208	6 09 49.619	24 26 00.896	3.218	16.15	0.78	0.92	...	...	...	...	0	PNM	0.0	g
209	6 07 54.839	24 23 42.578	3.303	14.43	0.57	0.65	16	-8.8	2.4	93	0	PSM	1.0	i
210	6 08 54.002	24 27 56.816	3.347	17.91	1.16	1.58	...	...	...	...	0	PM	0.5	g
211	6 07 58.271	24 23 00.672	3.347	13.94	0.48	0.56	4	-7.6	0.1	94	96	PSPM	1.0	–
212	6 07 49.011	24 23 59.497	3.392	14.27	0.59	0.66	3	14.8	0.4	0	0	PMSNM	0.0	i
213	6 09 49.600	24 36 37.080	3.415	14.23	0.94	1.03	2	18.2	0.5	0	0	PNM	0.0	g
214	6 10 11.151	24 14 01.601	3.439	14.68	0.65	0.78	3	-7.7	0.4	94	0	PSM	1.0	i
215	6 07 40.099	24 23 02.375	3.463	17.91	...	1.07	...	...	...	...	0	PNM	0.0	g
216	6 10 08.313	24 34 31.980	3.463	15.29	0.86	1.03	3	-7.8	0.8	94	0	PSM	1.0	g
217	6 08 11.994	24 33 56.728	3.511	14.67	0.70	0.88	7	34.7	13.9	0	0	PMSNM	0.0	i
218	6 08 30.296	24 26 28.431	3.561	14.49	0.61	0.69	3	-7.9	0.3	94	0	PSM	1.0	i
219	6 08 29.652	24 16 24.093	3.561	14.69	0.63	0.74	4	-8.1	0.9	94	0	PSM	1.0	i
220	6 09 21.441	24 24 09.742	3.587	16.41	0.71	0.84	...	...	...	...	0	PNM	0.0	i
221	6 09 10.382	24 13 03.339	3.587	17.22	1.36	1.51	1	-4.8	0.0	60	0	PSM	0.75	g
222	6 09 51.861	24 27 00.504	3.612	14.21	0.71	0.80	3	-8.9	0.2	93	67	PSPM	1.0	i
223	6 08 05.034	24 34 41.353	3.692	17.18	0.99	1.18	...	...	...	...	0	PNM	0.0	g
224	6 09 47.484	24 32 20.014	3.692	14.71	0.66	0.77	3	-8.8	0.2	93	0	PSM	1.0	i
225	6 09 15.573	24 10 42.158	3.710	14.87	0.83	0.92	37	-5.9	8.6	69	0	PSM	1.0	g

Table 2—Continued

No. [a]	RA h m s	DEC ° ′ ″	P_{rot} Days	V_0	$(B-V)_0$	$(V-I)_0$	N_{RV}	$\bar{RV}$ $km\ s^{-1}$	σ_{RV} $km\ s^{-1}$	P_{RV} %	P_{PM} %	mcode [b]	Weight	Sequence [c]
226	6 08 45.110	24 19 56.178	3.720	14.34	0.76	0.85	6	-8.0	0.3	94	86	PSPM	1.0	i
227	6 09 29.190	24 00 42.352	3.720	14.38	0.59	0.68	3	-9.8	0.2	83	0	PSM	1.0	i
228	6 09 26.342	24 23 19.569	3.748	15.68	0.88	0.96	3	-7.9	0.5	94	0	PSM	1.0	g
229	6 08 57.055	24 19 50.176	3.776	18.00	...	1.45	...	...	...	...	0	PNM	0.0	g
230	6 08 11.813	24 27 07.158	3.776	14.57	0.58	0.66	3	-8.1	0.6	94	0	PSM	1.0	i
231	6 09 40.317	24 25 46.278	3.776	17.58	0.77	0.94	...	...	...	...	0	PNM	0.0	i
232	6 08 09.561	24 17 53.763	3.805	18.84	1.47	1.97	...	...	...	...	0	PM	0.5	g
233	6 09 42.754	24 33 25.135	3.834	18.51	...	1.36	...	...	...	...	0	PNM	0.0	g
234	6 08 41.849	24 19 07.220	3.864	17.17	1.25	1.33	...	...	...	...	0	PM	0.5	g
235	6 10 01.280	24 13 43.061	3.864	14.56	0.58	0.69	3	-7.8	0.1	94	0	PSM	1.0	i
236	6 08 26.700	24 09 39.941	3.924	14.54	0.71	0.84	...	...	...	...	0	PM	0.5	i
237	6 08 10.447	24 24 23.811	3.955	14.84	0.64	0.73	3	-7.3	0.1	92	0	PSM	1.0	i
238	6 08 07.898	24 32 58.143	3.955	14.58	0.60	0.66	3	-7.7	0.2	94	0	PSM	1.0	i
239	6 08 07.065	24 18 49.916	3.955	14.55	0.62	0.69	1	-6.5	0.0	84	72	PSPM	1.0	i
240	6 08 52.437	24 03 06.294	3.986	14.46	0.56	0.64	3	-8.1	0.5	94	0	PSM	1.0	i
241	6 09 04.263	24 12 41.922	3.986	14.71	0.68	0.77	3	-8.1	0.1	94	0	PSM	1.0	i
242	6 09 31.907	24 10 38.347	3.986	14.41	0.71	0.82	22	-8.1	5.8	94	0	PSM	1.0	i
243	6 09 42.535	24 02 08.190	4.187	14.94	0.76	0.85	3	-7.9	0.5	94	0	PSM	1.0	i
244	6 07 52.604	24 20 02.385	4.222	14.57	0.57	0.65	3	-7.0	0.2	91	0	PSM	1.0	i
245	6 07 44.371	24 30 26.182	4.258	14.63	0.62	0.74	16	-7.0	5.0	91	0	PSM	1.0	i
246	6 10 10.538	24 24 14.398	4.258	14.73	0.64	0.73	5	-8.9	1.2	93	0	PSM	1.0	i
247	6 09 02.678	24 12 51.082	4.258	14.96	0.77	0.85	3	-7.6	0.3	94	0	PSM	1.0	i
248	6 10 01.754	24 20 12.094	4.294	14.75	0.68	0.77	3	-8.7	0.4	94	0	PSM	1.0	i
249	6 08 33.180	24 19 13.228	4.332	14.68	0.63	0.72	3	-8.2	0.4	94	0	PSM	1.0	i
250	6 08 52.234	24 23 28.145	4.332	14.55	0.65	0.76	3	-9.5	0.0	89	0	PSM	1.0	i
251	6 09 57.251	24 10 15.708	4.369	15.23	0.87	1.01	...	...	...	...	0	PM	0.5	i
252	6 09 02.150	24 29 31.223	4.408	15.26	0.75	0.86	3	-7.5	0.8	93	0	PSM	1.0	i
253	6 09 31.231	24 07 02.850	4.447	14.55	0.64	0.71	3	-8.1	0.7	94	0	PSM	1.0	i
254	6 09 34.139	24 18 09.075	4.447	15.00	0.77	0.90	3	-6.6	0.3	86	0	PSM	1.0	i
255	6 08 57.405	24 15 05.026	4.487	15.02	0.76	0.89	3	-9.0	0.4	92	0	PSM	1.0	i
256	6 09 21.896	24 17 17.006	4.487	14.86	0.69	0.77	4	-8.7	0.4	94	0	PSM	1.0	i
257	6 10 07.151	24 02 55.390	4.527	16.24	1.03	1.08	1	19.2	0.0	0	0	PM	0.5	g
258	6 09 50.072	24 17 02.813	4.527	14.97	0.76	0.82	3	-9.0	0.3	92	0	PSM	1.0	i
259	6 08 42.529	24 23 37.236	4.569	16.37	0.96	1.13	1	2.2	0.0	0	0	PM	0.5	g
260	6 08 46.616	24 31 43.038	4.611	14.96	0.71	0.86	3	-7.9	1.0	94	0	PSM	1.0	i
261	6 08 18.827	24 19 18.900	4.611	13.55	1.57	1.60	...	...	...	...	0	PNM	0.0	g
262	6 09 06.393	24 26 41.738	4.654	15.23	0.79	0.89	17	-0.7	16.3	0	0	PMSNM	0.0	i
263	6 09 23.478	24 16 56.737	4.654	16.94	0.76	0.95	...	...	...	...	0	PNM	0.0	i
264	6 09 03.068	24 19 36.210	4.697	15.15	0.80	0.90	14	-9.2	9.1	91	0	PSM	1.0	i
265	6 09 57.284	24 37 49.899	4.697	15.09	0.75	0.87	3	-8.5	0.1	94	0	PSM	1.0	i
266	6 08 56.418	24 27 10.618	4.742	14.91	0.70	0.77	3	-6.2	0.1	79	0	PSM	1.0	i
267	6 09 56.437	24 25 51.846	4.742	14.19	0.67	0.85	3	-7.9	1.0	94	58	PSPM	1.0	i
268	6 09 31.418	24 27 49.682	4.742	14.59	0.64	0.71	3	-8.1	0.3	94	0	PSM	1.0	i
269	6 08 07.623	24 03 16.758	4.787	16.29	0.92	1.05	...	...	...	...	0	PM	0.5	i
270	6 08 34.962	24 17 08.121	4.833	18.49	1.35	1.82	...	...	...	...	0	PM	0.5	g

Table 2—Continued

No. [a]	RA $h\ m\ s$	DEC $^\circ\ '\ ''$	P_{rot} Days	V_0	$(B-V)_0$	$(V-I)_0$	N_{RV}	$\bar{RV}$ $km\ s^{-1}$	σ_{RV} $km\ s^{-1}$	P_{RV} %	P_{PM} %	mcode [b]	Weight	Sequence [c]
271	6 10 04.706	24 17 34.770	4.833	14.81	0.70	0.71	3	-7.4	0.2	93	0	PSM	1.0	i
272	6 09 39.005	24 16 44.164	4.833	15.01	0.71	0.83	4	-7.4	0.4	93	0	PSM	1.0	i
273	6 09 11.862	24 26 16.188	4.929	14.43	0.59	0.67	4	-6.1	0.2	75	68	PSPM	1.0	i
274	6 08 23.661	23 59 35.130	4.929	15.07	0.69	0.73	1	-7.6	0.0	94	0	PSM	0.75	i
275	6 09 30.074	24 35 49.880	4.978	18.27	1.31	1.78	...	...	...	...	0	PM	0.5	g
276	6 08 27.707	24 33 11.725	5.028	15.16	0.78	0.82	5	-8.4	1.1	94	0	PSM	1.0	i
277	6 09 41.383	24 36 44.242	5.028	15.05	0.70	0.85	3	-8.3	0.6	94	0	PSM	1.0	i
278	6 09 30.484	24 03 16.223	5.079	18.15	1.29	1.74	...	...	...	...	0	PM	0.5	g
279	6 09 58.806	24 14 43.266	5.079	14.88	0.73	0.83	3	-9.2	0.3	91	0	PSM	1.0	i
280	6 08 47.292	24 00 33.639	5.131	16.67	0.87	0.94	...	...	...	...	0	PNM	0.0	i
281	6 08 57.228	24 15 53.318	5.184	17.23	1.24	1.38	1	-11.6	0.0	60	0	PSM	0.75	g
282	6 09 19.649	24 30 52.741	5.238	15.12	0.76	0.84	3	-7.6	0.4	94	0	PSM	1.0	i
283	6 09 19.242	24 17 22.390	5.248	14.93	0.72	0.83	17	-8.9	6.8	93	0	PSM	1.0	i
284	6 10 14.646	24 31 34.537	5.293	17.53	1.25	1.46	1	1.5	0.0	60	0	PSM	0.75	g
285	6 09 39.067	24 04 43.083	5.293	13.16	0.47	0.63	3	25.0	0.3	0	0	PMSNM	0.0	–
286	6 08 42.968	24 26 34.096	5.408	15.06	0.77	0.86	3	-9.5	0.4	88	0	PSM	1.0	i
287	6 09 43.444	24 24 33.747	5.467	14.88	0.70	0.73	3	-8.0	0.5	94	0	PSM	1.0	i
288	6 08 47.605	24 09 42.241	5.467	15.16	0.75	0.81	1	-7.3	0.0	93	0	PSM	0.75	i
289	6 09 56.346	23 59 35.102	5.467	15.85	0.95	1.17	2	-6.5	1.3	84	0	PSM	1.0	i
290	6 08 35.103	24 27 16.983	5.527	15.04	0.80	0.90	3	-9.2	0.5	91	0	PSM	1.0	i
291	6 08 39.717	24 19 24.104	5.527	16.93	1.17	1.25	1	-6.5	0.0	60	0	PSM	0.75	g
292	6 08 44.894	24 22 52.646	5.527	15.30	0.89	1.00	3	-8.9	0.4	93	0	PSM	1.0	i
293	6 08 48.087	24 37 50.002	5.527	15.09	0.73	0.71	3	-8.4	0.5	94	0	PSM	1.0	i
294	6 09 05.385	24 12 18.013	5.527	15.24	0.79	0.84	3	-7.9	0.3	94	0	PSM	1.0	i
295	6 09 26.543	24 25 37.015	5.589	15.96	0.73	0.86	...	...	...	...	0	PNM	0.0	i
296	6 08 57.455	23 59 36.228	5.589	16.39	0.97	1.10	...	...	...	...	0	PM	0.5	i
297	6 08 37.291	24 22 17.840	5.652	15.30	0.80	0.85	3	-8.2	0.7	94	0	PSM	1.0	i
298	6 09 22.881	24 34 06.444	5.652	15.44	0.81	0.96	3	-8.8	0.3	93	0	PSM	1.0	i
299	6 09 35.677	24 22 53.174	5.652	17.68	1.12	1.53	...	...	...	...	0	PM	0.5	g
300	6 08 17.686	24 16 05.170	5.652	15.16	0.72	0.77	3	-9.5	0.5	89	0	PSM	1.0	i
301	6 09 21.841	24 18 21.187	5.652	15.36	0.81	0.87	3	-8.7	0.1	94	0	PSM	1.0	i
302	6 08 17.040	24 27 01.980	5.717	15.14	0.72	0.78	3	-7.7	0.2	94	0	PSM	1.0	i
303	6 09 37.344	24 36 05.584	5.717	16.01	0.89	1.03	...	...	...	...	0	PM	0.5	i
304	6 08 43.414	24 16 07.264	5.717	15.20	0.78	0.82	3	-9.2	0.4	91	0	PSM	1.0	i
305	6 08 06.681	24 21 50.339	5.783	17.51	1.27	1.41	1	-8.8	0.0	60	0	PSM	0.75	g
306	6 08 30.837	24 22 17.606	5.783	15.71	0.84	0.91	3	18.5	1.5	0	0	PMSNM	0.0	i
307	6 08 37.439	24 32 39.954	5.783	17.59	1.10	1.51	...	...	...	...	0	PM	0.5	g
308	6 09 26.503	24 20 39.313	5.783	16.52	1.06	1.16	...	...	...	...	0	PM	0.5	g
309	6 09 30.043	24 32 08.492	5.783	16.52	1.05	1.17	1	-6.7	0.0	60	0	PSM	0.75	g
310	6 08 46.587	24 17 45.379	5.783	16.75	1.08	1.28	1	-13.3	0.0	60	0	PSM	0.75	g
311	6 07 49.432	24 09 13.306	5.783	15.33	0.74	0.77	...	...	...	...	0	PM	0.5	i
312	6 07 55.679	24 12 03.477	5.783	15.26	0.76	0.83	...	...	...	...	0	PM	0.5	i
313	6 08 59.049	24 18 25.005	5.783	15.41	0.85	0.92	3	-9.2	0.7	91	0	PSM	1.0	i
314	6 09 11.689	24 11 23.933	5.783	15.30	0.79	0.83	3	-9.0	0.1	93	0	PSM	1.0	i
315	6 08 35.415	24 19 59.268	5.850	16.16	0.96	1.06	1	-8.6	0.0	94	0	PSM	0.75	i

Table 2—Continued

No. [a]	RA $h\ m\ s$	DEC $^\circ\ '\ ''$	P_{rot} Days	V_0	$(B-V)_0$	$(V-I)_0$	N_{RV}	$\bar{RV}$ $km\ s^{-1}$	σ_{RV} $km\ s^{-1}$	P_{RV} %	P_{PM} %	mcode [b]	Weight	Sequence [c]
316	6 09 34.463	24 02 52.705	5.850	15.06	0.73	0.81	3	-7.6	1.3	94	0	PSM	1.0	i
317	6 09 01.930	24 32 08.753	5.919	15.38	0.75	0.87	3	-7.4	0.2	93	0	PSM	1.0	i
318	6 08 10.169	24 35 08.167	5.919	15.71	0.64	0.79	...	...	...	...	0	PNM	0.0	–
319	6 10 03.774	24 32 54.710	5.919	14.46	0.58	0.70	3	21.4	0.3	0	0	PMSNM	0.0	–
320	6 08 33.281	24 05 33.538	5.919	15.26	0.75	0.80	3	-7.7	0.1	94	0	PSM	1.0	i
321	6 09 16.099	24 18 03.293	5.919	16.62	1.04	1.17	1	-9.6	0.0	60	0	PSM	0.75	g
322	6 08 12.048	24 21 26.760	5.990	15.25	0.76	0.81	3	-8.4	0.1	94	0	PSM	1.0	i
323	6 09 38.851	24 28 53.725	5.990	16.07	0.98	1.06	1	-8.3	0.0	94	0	PSM	0.75	i
324	6 08 54.406	24 03 08.024	6.029	14.37	0.56	0.66	19	-7.5	17.5	93	0	PSM	1.0	–
325	6 07 46.193	24 22 48.999	6.137	16.86	0.87	1.12	...	...	...	...	0	PNM	0.0	i
326	6 08 29.814	24 29 17.806	6.137	15.60	0.87	0.92	3	-8.1	0.5	94	0	PSM	1.0	i
327	6 09 39.711	24 38 44.233	6.137	13.21	0.24	0.38	...	...	...	...	0	PNM	0.0	–
328	6 08 41.064	24 17 20.666	6.137	15.44	0.81	0.85	3	-8.6	0.8	94	0	PSM	1.0	i
329	6 07 56.510	24 08 59.202	6.137	13.20	0.56	0.61	...	...	...	...	0	PM	0.5	–
330	6 09 15.117	24 11 03.437	6.137	14.83	0.69	0.76	4	-7.2	0.2	92	0	PSM	1.0	i
331	6 07 43.568	24 24 01.585	6.213	16.49	1.11	1.36	1	-6.2	0.0	60	0	PSM	0.75	g
332	6 08 39.664	24 37 15.320	6.291	15.34	0.73	0.81	3	-8.0	0.6	94	0	PSM	1.0	i
333	6 09 29.190	24 21 51.205	6.291	15.66	0.88	0.92	4	-8.7	0.9	94	0	PSM	1.0	i
334	6 09 22.900	24 15 26.305	6.291	15.54	0.84	0.89	4	-7.3	0.8	93	0	PSM	1.0	i
335	6 07 50.235	24 27 17.643	6.372	15.71	0.85	1.01	...	...	...	...	0	PM	0.5	i
336	6 08 47.994	24 36 02.185	6.372	15.32	0.74	0.80	3	-8.9	0.2	93	0	PSM	1.0	i
337	6 09 01.070	24 24 53.186	6.372	17.71	1.08	1.48	...	...	...	...	0	PM	0.5	i
338	6 10 20.269	24 20 22.112	6.372	18.21	...	0.95	...	...	...	...	0	PNM	0.0	g
339	6 09 06.747	24 12 45.225	6.372	17.30	1.30	1.40	...	...	...	...	0	PM	0.5	g
340	6 08 32.162	24 20 36.285	6.454	15.46	0.83	0.85	4	-7.2	0.5	92	0	PSM	1.0	i
341	6 09 06.311	24 17 05.162	6.454	17.13	1.37	1.55	...	...	...	...	0	PM	0.5	g
342	6 09 14.073	24 13 36.737	6.454	15.45	0.82	0.86	3	-8.5	0.9	94	0	PSM	1.0	i
343	6 09 33.001	24 25 17.761	6.538	15.57	0.84	0.91	3	-9.3	0.5	91	0	PSM	1.0	i
344	6 10 07.831	24 28 11.091	6.538	15.87	0.88	1.04	3	-7.6	0.6	94	0	PSM	1.0	i
345	6 10 19.474	24 35 57.598	6.538	16.95	1.13	1.32	1	-10.8	0.0	60	0	PSM	0.75	g
346	6 09 53.330	24 37 59.958	6.538	16.55	1.04	1.16	...	...	...	...	0	PM	0.5	i
347	6 09 31.897	24 36 14.435	6.538	15.64	0.87	0.94	3	-8.4	0.5	94	0	PSM	1.0	i
348	6 08 34.450	24 08 13.932	6.538	15.52	0.80	0.85	3	-7.0	0.5	91	0	PSM	1.0	i
349	6 09 02.357	24 00 50.935	6.538	16.31	0.82	0.98	...	...	...	...	0	PNM	0.0	i
350	6 09 30.733	24 16 04.758	6.538	17.66	1.28	1.73	...	...	...	...	0	PM	0.5	g
351	6 10 08.428	24 23 24.650	6.625	17.20	1.04	1.38	...	...	...	...	0	PM	0.5	i
352	6 09 57.754	24 29 45.608	6.625	18.17	1.27	1.72	...	...	...	...	0	PM	0.5	g
353	6 09 06.487	24 21 30.234	6.625	15.77	0.91	0.96	3	-8.2	0.7	94	0	PSM	1.0	i
354	6 09 49.442	24 15 47.159	6.625	15.92	0.95	1.02	...	...	...	...	0	PM	0.5	i
355	6 08 51.065	24 23 50.186	6.805	17.77	1.14	1.56	...	...	...	...	0	PM	0.5	g
356	6 09 14.818	24 29 10.417	6.805	15.62	0.82	0.87	3	-8.9	0.5	93	0	PSM	1.0	i
357	6 09 42.591	24 20 51.981	6.805	15.89	0.91	1.02	6	-8.1	1.4	94	0	PSM	1.0	i
358	6 09 37.160	24 21 22.853	6.805	12.62	0.59	0.63	1	-2.1	0.0	0	0	PNM	0.0	–
359	6 09 07.478	24 08 33.686	6.805	18.72	1.44	1.93	...	...	...	...	0	PM	0.5	g
360	6 09 40.277	24 01 16.712	6.805	15.70	0.87	0.93	3	-8.3	0.4	94	0	PSM	1.0	i

Table 2—Continued

No. [a]	RA $h\ m\ s$	DEC $\circ\ '\ ''$	P_{rot} Days	V_0	$(B-V)_0$	$(V-I)_0$	N_{RV}	$\bar{RV}$ $km\ s^{-1}$	σ_{RV} $km\ s^{-1}$	P_{RV} %	P_{PM} %	mcode [b]	Weight	Sequence [c]
361	6 08 16.778	24 26 26.893	6.898	16.44	0.97	1.09	1	-5.9	0.0	60	0	PSM	0.75	i
362	6 09 03.068	24 34 56.487	6.898	15.46	0.82	0.93	3	-7.7	0.3	94	0	PSM	1.0	i
363	6 09 47.530	24 03 37.303	6.898	15.89	0.97	1.06	1	-8.8	0.0	93	0	PSM	0.75	i
364	6 08 07.462	24 35 35.735	6.995	16.50	1.05	1.14	1	-6.7	0.0	60	0	PSM	0.75	i
365	6 08 44.310	24 22 47.125	6.995	15.16	0.94	1.00	16	-13.6	16.8	0	0	PMSNM	0.0	i
366	6 10 20.482	24 22 10.925	6.995	16.74	1.09	1.26	1	-8.6	0.0	60	0	PSM	0.75	i
367	6 09 26.798	24 27 54.914	6.995	15.88	0.93	0.95	3	-8.7	0.1	94	0	PSM	1.0	i
368	6 09 07.452	24 19 05.517	6.995	17.96	1.19	1.61	...	...	...	...	0	PM	0.5	g
369	6 08 35.743	24 13 31.471	6.995	15.16	0.61	0.70	...	...	...	...	0	PNM	0.0	–
370	6 07 58.130	24 20 10.838	7.301	17.29	1.19	1.34	...	...	...	...	0	PM	0.5	g
371	6 09 10.652	24 28 03.971	7.301	15.93	0.94	0.95	6	-7.7	1.4	94	0	PSM	1.0	i
372	6 09 06.541	24 31 26.037	7.301	17.09	1.12	1.35	...	...	...	...	0	PM	0.5	i
373	6 10 18.760	24 32 44.719	7.301	16.07	0.98	1.08	1	-9.4	0.0	90	0	PSM	0.75	i
374	6 08 32.799	24 25 11.602	7.409	16.99	1.17	1.28	1	-15.7	0.0	60	0	PSM	0.75	i
375	6 08 03.144	24 28 54.638	7.520	16.08	0.90	0.98	1	-9.1	0.0	92	0	PSM	0.75	i
376	6 07 40.224	24 33 40.509	7.520	16.06	0.51	0.65	...	...	...	...	0	PNM	0.0	–
377	6 09 39.402	24 27 23.465	7.520	16.12	0.95	1.02	...	...	...	...	0	PM	0.5	i
378	6 07 41.261	24 13 00.496	7.520	13.65	0.63	0.68	2	14.5	0.2	0	0	PM	0.5	–
379	6 08 25.847	24 12 53.774	7.520	16.27	0.98	1.05	1	-7.5	0.0	93	0	PSM	0.75	i
380	6 08 22.319	24 15 02.506	7.520	15.90	0.88	0.95	1	-7.7	0.0	94	0	PSM	0.75	i
381	6 09 44.244	24 24 54.326	7.635	17.79	1.15	1.56	...	...	...	...	0	PM	0.5	i
382	6 10 24.096	24 16 45.064	7.635	17.46	...	1.33	...	...	...	...	0	PNM	0.0	g
383	6 09 18.809	24 27 05.043	7.753	15.97	0.91	0.93	1	-7.2	0.0	92	0	PSM	0.75	i
384	6 09 02.445	24 16 25.405	7.753	13.71	0.64	0.70	6	-3.3	0.5	0	88	PMSNM	0.0	–
385	6 10 14.196	24 32 30.334	7.875	16.40	1.06	1.13	1	-6.9	0.0	60	0	PSM	0.75	i
386	6 10 04.916	24 34 59.089	7.875	16.26	1.00	1.10	...	...	...	...	0	PM	0.5	i
387	6 08 58.164	24 33 11.595	8.001	13.22	0.66	0.74	1	-1.8	0.0	0	0	PNM	0.0	–
388	6 10 15.215	24 28 58.930	8.001	16.48	1.11	1.19	1	-9.5	0.0	60	0	PSM	0.75	i
389	6 08 40.793	24 11 50.548	8.001	17.04	1.19	1.28	1	-6.1	0.0	60	0	PSM	0.75	i
390	6 08 49.222	24 05 50.388	8.001	15.97	0.88	0.96	3	-6.2	0.7	77	0	PSM	1.0	i
391	6 08 48.278	24 17 59.077	8.001	16.53	1.14	1.16	...	...	...	...	0	PM	0.5	i
392	6 08 03.369	24 34 09.918	8.131	16.36	0.98	1.07	...	...	...	...	0	PM	0.5	i
393	6 09 32.508	24 27 23.802	8.131	17.25	1.13	1.37	1	-4.5	0.0	60	0	PSM	0.75	i
394	6 10 12.194	24 30 50.125	8.265	14.86	0.87	0.96	3	-17.8	0.4	0	0	PMSNM	0.0	–
395	6 08 58.960	24 14 41.646	8.265	15.60	1.01	1.09	5	-12.0	7.0	2	0	PMSNM	0.0	i
396	6 08 09.791	24 34 28.478	8.404	12.28	0.65	0.68	...	...	...	...	0	PNM	0.0	–
397	6 09 17.572	24 28 20.457	8.404	16.07	0.37	0.41	...	...	...	...	0	PNM	0.0	–
398	6 10 02.164	24 34 37.295	8.404	16.05	0.91	0.98	1	22.2	0.0	0	0	PM	0.5	i
399	6 08 09.528	24 05 50.258	8.404	14.51	0.77	0.82	3	17.7	0.3	0	0	PMSNM	0.0	–
400	6 07 40.808	24 14 23.374	8.404	16.10	0.91	1.05	...	...	...	...	0	PM	0.5	i
401	6 08 36.304	24 20 53.430	8.547	17.83	1.14	1.56	...	...	...	...	0	PM	0.5	i
402	6 08 06.018	24 04 42.033	8.547	16.58	0.95	1.12	1	-5.2	0.0	60	0	PSM	0.75	i
403	6 08 21.634	24 07 09.785	8.547	14.91	0.58	0.67	3	11.3	0.1	0	0	PMSNM	0.0	–
404	6 09 32.039	24 01 35.004	8.547	17.72	1.16	1.57	...	...	...	...	0	PM	0.5	i
405	6 09 22.543	24 27 55.834	8.696	17.06	1.18	1.27	...	...	...	...	0	PM	0.5	i

Table 2—Continued

No. [a]	RA $h\ m\ s$	DEC $\circ\ \prime\ \prime\prime$	P_{rot} Days	V_0	$(B-V)_0$	$(V-I)_0$	N_{RV}	$\bar{RV}$ $km\ s^{-1}$	σ_{RV} $km\ s^{-1}$	P_{RV} %	P_{PM} %	mcode [b]	Weight	Sequence [c]
406	6 09 54.242	24 29 39.408	8.696	16.55	1.14	1.18	1	-6.9	0.0	60	0	PSM	0.75	i
407	6 08 23.874	24 13 55.435	8.696	17.38	1.21	1.41	...	...	...	...	0	PM	0.5	i
408	6 08 35.214	24 18 24.009	8.696	13.29	0.85	0.89	...	...	...	...	0	PNM	0.0	–
409	6 09 51.267	24 10 01.865	8.696	17.13	1.32	1.37	1	-9.4	0.0	60	0	PSM	0.75	i
410	6 08 23.306	24 15 20.277	8.850	16.50	1.08	1.08	1	-7.6	0.0	60	0	PSM	0.75	i
411	6 09 24.502	24 06 12.800	8.850	17.20	0.95	1.32	...	...	...	...	0	PM	0.5	i
412	6 10 01.924	24 17 07.950	8.850	17.01	1.18	1.29	1	-8.5	0.0	60	0	PSM	0.75	i
413	6 08 15.684	24 01 21.999	9.174	16.37	0.88	1.00	...	...	...	...	0	PNM	0.0	–
414	6 08 47.979	24 07 47.352	9.174	16.58	1.04	1.31	1	-4.4	0.0	60	0	PSM	0.75	i
415	6 08 19.641	24 20 51.123	9.345	16.88	1.15	1.23	1	-9.5	0.0	60	0	PSM	0.75	i
416	6 10 10.970	24 19 33.896	9.345	17.13	1.13	1.32	1	-9.7	0.0	60	0	PSM	0.75	i
417	6 09 51.346	24 26 52.237	9.468	18.16	1.28	1.74	...	...	...	...	0	PM	0.5	i
418	6 08 45.021	24 23 18.649	9.523	16.86	1.11	1.25	1	-5.0	0.0	60	0	PSM	0.75	i
419	6 08 58.617	24 22 52.028	9.523	18.42	1.32	1.78	...	...	...	...	0	PM	0.5	i
420	6 07 54.553	24 35 49.715	9.708	17.04	1.04	1.25	1	-7.4	0.0	60	0	PSM	0.75	i
421	6 08 51.936	24 14 04.759	9.708	17.09	1.21	1.33	1	-9.3	0.0	60	0	PSM	0.75	i
422	6 07 48.986	24 02 02.793	9.708	17.12	1.13	1.31	1	-8.1	0.0	60	0	PSM	0.75	i
423	6 08 24.521	24 15 09.915	9.900	15.51	0.83	0.85	3	-18.5	0.1	0	0	PMSNM	0.0	–
424	6 09 24.357	24 26 20.047	10.132	14.74	0.68	0.76	22	-7.4	28.4	93	0	PSM	1.0	–
425	6 08 57.022	24 12 04.796	10.308	14.65	0.95	1.01	4	7.3	0.2	0	0	PNM	0.0	–
426	6 08 25.052	24 00 03.419	10.308	16.94	0.87	0.92	...	...	...	...	0	PNM	0.0	–
427	6 10 11.686	24 06 37.032	10.986	14.99	0.75	0.84	3	25.0	0.5	0	0	PMSNM	0.0	–
428	6 09 07.981	24 38 47.886	11.233	17.35	1.00	1.38	...	...	...	...	0	PM	0.5	–
429	6 09 57.172	24 32 03.370	12.044	15.98	0.97	1.06	...	...	...	...	0	PM	0.5	–
430	6 09 00.388	24 28 45.341	12.652	13.72	0.69	0.80	2	-16.0	0.4	0	0	PM	0.5	–
431	6 07 47.647	24 05 24.845	13.326	13.33	0.68	0.66	4	13.6	0.2	0	0	PMSNM	0.0	–
432	6 07 49.959	24 04 37.707	13.691	13.80	1.31	1.43	...	...	...	...	0	PNM	0.0	–
433	6 09 29.636	24 07 32.039	13.691	15.47	0.71	0.83	3	-22.8	1.2	0	0	PMSNM	0.0	–
434	6 07 51.071	24 18 28.891	14.483	12.40	0.65	0.69	1	49.7	0.0	0	0	PNM	0.0	–
435	6 09 49.301	24 06 50.332	14.915	16.37	0.96	1.07	...	...	...	...	0	PM	0.5	–
436	6 08 26.765	24 29 24.741	15.373	16.08	0.95	1.05	1	27.2	0.0	0	0	PM	0.5	–
437	6 08 17.073	24 32 57.587	15.373	14.94	0.75	0.82	...	...	...	...	0	PM	0.5	–
438	6 10 18.062	24 33 54.647	17.605	15.20	0.82	0.96	3	30.2	0.4	0	0	PMSNM	0.0	–
439	6 08 35.834	24 27 48.954	23.215	13.56	0.80	0.87	2	21.8	0.0	0	0	PNM	0.0	–
440	6 10 06.758	24 37 15.182	52.465	15.18	1.19	1.46	...	...	...	...	0	PNM	0.0	–
441	6 08 30.040	24 31 58.076	58.464	16.76	1.42	1.65	1	-16.4	0.0	60	0	PSM	0.75	–

[a]Running number assigned to 310 rotators after sorting by rotation period.

[b]etter code denoting a star's cluster membership status (see introductory text of Appendix for code meaning).

[c]etters "i", "c", and "g" mark stars on the I and C sequances or in the gap, respectively.

C. THE ROTATION PERIOD DISTRIBUTION OF NON-MEMBERS

In this section, we display and briefly comment upon the rotation period distribution of the non-members among the 441 rotators, which presumably are mostly field stars belonging to the Galactic disk. Unlike the cluster members we do not know the ages, distances, or masses of these stars. We will therefore only comment on a comparison between the two distributions and on distinct features in the period distribution of the 131 non-members shown in Figure 16. First, rotation periods are detected over approximately the same range ($\sim$0.1 - 15 days) as for the 150 Myr cluster members, with only a few stars rotating slower. Second, there appears to be no indication of a bimodal distribution, but rather a distribution with a peak of ultra fast rotators and a long tail of periods up to and beyond 15 days. Third, and most strikingly, as shown by the 0.1 day resolution of the insert in Figure 16, the non-member distribution exhibits a very distinct peak between 0.1 and 0.2 days. The phased light curves for these stars (Appendix A) shows that the majority of these stars have large and well defined photometric variability with with peak-to-peak amplitudes of $0\overset{\mathrm{m}}{.}1$ or higher. It is possible that most of these stars are contact binaries of, e.g., the W UMa-type. Such systems typically have orbital periods of order 0.2-0.5 days and occur with a frequency of $\sim$0.2% (OGLE Variable Star Catalog; Rucinski 1997). The frequency of rapidly varying non-members found in the field of M35 is $\sim$20 out of 13700 or $\sim$0.15% and thus in good agreement with that found from the OGLE Catalog. Indeed, if the light curves for these stars represent eclipses rather than spot-modulation, then the measured periods must be doubled bringing them into the expected range for W Uma systems.

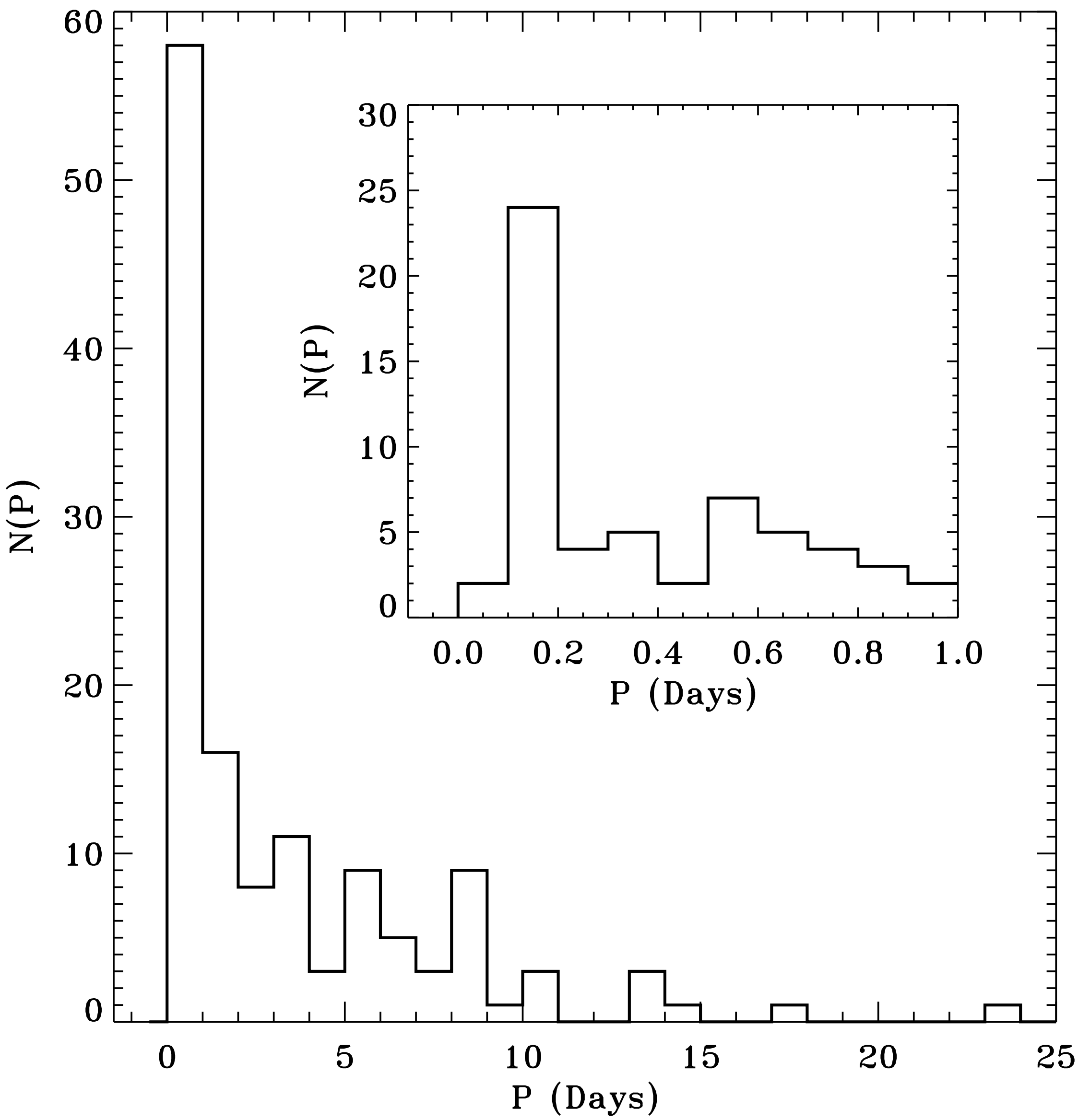

Fig. 16.— The rotation period distribution of the 131 radial-velocity and/or photometric non-members. The insert shows the distribution of periods less than 1 day with increased resolution of 0.1 day.

REFERENCES

Alphenaar, P., & van Leeuwen, F. 1981, Informational Bulletin on Variable Stars, 1957, 1

Barnes, S., & Sofia, S. 1996, ApJ, 462, 746

Barnes, S. A. 2003, ApJ, 586, 464

—. 2007, ApJ, 669, 1167

Barrado y Navascués, D., Deliyannis, C. P., & Stauffer, J. R. 2001, ApJ, 549, 452

Benz, W., Mayor, M., & Mermilliod, J. C. 1984, A&A, 138, 93

Bouvier, J., Forestini, M., & Allain, S. 1997, A&A, 326, 1023

Braden, E., Mathieu, R. D., & Meibom, S. 2008, in preparation.

Cudworth, K. M. 1971, AJ, 76, 475

Deliyannis, C. P. 2008, private comm.

Duvall, T. L., Dziembowski, W. A., Goode, P. R., Gough, D. O., Harvey, J. W., & Leibacher, J. W. 1984, Nature, 310, 22

Edwards, S., Strom, S. E., Hartigan, P., Strom, K. M., Hillenbrand, L. A., Herbst, W., Attridge, J., Merrill, K. M., Probst, R., & Gatley, I. 1993, AJ, 106, 372

Eff-Darwich, A., Korzennik, S. G., & Jiménez-Reyes, S. J. 2002, ApJ, 573, 857

Endal, A. S., & Sofia, S. 1981, ApJ, 243, 625

Geller, A., Mathieu, R. D., Harris, H. C., & McClure, R. 2008, submitted to AJ

Goode, P. R., Dziembowski, W. A., Korzennik, S. G., & Rhodes, E. J. 1991, ApJ, 367, 649

Gough, D. O. 1982, Nature, 298, 334

Herbst, W., Eislöffel, J., Mundt, R., & Scholz, A. 2007, in Protostars and Planets V, ed. B. Reipurth, D. Jewitt, & K. Keil, 297–311

Herbst, W., & Wittenmyer, R. 1996, Bulletin of the American Astronomical Society, 28, 1338

Honeycutt, R. K. 1992, PASP, 104, 435

Horne, J. H., & Baliunas, S. L. 1986, ApJ, 302, 757

Jianke, L., & Collier Cameron, A. 1993, MNRAS, 261, 766

Kalirai, J. S., Fahlman, G. G., Richer, H. B., & Ventura, P. 2003, AJ, 126, 1402

Kawaler, S. D. 1988, ApJ, 333, 236

—. 1989, ApJ, 343, L65

Koenigl, A. 1991, ApJ, 370, L39

Kraft, R. P. 1967, ApJ, 150, 551

Krishnamurthi, A., Pinsonneault, M. H., Barnes, S., & Sofia, S. 1997, ApJ, 480, 303

Lockwood, G. W., Thompson, D. T., Radick, R. R., Osborn, W. H., Baggett, W. E., Duncan, D. K., & Hartmann, L. W. 1984, PASP, 96, 714

MacGregor, K. B., & Brenner, M. 1991, ApJ, 376, 204

Mathieu, R. D. 2000, in ASP Conf. Ser. 198: Stellar Clusters and Associations: Convection, Rotation, and Dynamos, 517

McNamara, B., & Sekiguchi, K. 1986, AJ, 91, 557

Meibom, S., Barnes, S. A., Dolan, C., & Mathieu, R. D. 2001, in ASP Conf. Ser. 243: From Darkness to Light: Origin and Evolution of Young Stellar Clusters, 711

Meibom, S., & Mathieu, R. D. 2005, ApJ, 620, 970

Meibom, S., Mathieu, R. D., & Stassun, K. G. 2006, ApJ, 653, 621

—. 2008, in preparation.

Meys, J. J. M., Alphenaar, P., & van Leeuwen, F. 1982, Informational Bulletin on Variable Stars, 2115, 1

Najita, J. 1995, in Revista Mexicana de Astronomia y Astrofisica Conference Series, 293

Nordhagen, S., Herbst, W., Rhode, K. L., & Williams, E. C. 2006, AJ, 132, 1555

Perryman, M. A. C., Brown, A. G. A., Lebreton, Y., Gomez, A., Turon, C., de Strobel, G. C., Mermilliod, J. C., Robichon, N., Kovalevsky, J., & Crifo, F. 1998, A&A, 331, 81

Pinsonneault, M. H., Kawaler, S. D., & Demarque, P. 1990, ApJS, 74, 501

Pinsonneault, M. H., Kawaler, S. D., Sofia, S., & Demarque, P. 1989, ApJ, 338, 424

Prosser, C. F., Shetrone, M. D., Dasgupta, A., Backman, D. E., Laaksonen, B. D., Baker, S. W., Marschall, L. A., Whitney, B. A., Kuijken, K., & Stauffer, J. R. 1995, PASP, 107, 211

Radick, R. R., Thompson, D. T., Lockwood, G. W., Duncan, D. K., & Baggett, W. E. 1987, ApJ, 321, 459

Rucinski, S. M. 1997, AJ, 113, 1112

Scargle, J. D. 1982, ApJ, 263, 835

Schatzman, E. 1962, Annales d'Astrophysique, 25, 18

Shu, F., Najita, J., Ostriker, E., Wilkin, F., Ruden, S., & Lizano, S. 1994, ApJ, 429, 781

Sills, A., Pinsonneault, M. H., & Terndrup, D. M. 2000, ApJ, 534, 335

Skumanich, A. 1972, ApJ, 171, 565

Soderblom, D. R. 1982, ApJ, 263, 239

Soderblom, D. R., Jones, B. F., & Walker, M. F. 1983, ApJ, 274, L37

Soderblom, D. R., Stauffer, J. R., Hudon, J. D., & Jones, B. F. 1993a, ApJS, 85, 315

Soderblom, D. R., Stauffer, J. R., MacGregor, K. B., & Jones, B. F. 1993b, ApJ, 409, 624

Stassun, K. G., Ardila, D. R., Barsony, M., Basri, G., & Mathieu, R. D. 2004, AJ, 127, 3537

Stassun, K. G., Mathieu, R. D., Mazeh, T., & Vrba, F. J. 1999, AJ, 117, 2941

Stauffer, J. R., Hartmann, L., Soderblom, D. R., & Burnham, N. 1984, ApJ, 280, 202

Stauffer, J. R., & Hartmann, L. W. 1987, ApJ, 318, 337

Stauffer, J. R., Hartmann, L. W., Burnham, J. N., & Jones, B. F. 1985, ApJ, 289, 247

Stauffer, J. R., Hartmann, L. W., & Jones, B. F. 1989, ApJ, 346, 160

Stelzer, B., Fernández, M., Costa, V. M., Gameiro, J. F., Grankin, K., Henden, A., Guenther, E., Mohanty, S., Flaccomio, E., Burwitz, V., Jayawardhana, R., Predehl, P., & Durisen, R. H. 2003, A&A, 411, 517

Terndrup, D. M., Stauffer, J. R., Pinsonneault, M. H., Sills, A., Yuan, Y., Jones, B. F., Fischer, D., & Krishnamurthi, A. 2000, AJ, 119, 1303

van Leeuwen, F., & Alphenaar, P. 1982, The Messenger, 28, 15

Vasilevskis, S., Klemola, A., & Preston, G. 1958, AJ, 63, 387

von Hippel, T., Steinhauer, A., Sarajedini, A., & Deliyannis, C. P. 2002, AJ, 124, 1555

Yi, S. K., Kim, Y., & Demarque, P. 2003, ApJS, 144, 259
